Spring 2014

VARIABILITY IN UV DISINFECTION OF MUNICIPAL WASTEWATER

Angela Patricia Ortiz
Purdue University

Graduate School ETD Form 9
(Revised 01/14)

PURDUE UNIVERSITY
GRADUATE SCHOOL
Thesis/Dissertation Acceptance

This is to certify that the thesis/dissertation prepared

By Angela P. Ortiz

Entitled
VARIABILITY IN UV DISINFECTION OF MUNICIPAL WASTEWATER

For the degree of Master of Science in Civil Engineering

Is approved by the final examining committee:

Ernest R. Blatchley

Loring Nies

Chad T. Jafvert

To the best of my knowledge and as understood by the student in the *Thesis/Dissertation Agreement. Publication Delay, and Certification/Disclaimer (Graduate School Form 32)*, this thesis/dissertation adheres to the provisions of Purdue University's "Policy on Integrity in Research" and the use of copyrighted material.

Ernest R. Blatchley

Approved by Major Professor(s): _____

_____

Approved by: Michael E. Kreger 04/28/2014

Head of the Department Graduate Program Date

VARIABILITY IN UV DISINFECTION OF MUNICIPAL WASTEWATER

A Thesis

Submitted to the Faculty

of

Purdue University

by

Angela P. Ortiz

In Partial Fulfillment of the

Requirements for the Degree

Of

Master of Science in Civil Engineering

May 2014

Purdue University

West Lafayette, Indiana

Le dedico esta tesis a toda mi familia por apoyarme constantemente. Especialmente quiero agradecerle a mi madre Carmen Elvira Diaz por creer firmemente en mis capacidades, por su constante apoyo y amor. También a Michael Rodriguez por acompañarme en cada paso de este proceso y brindarme fuerza y ánimo cuando lo necesité. Finalmente, quiero dedicarle mi trabajo a mi padre Jorge Alberto Ortiz quien con sus consejos sinceros y veraces, y su amor, ha sido parte fundamental para yo tomar el impulso de perseguir esta meta y alcanzarla.

ACKNOWLEDGEMENTS

I would like to express my deepest gratitude to my committee chair, Professor Ernest R. Blatchley III, who gave me the opportunity to initiate my research experience, trusting that I had the potential to undertake the challenge. His consistent knowledge-enriched guidance provided me the tools to overcome obstacles along this process. I would especially like to thank Professor Blatchley for the compassion he demonstrated when my familial circumstances became difficult.

I would also like to thank Citizens Energy for providing the necessary funding that made this project possible, and in particular, Daphne Chiu who provided significant support in facilitating my data collection.

Additionally, I would like to recognize the School of Civil Engineering for providing supplementary funding by giving me a Teaching Assistant position, which further enhanced my experience as a graduate student at Purdue University.

Moreover, I would like to thank my other committee members, Professor Larry Nies and Professor Chad Jafvert, for their academic support and, especially, their patience throughout this project.

Furthermore, I would like to express my deepest thanks to the Statistical Consulting Service at Purdue University, in particular, Jyotishka Datta who was an invaluable help in the statistical analysis portion of this project.

Finally, I would like to thank my fellow research partners, including Caitlin A. Grady for the assistance she offered in performing several experiments and Yousra Ahmed for providing her insight and help with these experiments.

TABLE OF CONTENTS

Page

LIST OF FIGURES

Figure Page

LIST OF TABLES

ABSTRACT

Angela P. Ortiz Diaz. MSCE, Purdue University, May 2014. Variability in UV Disinfection of Municipal Wastewater. Major Professor: Ernest R. Blatchley III.

Variability in the performance of UV disinfection systems is hypothesized to be attributable to variability in the parameters that influence the overall performance. Predictability of process performance in UV disinfection systems should be possible, if variability in these input parameters can be defined. The objective of this project was to define variability in parameters that are known to affect the performance of UV disinfection systems so as to inform design and operation conditions for a large-scale UV disinfection system that was recently applied at the Belmont facility in Indianapolis, Indiana, and other systems. The present study focused on quantification of variability in several input parameters, including viable *E. coli* concentration in undisinfected secondary effluent, UV_{254} dose-response behavior of the target organism (*E. coli*), UV_{254} transmittance (UVT_{254}) of the water, total suspended solids (TSS), flow rate (Q), and precipitation. These data were subjected to correlation analysis to identify dependence among these parameters, and thus have a better understanding of the variability in the performance of this UV system.

In addition, measurements of the actual performance of the existing, full-scale UV disinfection system at the Belmont facility were conducted using Ambient Biodosimetry (AB). This method allowed for quantification of *E. coli* inactivation across the UV system over a range of operating conditions. The results of these experiments indicated that the system consistently exceeds treatment requirements, as defined by the Belmont NPDES permit, with a fraction of the existing hardware. This suggests that the existing system at Belmont may be over-designed, and that opportunities exist to improve the efficiency of the system's operation.

In the future, these data will be used in the development of a stochastic model that will predict performance variability. In turn, these model predictions will be used to inform the design and/or operation of UV wastewater disinfection systems.

CHAPTER 1. INTRODUCTION

During the 1970s, concerns arose regarding the use of chlorine as a disinfectant because of its potential negative environmental and human impacts relating to disinfection by-product (DBP) formation, as well as its safe storage and handling. Implementation of UV disinfection in wastewater treatment plants (WWTPs) has become a popular alternative disinfection method because it is a broad-spectrum antimicrobial agent, it promotes minimal DBP formation, it typically has lower overall capital and operational costs than other methods, and it requires a relatively small footprint as the reactions of interest are very fast (Whitby & Scheible, 2004).

After the discovery of disinfection by-products and their potential detrimental effects on the biota of receiving waters and human health, governments throughout North America were motivated to reduce the concentrations of chlorine disinfection by-products in effluent waters (USEPA, 1976). This also motivated research efforts in alternative disinfection methods, such as ozone, bromine chloride, chlorine dioxide, and UV. As a result of a financial investment from the United States Environmental Protection Agency's Innovative and Alternative Technology program, the effectiveness of UV disinfection was demonstrated. And a few years later, the successful implementation of a gravity-fed, open channel system with lamps oriented parallel to the direction of flow marked the establishment of UV disinfection for wastewater treatment (Whitby & Scheible, 2004).

As the application of UV disinfection for wastewater continues to expand, it offers several well-known advantages, including minimal formation of harmful disinfection by-products (DBPs). DBPs in final effluent discharge waters have been shown to have negative effects in humans and aquatic biota (Lazarova *et al.*, 1999; Das, 2002). Another advantage is the competitive capital and operational costs of UV compared to chlorine disinfection, as well as its safer operation and handling (Lazarova *et al.*, 1999; Das, 2002).

In addition to disinfection, UV irradiation has also been applied in advanced oxidation processes (AOP) that are used to treat toxic non-biodegradable contaminants, such as pesticides. The AOPs that involve UV generally require relatively high doses (as compared to those required for disinfection) in conjunction with a photocatalytic agent to promote the formation of radical intermediates, such as hydroxyl radical. The hydroxyl radical is highly reactive, and it will further react with contaminants in the water to convert them, to a large extent, into more stable inorganic compounds (Kruithof *et al.*, 2002; Zwiener *et al.*, 1995; Glaze *et al.*, 1987).

As more WWT facilities are switching to UV disinfection, there is an increasing need to more accurately predict the performance of UV reactor systems. Currently, in the U.S. there are several large drinking water and wastewater facilities that are planning to switch to UV disinfection. These facilities service large populations, such as the cities of Chicago and New York. The city of Chicago, for example, has the Stickney Water Reclamation Plant (WRP), the largest WWTP in the world, which serves about 2.38 million people, with a design flow rate of 1.2 billion gallons per day (BGD). Treated wastewater from the Stickney facility is discharged to the Chicago Sanitary and Ship Canal. This waterway is considered an incidental contact water, and this is, in part, why this facility is not currently required to disinfect its effluent (IEPA, 2013; MWRDGC, 2013). The Stickney (WRP) will be required to disinfect in the near future.

The Castkill/Delaware UV disinfection facility in the state of New York is currently the largest UV disinfection system in the world. Although this is a drinking water facility, the mechanisms of UV disinfection are the same for both drinking and wastewater, with final effluent requirements and source water quality being the main differences. This facility was designed to treat 2.02 BGD to be distributed to the city of New York (Trojan UV 2014).

The Catskill/Delaware UV system is an excellent example of the growing reliance that UV disinfection is gaining among utilities and consulting engineers. As more wastewater and drinking water treatment facilities look for alternative disinfection processes to be incorporated, UV will continue to attract their attention because it has been demonstrated to comply with existing disinfection standards, and in many cases it has been demonstrated to be cost competitive with the other alternatives (Lazarova *et al.*, 1999; Das, 2002).

From the engineering perspective, having a more comprehensive and accurate understanding of the behavior of UV disinfection systems is beneficial to the development of UV. Research that demonstrates the true capabilities of UV disinfection, including its weaknesses, will be useful for future designs of reactor systems, and improve maintenance and operation practices of existing UV systems. Moreover, development of improved predictive methods to estimate the performance of UV disinfection systems will allow optimization of system designs, while improving system reliability and conformance to treatment regulations.

It has been hypothesized that in order to understand the variability in process performance of UV reactor systems, an understanding of the variability in other input parameters known to influence disinfection performance is crucial; that is, if the variability of input parameters is well understood, an accurate prediction of the overall performance of the reactor can be made.

This research project focused on measurement of parameters that are known to affect process performance of UV disinfection systems, as well as measurement of actual variability in process performance of a full-scale UV system. This study took advantage of the recently installed full-scale UV disinfection system at the Belmont WWTP located in Indianapolis, Indiana. Data collected included UV_{254} dose-response data of the target organism using undisinfected secondary effluent samples, ambient biodosimetry (AB) data from the UV reactor system, UV transmittance (UVT_{254}) of the water at the time of sampling, flow rate through the UV system, nominal UV_{254} dose delivered as calculated by the PLC system, total suspended solids, and precipitation. These data were subjected to correlation analysis to identify dependence among these parameters, and thus have a better understanding of the variability in the performance of this UV system. In the future, these data will be used in the development of a stochastic model to describe and predict variability so as to inform the design and/or operation of UV wastewater disinfection systems.

CHAPTER 2. LITERATURE REVIEW

2.1 Mechanisms of disinfection

UV radiation achieves inactivation of microorganisms primarily by causing damage to their RNA and DNA. UV irradiation causes dimers to form in nucleic acids; these are covalent bonds that form between adjacent pyrimidines (thymine and cytosine) on the same DNA or RNA strand, and they are the most common damage resulting from UV disinfection (see Figure 1). The result is inhibition of the ability to reproduce on the part of the microorganism. Once the microorganism is inactivated, it loses its ability to infect its host and cause disease. UV radiation is absorbed most strongly by DNA and RNA nucleotides in the range of 230 nm to 260 nm (Jagger, 1967). This knowledge informed selection of UV lamps that are used in disinfection systems. The optimal germicidal wavelengths are generally found in the UV-C region of the electromagnetic spectrum, which ranges from wavelengths of 200 nm to 280 nm (see Figure 3).

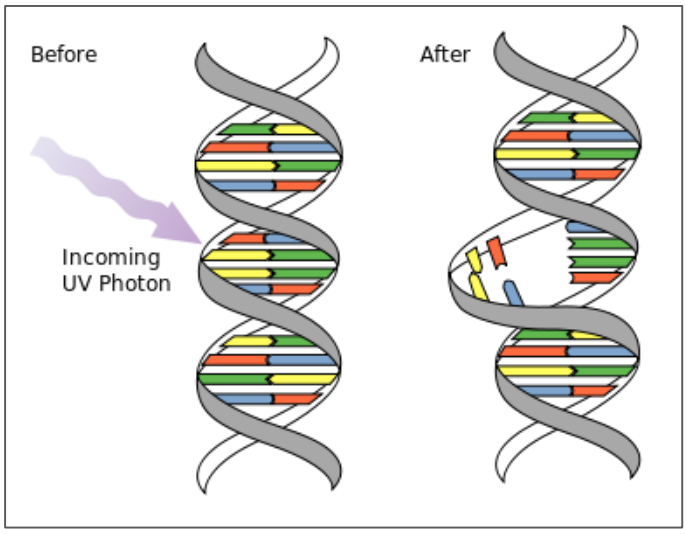

Figure 1. Dimerization of pyrimidines in a DNA strand caused by UV irradiation. Source: http://en.wikipedia.org/wiki/Pyrimidine_dimer.

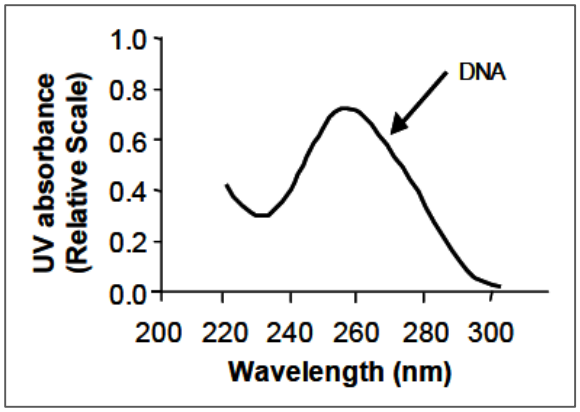

Figure 2. DNA absorbance spectrum. Source: Jagger (1967).

There is evidence that UV radiation in the UV-B and UV-A spectrum, which is the most abundant type of radiation in our atmosphere, can also have germicidal properties. However, radiation in the UV-B and UV-A portions of the spectrum is less effective for causing damage to nucleic acids, and as such requires a longer exposure time than UV-C radiation at the same fluence rate to achieve a given reduction of viable microorganisms in water. Examples of applications of UV-B and UV-A for water disinfection are the Solar Water Disinfection (SODIS) (McGuigan *et al.*, 2012) and the continuous-flow solar disinfection reactor system developed by Mbonimpa et al. (2012). These methods take advantage of ambient solar UV radiation to disinfect water for drinking, and they have been typically used or intended for use in developing countries where improved sources of water are difficult to access.

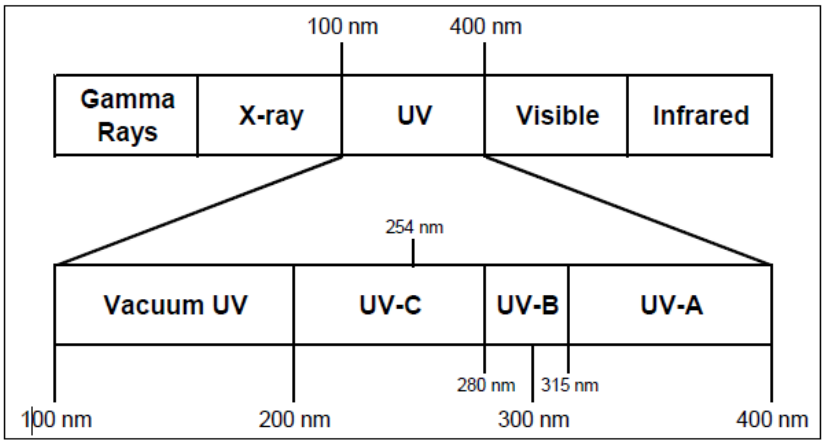

Figure 3. UV radiation in the electromagnetic spectrum. Source: *USEPA UV Disinfection Guidance Manual* (2006).

The dose of UV radiation is defined as the product of the time of exposure (τ) and the imposed fluence rate (F) (USEPA, 2006a). The UV dose is typically expressed in mJ/cm^2. More specifically, UV dose is the time-integral of the imposed fluence rate:

$$D = \int_0^{\tau} F(t) \cdot dt \qquad \text{Eq. 1}$$

Where F(t) = fluence rate history for an irradiated object

t = time.

As clarified in the work by Bolton and Linden (2003), the *fluence rate* is defined as the total radiant power incident from all directions onto an infinitesimally small sphere; and, the *irradiance* is defined as the total radiation *incident* from all directions irradiated from *above* on an infinitesimally small element of surface of area.

In a continuous flow UV reactor, every microorganism or particle present in the water experiences a different UV dose by the time it exits the reactor. This is because within the reactor the microorganisms and particles travel through different paths; some may travel closer to the lamps experiencing an overall higher dose, while others may travel closer to the walls of the reactor resulting in an overall lower dose. Therefore, it is clear that continuous flow UV reactors deliver a distribution of UV doses (Cabaj *et al.*, 1996).

2.2 Kinetic models

The kinetics of microbial inactivation achieved by UV radiation, i.e., dose-response behavior, are often simulated by fitting with a kinetic model. If a kinetic model accurately describes the inactivation behavior of the target organism of interest, it will allow for an accurate prediction of inactivation that will result with a given UV dose. That is to say, the delivery of a specific UV dose will result in a predictable inactivation according to the kinetic model that is chosen.

All kinetic models of UV disinfection relate microbial inactivation to the applied dose. As such, UV dose represents the "master variable" in UV disinfection systems.

Common kinetic models include the Chick-Watson (single-event), Series-event, and Phenotypic Persistence and External Shieling (PPES) models. The Chick-Watson kinetic model has been widely used in wastewater disinfection. This model is based on the assumption that inactivation of

microorganisms by UV irradiation can be described by a model that is first-order with respect to the imposed fluence rate and the concentration of viable organisms (N) (Watson, 1908):

$$\frac{dN}{dt} = -kFN \qquad \text{Eq. 2}$$

Where k = Rate constant for inactivation (cm^2/mJ)

F = Fluence rate (mW/cm^2)

N = concentration of viable organisms

t = Exposure time (s).

Literal interpretation of the Chick-Watson model, as applied for UV disinfection, implies that a single photochemical event (e.g., formation of one dimer in a DNA strand) will lead to inactivation. The Chick-Watson (single-event) model has been observed to work well for description of the dose-response behavior of some simple microbes, including some viruses and bacteria (Severin *et al.*, 1983). However, the dose-response behavior of some bacteria, as well as some higher organisms is often not described well by the single-event model. A common deviation from simple first-order behavior is displayed by the existence of a "shoulder" in a dose-response relationship (see Figure 4).

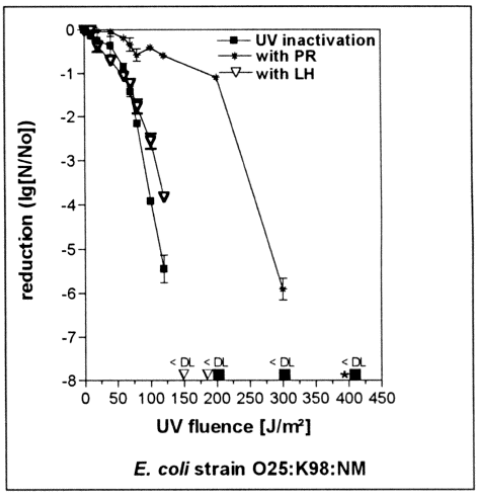

Figure 4. Example of "shoulder" behavior in the UV dose-response of *E. coli*. Source: Sommer (2000).

One explanation for this behavior is the need for multiple units of damage to cause inactivation. The Series-event model was developed to describe this behavior. The model assumes that all organisms within a population accumulate damage as a result of a series of identical photochemical events:

$$M_0 \xrightarrow{h\nu} M_1 \xrightarrow{h\nu} M_2 \xrightarrow{h\nu} \dots M_{n-1} \xrightarrow{h\nu} M_n \xrightarrow{h\nu} M_{n+1} \xrightarrow{h\nu} \dots \quad \text{Eq. 3}$$

Where M_i represents a microorganisms with i units of damage. A further assumption of this model is that organisms will retain viability until they accumulate n units of damage. If each photochemical event is assumed to follow first-order kinetics, then the fraction of organisms in a population that retain viability will be as follows (Severin *et al.*, 1983; 1984).

$$\frac{N}{N_0} = exp(-k \cdot F \cdot t) \sum_{i=0}^{n-1} \frac{(k \cdot F \cdot t)^i}{i!} \quad \text{Eq. 4}$$

Where N = Concentration of viable organisms that survive UV exposure

N_0 = Concentration of viable organisms prior to exposure to UV

k = inactivation rate constant

F = Fluence rate (mW/cm^2)

t = exposure time (s)

$F \cdot t$ = UV dose (mJ/cm^2)

n = inactivation threshold

Another common deviation from Chick-Watson behavior is the existence of "tailing" in an observed UV dose-response data set. Models that are used to describe this behavior generally assume that microbial populations can be described as two sub-populations: one that is susceptible to inactivation and another that resists inactivation. The existence of a resistant sub-population has been attributed to microbial association with particles and/or population heterogeneity. Based on this logic, Pennell *et al*. (2007), developed the Phenotypic Persistence and External Shielding (PPES) kinetic model.

The PPES model is a combination of the Chick-Watson and Series-Event kinetic models, where the sub-population (A_0) is assumed to be susceptible to UV exposure, and the second sub-population (B_0) is assumed to be resistant to UV. Therefore, N_0 is the sum of A_0 and B_0. The result is a mathematical expression that accurately describes the "shoulder", and "tailing" parts of the UV dose-response curve that are commonly observed. The expression is as follows:

$$\frac{N(t)}{N_0} = \frac{A_0}{N_0}\left(exp(-k_A \cdot F \cdot t)\sum_{i=0}^{n-1}\frac{(k_A \cdot F \cdot t)^i}{i!}\right) + \frac{B_0}{N_0} \cdot exp(-k_B \cdot F \cdot t) \qquad \text{Eq. 5}$$

Where A_0 = Microorganism subpopulation assumed to be susceptible to UV

B_0 = Microorganism subpopulation assumed to be resistant to UV

k_A = Inactivation constant for the susceptible subpopulation (cm^2/mJ)

k_B = Inactivation constant for the resistant subpopulation (cm^2/mJ)

$F \cdot t$ = UV dose (mJ/cm^2)

2.2.1 Segregated Flow Model for Continuous Flow Reactors

The inactivation by continuous flow UV reactors can be predicted by applying the Segregated Flow Model (SFM).

$$\left(\frac{N}{N_0}\right)_{reactor} = \int_0^{\infty} \left(\frac{N}{N_0}\right)_{batch} \cdot E(D) \cdot dD \qquad \text{Eq. 6}$$

Where $\left(\frac{N}{N_0}\right)_{reactor}$ = inactivation of microorganisms achieved in flow through reactor

$\left(\frac{N}{N_0}\right)_{batch}$ = inactivation of microorganisms achieved in with dose *D* (UV disinfection kinetics)

E(D) = dose distribution

dD = differential dose

E(D)·dD = fraction of particles that receive a dose in a dose interval *D* to *D* + *dD*.

The SFM assumes that the organisms present in water that passes through a reactor do not exchange material with each other. As such, each organism passes through the reactor as a discrete (segregated) unit. Under these circumstances, integration of the UV disinfection kinetic model with the dose distribution function, over the range of possible doses, yields a prediction of overall inactivation achieved by the reactor. The SFM has been shown to yield accurate predictions of reactor behavior under conditions when all input parameters can be accurately measured (Naunovic *et al.*, 2008).

2.3 Assessment and design tools of UV reactor systems

Current methods to characterize the design and process performance of large-scale UV disinfection systems include biodosimetry, Computational Fluid Dynamics Irradiance Field (CFD-I) models, and Lagrangian Actinometry. Of these, biodosimetry is perhaps the most common methodology used by operators in WWTPs and drinking water facilities.

2.3.1 Biodosimetry

Biodosimetry involves a comparison of the performance of a continuous flow reactor with dose-response behavior, usually measured using a collimated beam test. It consists of developing a standard curve for the UV dose-response behavior of a challenge organism by determining the fractional survival of the challenge organism(s) as a function of UV dose. Dose delivery in this portion of the test usually involves a collimated UV source. Ideally, the challenge organism should have a similar sensitivity to UV radiation as the target pathogen or regulated microorganism.

The second step consists of testing the continuous flow (large-scale) reactor. A known concentration of the same challenge organism is injected at the influent of the reactor, then samples from the effluent are analyzed to determine the inactivation response achieved by the reactor, i.e., measure surviving organisms. The test conditions are also measured, e.g., flow rate, UVT, lamp status, and UV fluence rate, as measured by UV sensors.

The third step is to determine the reduction equivalent dose (RED) by comparing the results from the bench-scale and large-scale testing. The inactivation response of the challenge organism measured in the continuous-flow reactor is compared with the UV dose-response data to determine the RED. RED values are specific to challenge microorganisms used during experimental testing, and to test conditions of the full-scale testing (USEPA, 2006a; Cabaj *et al.*, 1996; Qualls & Johnson, 1983; Blatchley, 1997). The following figure illustrates the process described above.

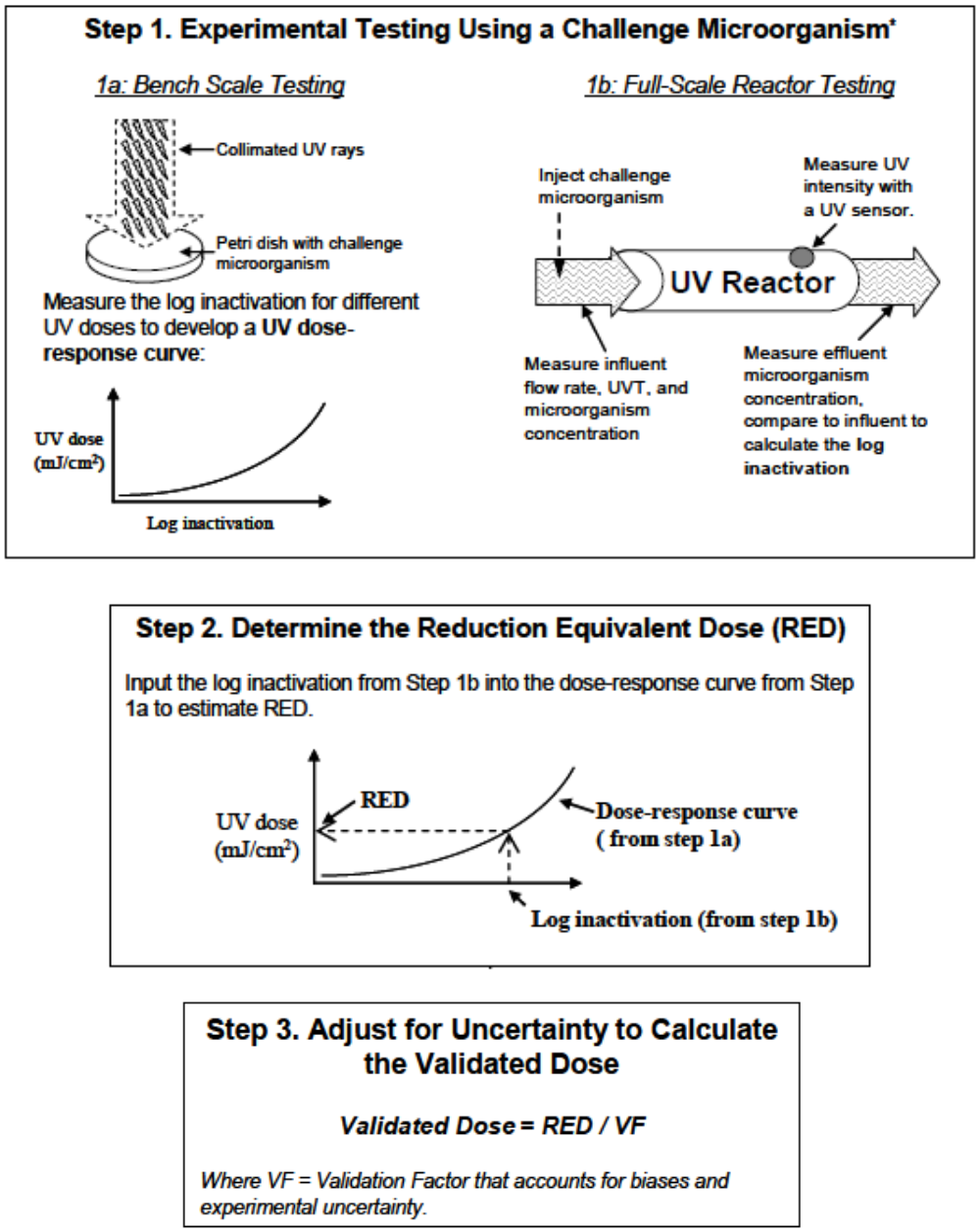

Figure 5. Overview of recommended experimental protocol. Source: *USEPA UV Disinfection Guidance Manual* (2006).

The primary advantage of biodosimetry is that it involves direct measurements of the concentration of the surviving challenge organism(s). This is beneficial for regulatory agencies; however, it fails to give a description of the actual UV dose distribution that a continuous-flow UV reactor system delivers.

2.3.2 Computational Fluid Dynamics Irradiance Fluence Rate Field

Computational Fluid Dynamics Irradiance (Fluence Rate) Field (CFD-I) models are used to simulate hydrodynamic behavior within a UV reactor, and because of its utility it is becoming more prevalent in the design of UV reactors (Wols *et al.*, 2011; Santoro *et al.*, 2005).

CFD uses numerical methods to solve the fundamental nonlinear differential equations (equations of motion and continuity, together with a turbulence closure model) and obtain the flow field of the water and the motion of particles for a predefined reactor geometry and conditions. Irradiance Field models account for the optical qualities of the water, output power of the lamps, and system geometry. The results of I-field modeling are integrated with CFD results to predict reactor behavior. Figure 6 is an illustration of a velocity field as simulated by CFD.

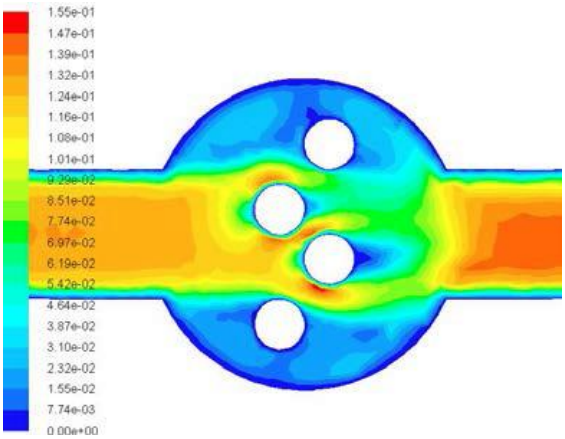

Figure 6. Velocity field CFD simulation. Source: Wols et al. (2012).

As mentioned before CFD-I analyses are performed for set of predetermined conditions, allowing simulation for those conditions. However, the results are deterministic, meaning that the CFD does not take into account the natural variability observed in UV reactor systems.

2.3.3 Lagrangian Actinometry

Lagrangian Actinometry involves the use of microspheres that have been conjugated to a UV-sensitive dye. As in biodosimetry, the dose-response behavior of microspheres is first defined by exposure to UV under a collimated beam to a range of doses. The response of microspheres is a change in in fluorescence intensity (FI) that is measured by flow cytometry (FC). After the UV response of microspheres has been determined, microspheres are injected to the influent of continuous-flow UV reactors and allowed to flow through. The microspheres are then collected at the effluent, separated from the water, and analyzed by FC. Mathematical deconvolution is employed to estimate the dose distribution delivered by the reactor (Blatchley *et al.*, 2006).

To date, Lagrangian Actinometry is the only method available for measurement of UV dose-distribution of a continuous flow reactor. This method has been used in conjunction with biodosimetry and CFD-I methods for validation of a wide range of UV reactor types (Blatchley *et al.*, 2008; Wols *et al.*, 2012).

2.4 Input parameters that introduce variability in process performance

The performance of UV disinfection systems is dependent on several factors that cannot be controlled and display variability over time. Figure 3 illustrates parameters that are known to influence the performance of UV disinfection reactors. Input parameters listed in the green boxes display variability, but can be measured and quantified. Parameters in the red box illustrate fixed attributes of a given reactor, and parameters in the yellow boxes illustrate attributes of the system that depend on other system characteristics, and their variability. Arrows indicate direction of dependence among process variables.

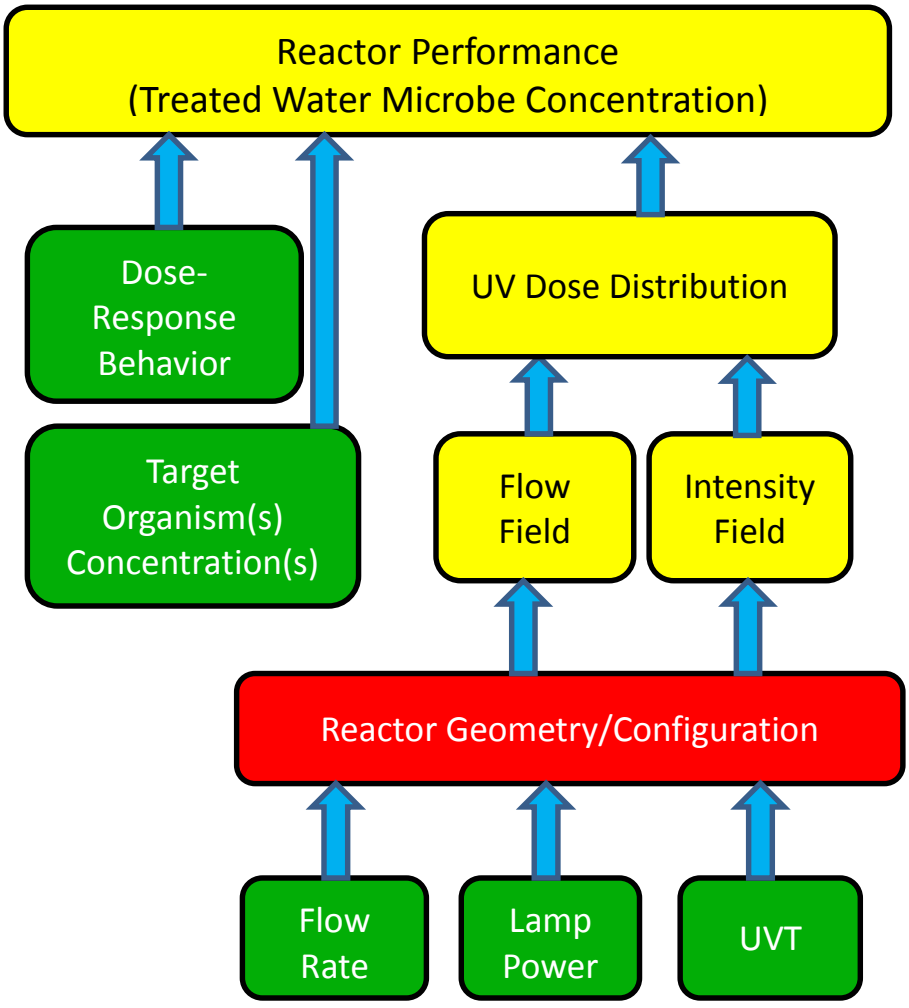

Figure 7. Parameters that influence the performance of UV disinfection reactors.

The microbial response to UV, or UV dose-response behavior, is a measure of the susceptibility of the target microorganism to UV radiation. Standardized methods for measurement of UV dose-response behavior were described previously.

Flow rate variations to a treatment process will show diurnal, seasonal and other variations. However, flow rate is often measured in real time; therefore robust flow rate data sets are often possible at municipal WWTPs.

UV transmittance also displays variability, and it affects the delivery of UV radiation to water. UVT is defined as the percentage of UV (λ = 254 nm) radiation passing through an optical path length of a sample. UVT can also be measured in real time; however, in the absence of this instrumentation, grab samples can be collected to for measurement of UVT with a conventional spectrophotometer.

Total suspended solids (TSS) is a measurement used to describe particles suspended in water. Water with high TSS concentration is often observed to shelter aquatic microbes from UV exposure (Blatchley *et al.*, 2001).

2.5 Current regulations

Current federal and state regulations pertaining to UV disinfection of municipal wastewater in the United States are based on limitations on discharge concentrations of target organism(s) and other contaminants. Examples of these regulations of limits on effluent quality include those imposed through the National Pollutant Discharge Elimination System (NPDES) permits and the Water Recycling Criteria (WRC) *Title 22* of the California Code of Regulations. It is relevant to note that some water regulations, such as Chapter 62: Domestic Wastewater Facilities of the Florida Administrative Code (FAC), recognize the potential "harmful effects of chlorine" and encourage "the use of alternative disinfection methods".

No uniform, standard operational UV dose has been defined for UV systems used to disinfect municipal wastewater because there is a great deal of variability associated with the UV disinfection process, and it would be arbitrary to assign one operational scheme for all target endpoints. However, there have been several recommendations included in federal, regional, or state standards that have been published to inform designers and operations personnel. Some of these include the *Ten States Standards*, which recommends a nominal dose for wastewater

disinfection of no less than 30 mJ/cm^2 (2004); however, no definition of dose or its measurements is included in *Ten States Standards. The Ultraviolet Disinfection Guidelines for Drinking Water and Water Reuse* suggests a design RED of 100 mJ/cm^2 for water reuse applications based on the a 5-$\log_{10}$ inactivation of poliovirus (2012).

Another difficulty with existing regulations is that they fail to recognize the existence or importance of the dose distribution that is delivered by all contemporary UV reactors. This is complicated by the existence of a wide range of UV "dose" definitions for UV reactors. In general, these characteristics of existing regulations effectively mandate conservatism in the design and operation of UV disinfection systems.

2.6 Belmont WWTP design features

The Belmont WWTP is one of two facilities responsible for treating wastewater in Indianapolis, Indiana. It has an average design flow of 120 million gallons per day (MGD) and a peak flow capability of 300 MGD. The Belmont facility recently underwent a substantial upgrade of its treatment hardware and capability. This upgrade was part of the recent Wet Weather Secondary Treatment (WWST) Expansion Project, which includes an Air Nitrification System (ANS). A UV disinfection system designed to handle a peak flow of 150 MGD was also installed. In accordance with Belmont's National Pollutant Discharge Elimination System (NPDES) permit, the facility is required to comply with limits of viable *E. coli* including a monthly geometric mean of 125 cfu/100 mL, and a daily maximum is 235 cfu/100 mL. These disinfection standards are to be complied with during the period of April 1 through October 31, annually. Here this period will be referred to as the *disinfection season*; otherwise, it will be specified as the *non-disinfection season*. During the period of November 1 through March 31, the Belmont WWTP it is not required to disinfect (IDEM, 2013).

The UV disinfection system at Belmont UV system consists of seven channels each with 2 banks of UV lamps, each bank has 24 modules, and each module has 8 lamps. The total number of lamps per bank is 192. An estimate of the electrical power cost for operation of this system was developed based on an assumed operating condition of all seven channels being operated, with all lamps in both banks of each channel being operated at full power.

A list of assumptions used in developing this estimate of electrical power cost is as follows:

1. Two banks of UV lamps in operation
2. Operation at full power equal to 250 watts per lamp
3. A total of 7 channels in operation
4. 184 days in the disinfection season (April 1st – October 31st)

Total number of lamps for the whole system is:

$$192\frac{lamps}{bank} \times 2\frac{bank}{channel} \times 7channels = 2688\ lamps$$

Cost per kW·hr is $0.06

$$2688\ lamps \times 250\ W \times \frac{1\ kW}{1000\ W} = 672\ kW$$

$$672\ kW \times 24\frac{hr}{day} \times \frac{\$0.06}{kW \cdot hr} = \$968/day$$

$$\frac{\$968}{day} \times 184\frac{days}{year} = \$178{,}000/year$$

The Southport WWTP is an additional treatment facility in the city of Indianapolis. This facility is similar in size with an average flow rate of 125 MGD and a peak flow of 150 MGD. The Southport WWTP is currently undergoing an expansion project to increase its treatment capacity. As with Belmont the project will include the installation of a UV disinfection system.

CHAPTER 3. METHODS AND MATERIALS

3.1. UV Dose-Response Experiments

Sampling and conducting of these experiments began in June of 2012 and finished in June of 2013. Secondary effluent samples were collected from a sampling station (see Figure 8) at the Belmont WWTP in 1 L glass bottles. The samples were immediately put in coolers that maintained a temperature between 1.7°C and 4.4°C. The analyses were initiated within 30 minutes of collection, when the Belmont Field Laboratory was used. When analyses were conducted at Purdue University, they were initiated within 2 hours of collection.

Figure 8. Secondary effluent sampling station

From each sample, subsamples were placed under a collimated beam in a shallow, well-mixed batch reactor and subjected to a range of UV doses (λ = 254 nm). The shallow batch reactors were 15 cm diameter Pyrex glass petri dishes. For each exposure, 150 mL of sample was poured to achieve a depth of ~1.0 cm. A small Teflon-coated stir bar was introduced in the sample to accomplish mixing during exposure. This arrangement is illustrated in Figure 9.

Target UV doses chosen included 40, 30, 20, 15, 10, and 5 mJ/cm^2. Additionally, one subsample received no exposure of UV, which was used as the control to measure N_0 (concentration of viable *E. coli* in undisinfected effluent). These values for UV doses were chosen as they are relevant to wastewater disinfection applications.

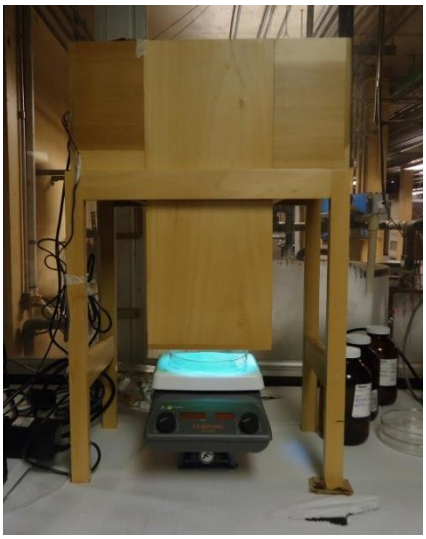

Figure 9. Collimated beam set-up at the Belmont WWTP Field Laboratory.

USEPA Method 1103.1 was applied to quantify viable *E. coli* concentrations after each exposure of UV radiation, and in undisinfected effluent samples. This method allows for a direct bacterial count from a water sample based on the development of colonies on the surface of a membrane filter. A water sample is filtered through a membrane which retains the bacteria. After filtration, the membrane is placed on a growth medium that is selective and differential, and incubated at 35°C to 44.5°C ± 0.2°C for about 24 hours. Following incubation, the filter is transferred to a filter pad saturated with urea substrate. After 15 minutes, yellow, yellow-green, or yellow-brown colonies are counted. Membranes that developed more than 100 colonies were classified as too numerous to count (TNTC) (USEPA, 2006b).

The dose was calculated following the protocols established by Bolton and Linden (2003). First the incident irradiance (I) of the collimated beam was measured with a radiometer at the center of the beam (International Light, model: IL1700). The UVT of the sample was measured with a spectrophotometer (Cary, model: 300 Bio). Several correction factors were included to allow accurate measurement of the applied UV dose. The corrections included the petri factor, the reflection factor, water factor, and divergence factor (Bolton & Linden, 2003).

The petri factor used to correct the irradiance reading taken at the center of the beam and petri dish to more accurately reflect the average incident irradiance over the surface area of the whole petri dish.

The reflection factor accounts for the reflection that takes place when a beam of radiation passes from one medium to another.

The water factor, accounts for the absorbance of radiation that the water sample may have.

The divergence factor accounts for the divergence of the radiation over the distance from the lamp to the suspension.

Equation 7 expresses the collective effects of the correction factors.

$$I_{avg} = \frac{I_R \cdot (1 - R)\left(\frac{L}{L + \ell}\right) \cdot P \cdot [1 - exp(-\alpha\ell)]}{\alpha\ell} \qquad \text{Eq. 7}$$

Where I_R = Irradiance measured with radiometer (mW/cm^2)

R = Reflection coefficient

L = Vertical distance from the lamp axis to the air:water interface

ℓ = Liquid depth in the Petri dish (1 cm)

P = Petri factor (0.846)

$\alpha = \frac{-ln(T)}{A}$ where T is the UVT (%) measured with a spectrophotometer, and A is the optical path length of the spectrophotometer.

For every day a UV dose-response experiment was performed, additional water quality parameters were obtained from the Belmont Monthly Reports. These included TSS in mg/L, average flow rate in MGD, and precipitation in inches.

A total of 46 UV dose-response experiments were performed. Due to construction that took place at the Belmont WWTP, the sampling location had to be changed, and as a result 19 samples were unfiltered secondary effluent samples and 27 were filtered effluent samples

3.2 Statistical analysis

Piece-wise regression was applied to the resulting UV dose-response curves to obtain fitting parameters of the PPES model. None of the resulting curves in this study displayed a shoulder, but tailing was evident in all data sets. Therefore, a modified form of the PPES model was applied for regression analysis:

$$\frac{N(t)}{N_0} = \frac{A_0}{N_0} \cdot exp(-k_A \cdot F \cdot t) + \frac{B_0}{N_0} \cdot exp(-k_B \cdot F \cdot t) \quad \text{Eq. 8}$$

A piece-wise regression tool was developed using the software SAS, to find the best fit for the PPES model parameters k_A, k_B, and the inflection point of the curve (c), which is equivalent to the UV dose in mJ/cm^2 for which the persistent *E. coli* population (B_0) remained. Once the value of c was obtained, B_0 was calculated as follows:

$$B_0 = \exp(-k_A \cdot c) \cdot N_0 \quad \text{Eq. 9}$$

Where B_0 = Microorganism sub-population assumed to be resistant to UV

k_A = Inactivation constant for the susceptible subpopulation (cm^2/mJ)

c = UV dose for which the resistant sub-population B_0 remains (mJ/cm^2)

The susceptible subpopulation (A_0) was calculated by subtracting B_0 from N_0, which was directly measured in the UV dose-response experiments.

Additionally, Pearson correlation coefficients were calculated between the following parameter estimates:

- PPES model parameters (each of them) vs. daily average flow
- PPES model parameters vs. TSS
- PPES model parameters and UVT
- UVT vs. TSS
- UVT vs. daily average flow
- UVT vs. daily max flow
- N_0 vs. TSS
- N_0 vs. daily average flow

Correlation coefficients are considered statistically significant when the P-value is less than 0.05 (Schervish, 1996). Parameters that express strong positive or negative correlations coefficients can be interpreted as having a significant linear relationship between them. Correlation coefficients were calculating using SAS.

3.3 Ambient Biodosimetry (AB)

Ambient biodosimetry experiments were performed during the disinfection season and the non-disinfection season. During the non-disinfection season the WWTP is not required to disinfect to comply with the NPDES discharge permit limitations for *E. coli*. Therefore, management at the Belmont facility allowed manipulation of the UV system without concern of violating the permit. This allowed the use of high flow rates or small number of channels to "challenge" the system. For some of the AB experiments, a fixed flow rate was diverted to the UV system, and samples were collected for different flow conditions. Flow conditions were defined by the number of channels open for operation and flow rate. Therefore, the more channels open, the lower the flow rate per channel, and vice versa. It is important to mention that due to the design of the system, when the system is set to manual operation, the power output of the lamps is automatically fixed to deliver full power. So the dose delivered changed based only on the UVT, number of operating channels, number of operating lamp banks and flow rate.

The Belmont UV system consists of seven channels, each with two banks of lamps in series, labeled A and B for the upstream and downstream locations respectively. As illustrated in Figure 11, samples were collected from position I (undisinfected water), position II (downstream of bank A), and position III (downstream of both banks A and B).

Figure 10. UV disinfection reactor at the Belmont WWTP

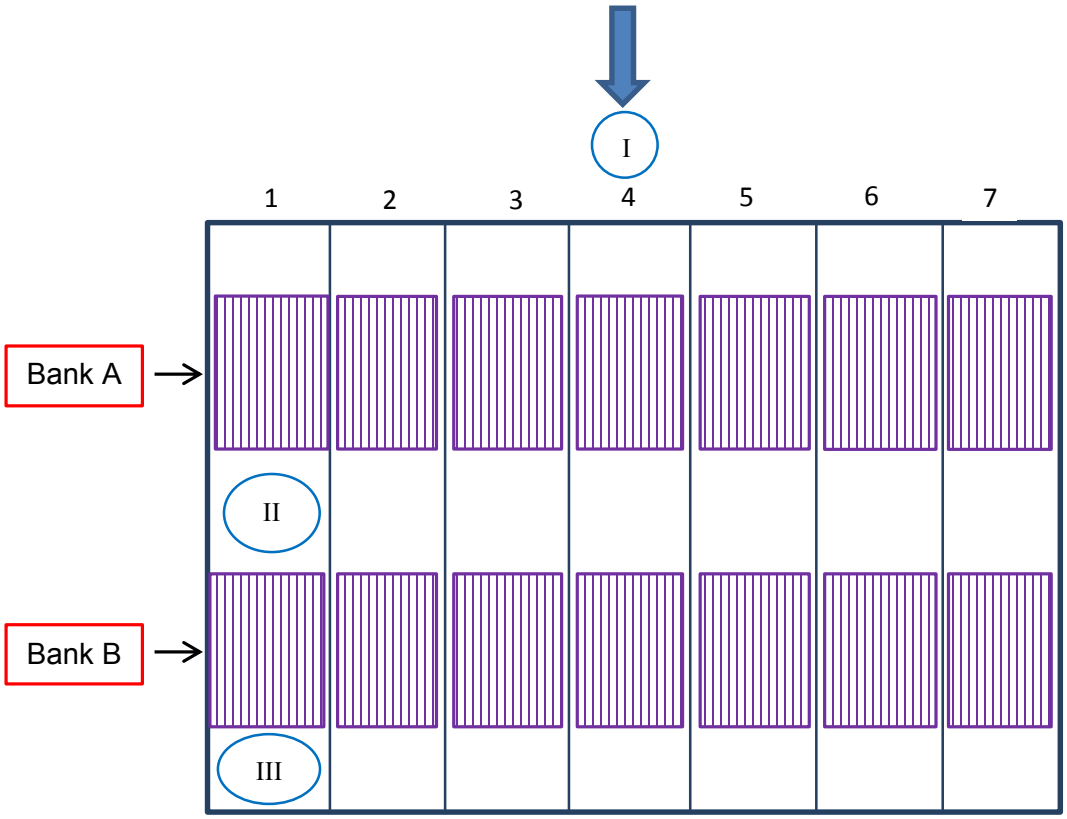

Figure 11. Schematic representation of the UV reactor of the Belmont WWTP. The arrow illustrates the direction of flow. Seven channels each with two banks of UV lamps. I, II, III indicate the locations where water samples were collected. Not to scale.

The samples were collected with plastic buckets, one for each sample location. Water from the bucket was transferred into sterile 1 L whirl packs, and immediately placed in a cooler. For most of AB experiments the analyses were performed in the Belmont Field Laboratory, and were initiated within a 1 hour of collection. When the analysis was done at Purdue University, it was initiated within two hours of sample collection. USEPA Method 1103.1 of membrane filtration was employed for *E. coli* quantification, as described previously (2006b).

CHAPTER 4. RESULTS AND DISCUSSION

4.1 Viable *E. coli* Concentration in Undisinfected Effluent (N_0)

A total of 49 undisinfected effluent samples were collected over a period beginning in July of 2012 and ending in June of 2013. The concentration of viable *E. coli* was measured in each sample. Figure 12 illustrates these results.

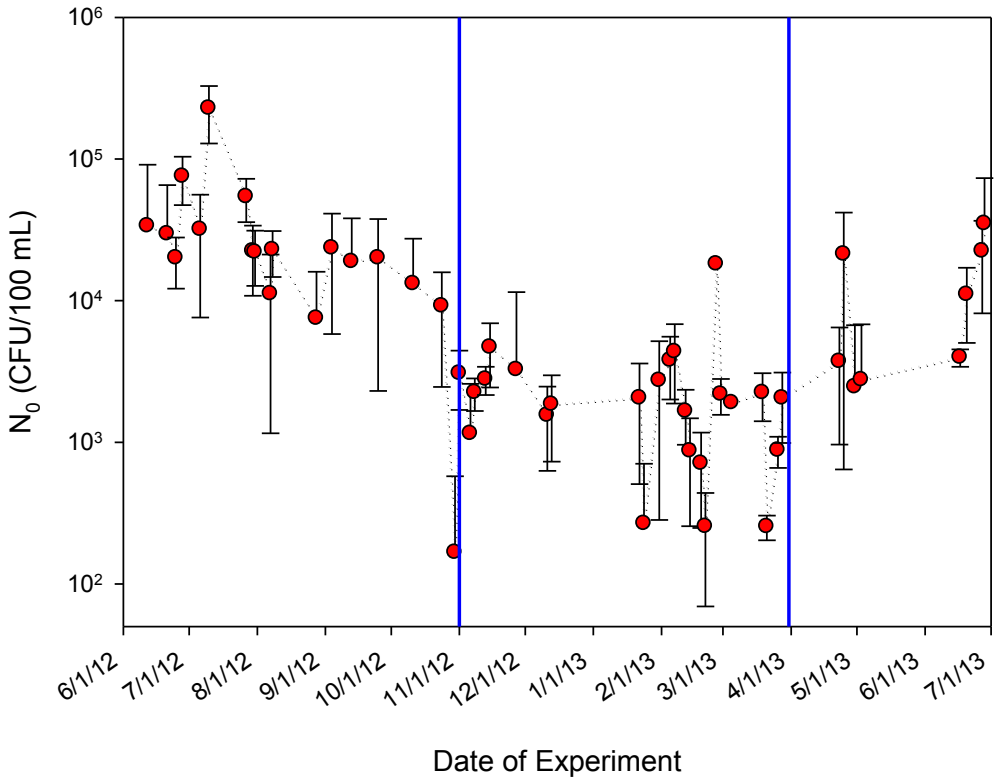

Figure 12. Viable *E. coli* concentrations in the undisinfected water (*e.g.*, before being subjected to UV radiation). The two blue lines indicate the beginning and the end of the non-disinfection season.

The data illustrated in Figure 12 were based on counts from three to nine plates per sample; the error bars represent the standard deviation that was measured among the plates counted for each experiment. Viable *E. coli* concentrations tended to be higher during the warmer months than the colder months. The seasonal trend of bacterial populations is wastewater effluent has been observed before. Figure 13 illustrate data collected from the West Lafayette, IN WWTP.

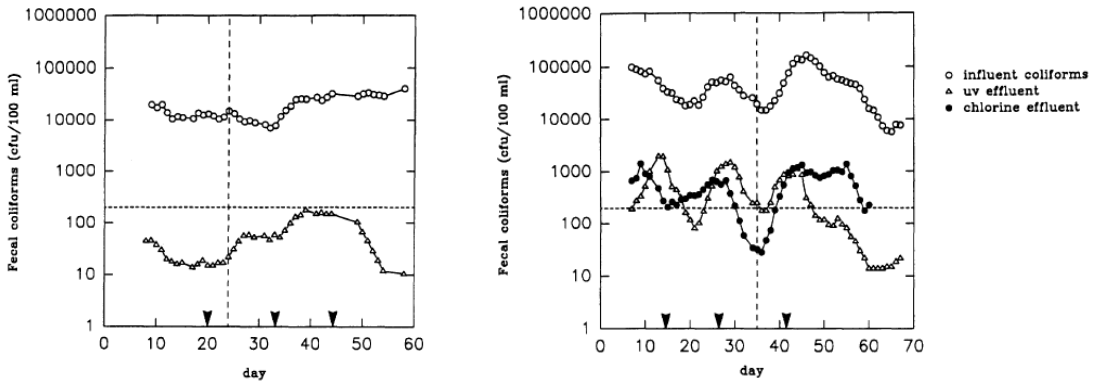

Figure 13. Fecal coliform concentrations collected in the winter of 1995(Left). Fecal coliform concentrations collected in the spring and summer of 1995 (Right). Source: Blatchley *et al*. (1996).

4.2 UV Dose-response Experiments

Figure 14 provides a graphical summary of bench scale collimated beam UV_{254} dose-response experiments results, which were conducted on undisinfected secondary effluent samples from the Belmont WWTP. The data displayed in Figure 14 are the results of UV dose-response experiments conducted on the dates included in Figure 12. The results show that the viable *E. coli* concentration was consistently reduced to below the NPDES permit limitations, based on maximum daily and the monthly geometric mean limits, with UV_{254} doses of 15 mJ/cm^2 or less. More specifically, doses of 15 mJ/cm^2 or more, provided by a collimated beam system, have yielded a concentration of 37 cfu/100 mL or less. Tailing was noted at doses at or above 20 mJ/cm^2; inactivation for doses of 20 mJ/cm^2 and greater was small compared with inactivation achieved at lower doses. Average viable *E. coli* concentrations were 5.0, 4.5, and 3.6 cfu/100 mL, for doses 20, 30, and 40 mJ/cm^2 respectively.

The data presented in Figure 14 provide strong evidence that a dose of 15 mJ/cm^2 will yield consistent compliance with the discharge permit limitations that are in place at the Belmont WWTP.

This dose is nominally 50% of the "dose" recommendation provided by *Ten States Standards*. This suggests that systems that are designed to conform to *Ten States Standards* (and other similar design guidelines) may be overdesigned.

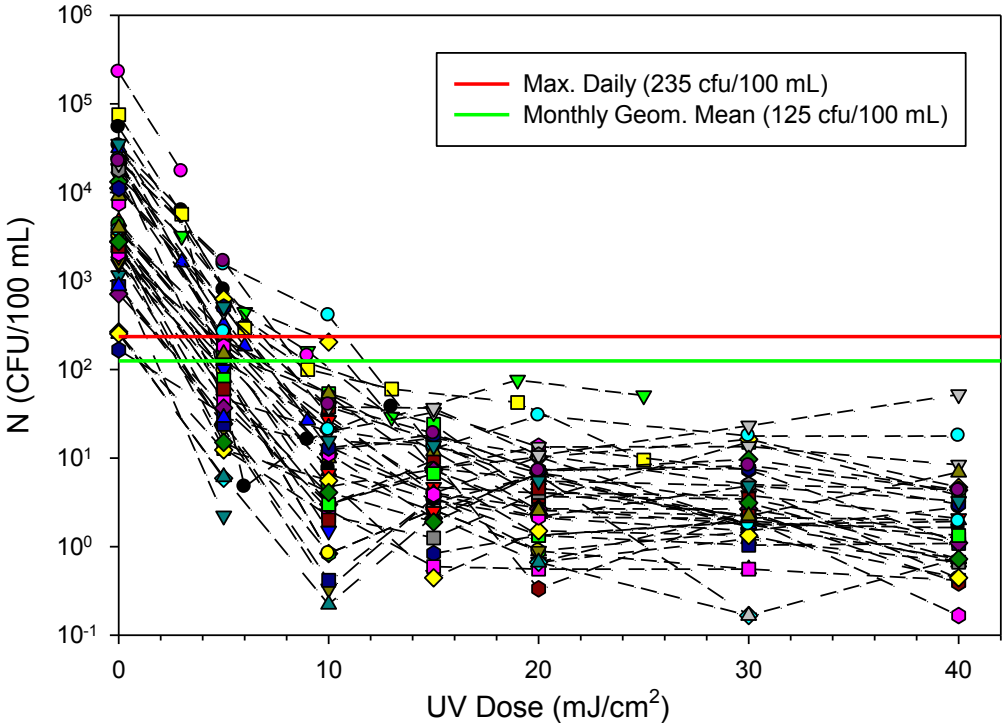

Figure 14. Viable *E. coli* concentration in secondary effluent samples from the Belmont WWTP, as a function of UV dose from collimated beam dose-response experiments. A total of 49 dose-response experiments are included in this graph. The horizontal red and green lines are included to illustrate the NPDES permit limitations for the Belmont facility, as defined by a daily maximum and monthly geometric mean of viable *E. coli* concentration, respectively.

The response behavior of ambient *E. coli* to UV exposure observed in this study is comparable to that reported in previous studies (Pennell *et al.*, 2007; Blatchley *et al.*, 2001).

To facilitate the comparison across sampling dates, the data presented in Figure 5 are also presented in normalized form (N/N_0). Figure 15 indicates that a UV dose of 15 mJ/cm^2 will achieve 2 – 4.5 $\log_{10}$ units of *E. coli* inactivation. This is a clear illustration of variability of a system attribute that is known to affect overall process performance in UV disinfection systems.

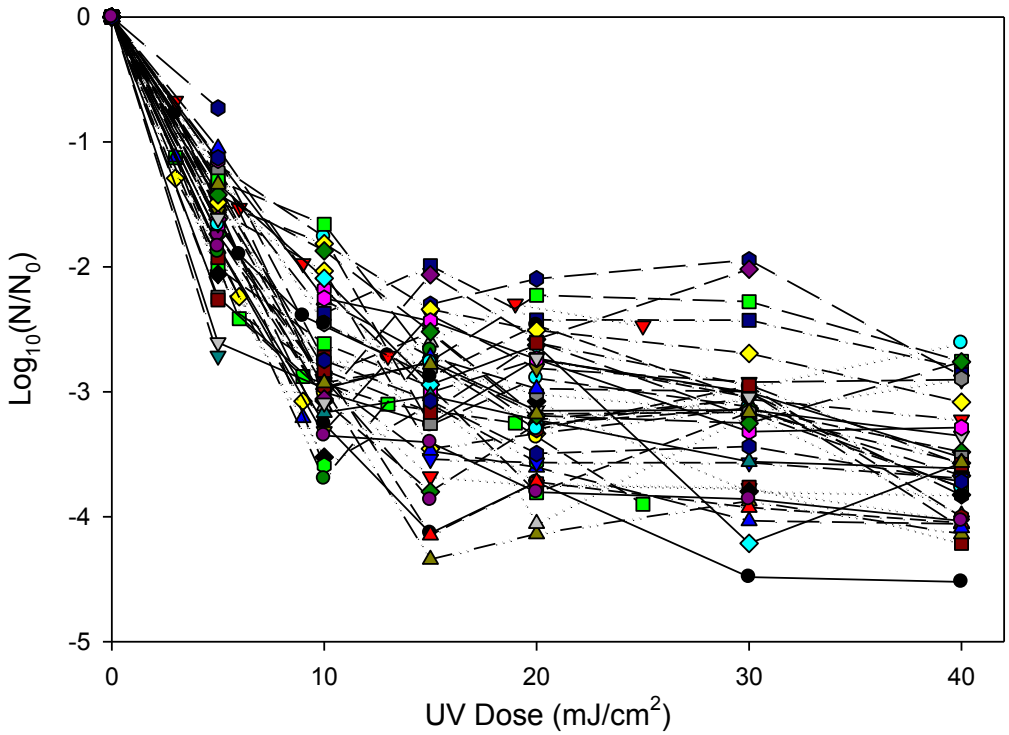

Figure 15. Fractional inactivation of *E. coli* (log_{10}-transformed) as a function of UV dose applied in collimated beam experiments.

Figure 16 illustrates variability that has been observed in UVT_{254} of undisinfected secondary effluent samples. For most samples UVT_{254} was observed to be between 60% to 80% (based on a 1.0 cm optical path). Clearly, variations in UVT_{254} will affect the disinfection performance of a UV disinfection system, as this will influence the irradiance field within the reactor. By extension, this variation in the irradiance field will affect the dose distribution and disinfection efficacy.

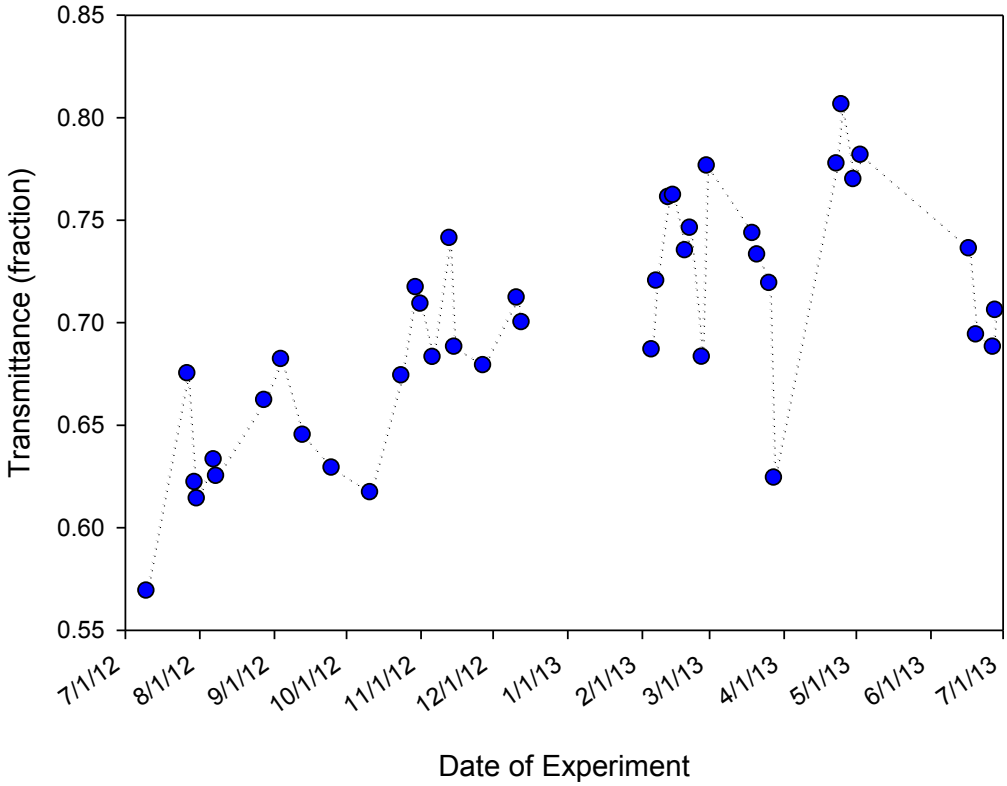

Figure 16. Measured UVT_{254} in undisinfected secondary effluent samples.

The gap in the middle of the data set (Figure 16) is attributed to measurements that were taken with a malfunctioning spectrophotometer and therefore were not included in the illustration.

4.3 PPES Model fitting

For each of the UV dose-response curves, the PPES model parameters (k_A, k_B, A_0, and B_0) were estimated by employing a piecewise regression tool. As explained in Methods and Materials section, the regression analysis also yielded an estimate of the inflection point c. Figure 17 illustrates the regression curve obtained for the one UV dose-response experiment. The plot demonstrates that the modified PPES model fits the data adequately with an R^2 value of 0.970. Regression fits for all UV dose-response experiments performed are included in Appendix A. Since the modified PPES is a 4-parameter model, high values for R^2 are expected.

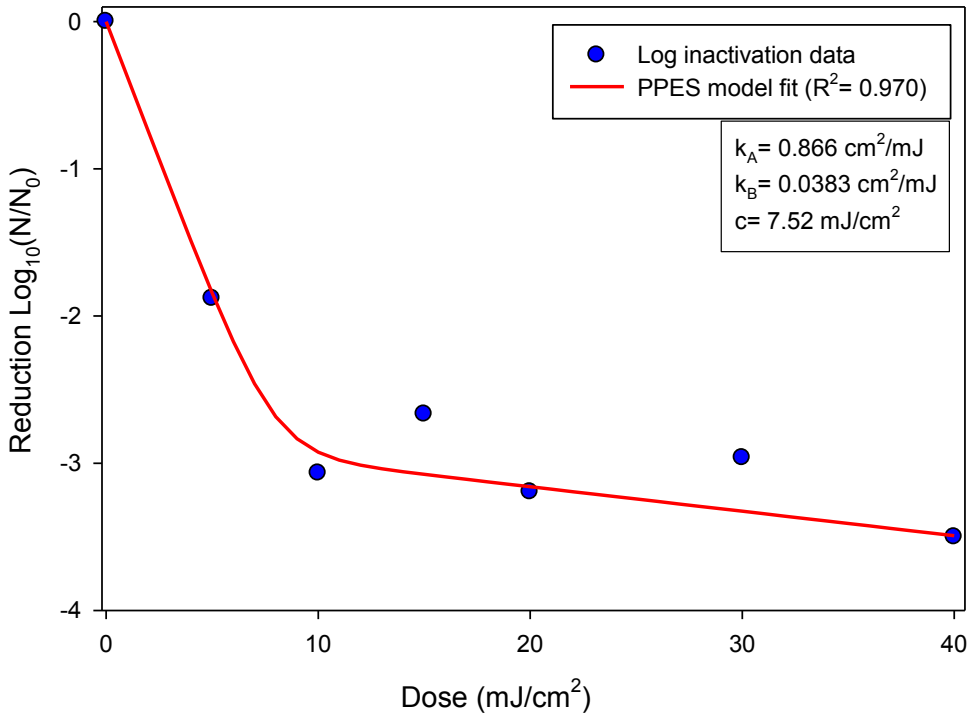

Figure 17. Fit of PPES model to UV dose-response data for experiment performed on 2/12/2013. The parameters k_A, k_B, and c values are shown.

Correlations between PPES parameters and measurements of daily average flow rate (Q), undisinfected effluent *E. coli* concentrations (N_0), UVT, TSS, and Precipitation (Prec) were calculated using the CORR procedure in SAS. Table 1 presents the correlation values and P-values for the aforementioned parameters.

Table 1. Pearson Correlation Coefficients and *p*-values for PPES model parameters (k_A, k_B, A_0, B_0, c) and measured parameters for UV dose-response experiment dates (Q, N_0, UVT, TSS, Prec). The number of observations was 49.

		N_0	UVT	TSS	k_A	k_B	c	A_0	B_0	Prec
Q	Corr	-0.212	**0.454**	**0.503**	0.015	-0.036	-0.133	-0.082	0.0823	**0.313**
	P-value	0.157	**0.0015**	**0.0004**	0.922	0.813	0.378	0.587	0.587	**0.0342**
	N_0	Corr	**-0.382**	0.0073	-0.099	0.225	**0.319**	**0.317**	**-0.317**	0.066
		P-value	**0.0088**	0.962	0.515	0.133	**0.0310**	**0.032**	**0.0319**	0.665
		UVT	Corr	0.0536	0.020	-0.119	-0.228	**-0.270**	**0.270**	-0.0379
			P-value	0.724	0.895	0.430	0.128	**0.070**	**0.0698**	0.803
			TSS	Corr	-0.045	0.001	0.0077	0.0251	-0.0251	**0.555**
				P-value	0.767	0.997	0.960	0.869	0.869	**<0.0001**
				k_A	Corr	0.144	**-0.773**	0.094	-0.0941	0.0015
					P-value	0.338	**<0.0001**	0.534	0.534	0.992
					k_B	Corr	-0.280	-0.128	0.128	0.167
						P-value	0.0597	0.398	0.398	0.268
						c	Corr	**0.471**	**-0.471**	-0.0451
							P-value	**0.001**	**0.001**	0.766
							A_0	Corr	-1.000	0.0240
								P-value	<0.0001	0.874
								B_0	Corr	-0.0240
									P-value	0.874

Parameters that are strongly correlated are highlighted in dark gray and parameters moderately correlated are highlighted in light gray. Correlations between two parameters were defined as "strong" when the corresponding p-value is less than 0.01, and a "moderate" correlation defined

when the corresponding p-value was between 0.05 and 0.1 (Fisher, 1938; Stigler, 2008). The analysis based on the 46 observations indicates that the parameters that are strongly correlated are **Q – UVT** (Corr = 0.454, *p*-value = 0.0015), **Q – TSS** (Corr = 0.503, *p*-value = 0.0004), **N_0 – UVT** (Corr = -0.382, *p*-value = 0.0088), **TSS – Prec** (Corr = 0.555, *p*-value < 0.0001), **k_A – c** (Corr = -0.773, *p*-value < 0.0001), **c – A_0** (Corr = 0.471, *p*-value = 0.001), and **c – B_0** (Corr = -0.471, *p*-value = 0.001).

Parameters that were moderately correlated included: **N_0 – c** (Corr = 0.319, *p*-value = 0.031), **N_0 – A_0 (**Corr = 0.317, *p*-value = 0.0319), **N_0 – B_0** (Corr = -0.317, *p*-value = 0.0319), **UVT – A_0** (Corr = -0.270, *p*-value = 0.0698), **UVT – B_0** (Corr = 0.270, *p*-value = 0.0698), **Q – Pec** (Corr = 0.313, *p*-value = 0.0342).

Because of the assumptions contained in the PPES model, the parameters that were expected to display correlation were $N_0 – A_0$, $N_0 – B_0$, $c – B_0$, and $k_A – c$, which was confirmed by the analysis. The reason to expect these correlations are:

1. As was mentioned in the Chapter 3 section 2, *c* is the UV dose for which the persistent *E. coli* population (B_0) remains. Therefore, in order to obtain B_0 we need to know *c*. *i.e.*, B_0 is dependent on *c*. (see equation 9).
2. $N_0 = A_0 + B_0$ Eq. 10

   Therefore these three parameters may be correlated.

To illustrate the correlations indicated in Table 1, scatter plots are presented in the figures that follow. The plots include the 95% prediction ellipse, which contains 95% of the observed data points, and it also indicates region in which a future observation can be expected. Also, the prediction ellipse gives an indication of the direction and strength of correlation between two parameters. A large ratio of the length of the major to minor axis is an indication of a large positive or negative correlation between two variables.

Discussions follow the figures for those parameters that were found to be strongly correlated and moderately correlated. Two parameters are examined in each discussion and possible explanations are provided for the correlation observed. Redundancy in these discussions is to be expected as many of these parameters are correlated with more than one parameter.

4.3.1 Correlations between Q – TSS, Q – Prec and TSS – Prec

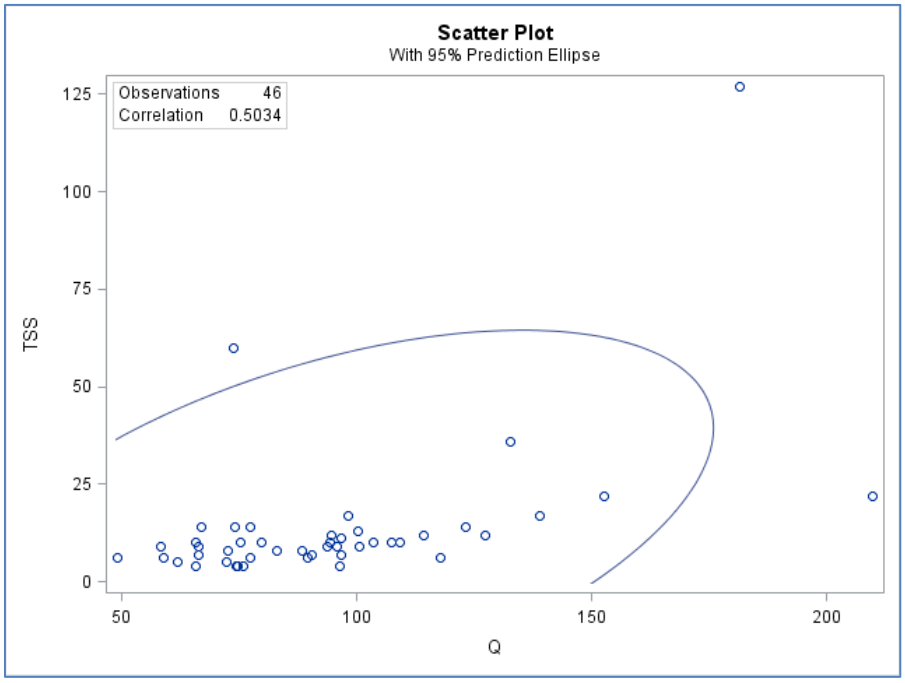

Figure 18. Scatter plot of TSS (mg/L) vs. Q (MGD), where Corr = 0.503, p-value = 0.0004.

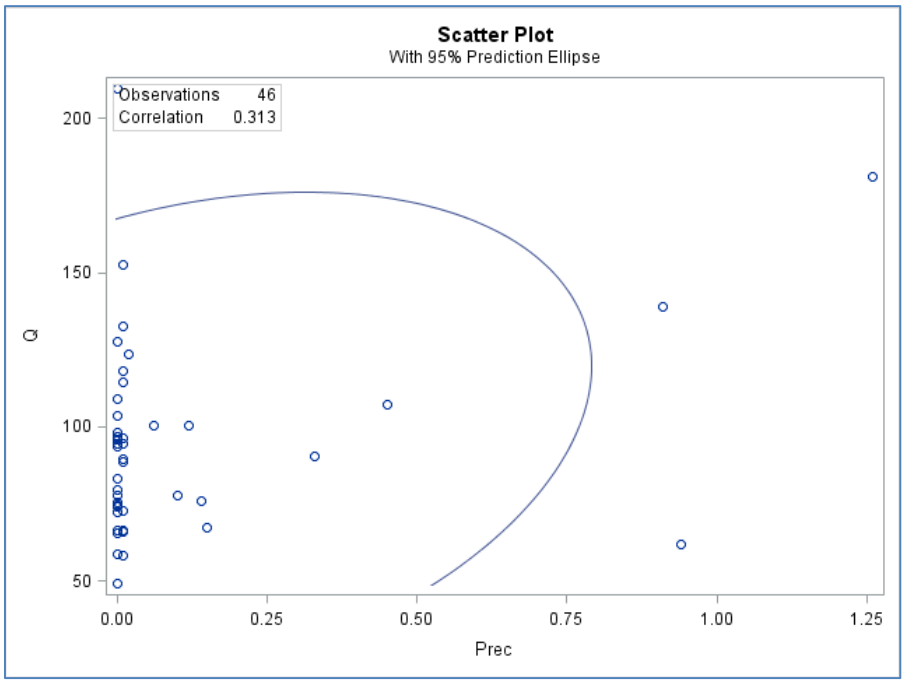

Figure 19. Scatter plot of Precipitation (in) vs. Q (MGD), where Corr = 0.313, p-value = 0.0342.

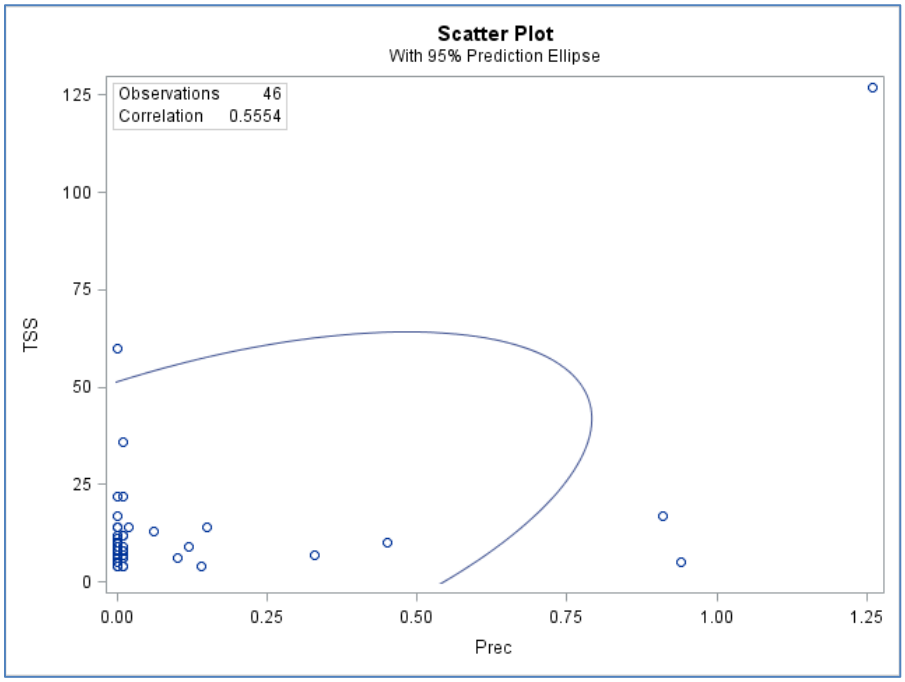

Figure 20. Scatter plot of Precipitation (in) vs. TSS (mg/L), where Corr = 0.555, p-value < 0.0001.

Figures 18, 19, and 20 display strong positive correlations between the parameters Q – TSS, Q – Prec, and TSS – Prec. This suggests that these parameters influence each other. From experience, this correlation is compatible with field observations, that is, when there is a rain event the flow rate at the WWTP increases, and in many cases the visual quality of the water tends to decrease.

The Belmont WWTP reported a TSS value of 127 mg/L on the date 2/26/13. This value is unusually high, and as such it lies far from the contour of the prediction ellipse. One explanation for the high value of TSS is that the precipitation reported for that same day was coincidentally the highest reported for the data set here analyzed, the corresponding precipitation was 1.26 in.

4.3.2 Correlations between UVT – Q

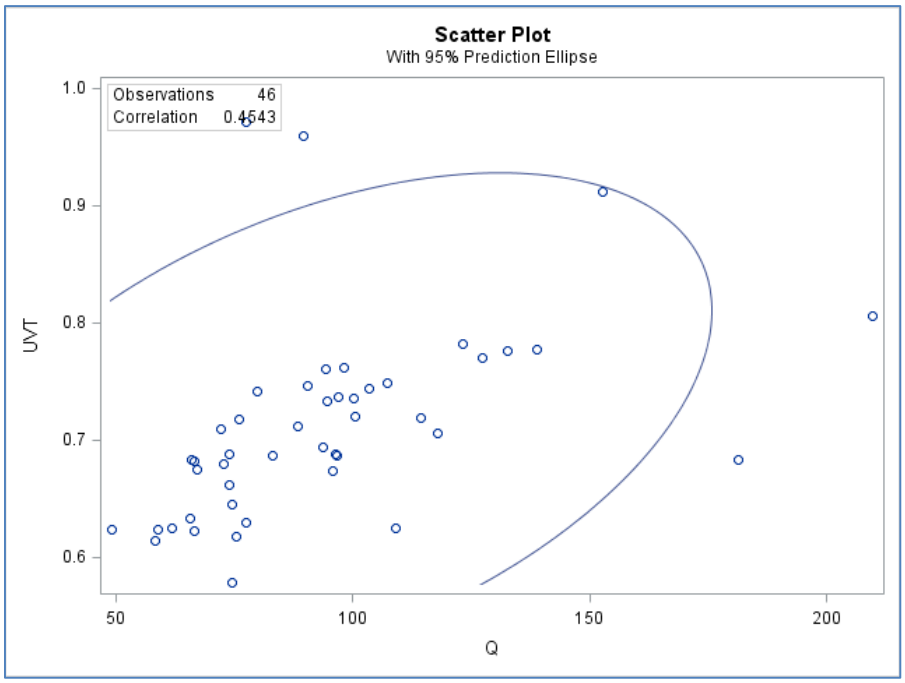

Figure 21. Scatter plot of UVT (%) vs. Q (MGD), where Corr = 0.454, p-value = 0.0015.

It appears that Q and UVT are positively correlated; as Q increases UVT increases as well. Although, the analysis did not yield a correlation between UVT and TSS, and UVT and precipitation, it is possible that UVT is indirectly influenced by TSS and precipitation because as it is illustrated in Figure 21, Q and UVT are strongly correlated, and it has been shown that Q is related to precipitation, and TSS, as discussed in section 4.3.1.

4.3.3 Correlation between N_0 – UVT, A_0 – UVT, B_0 – UVT

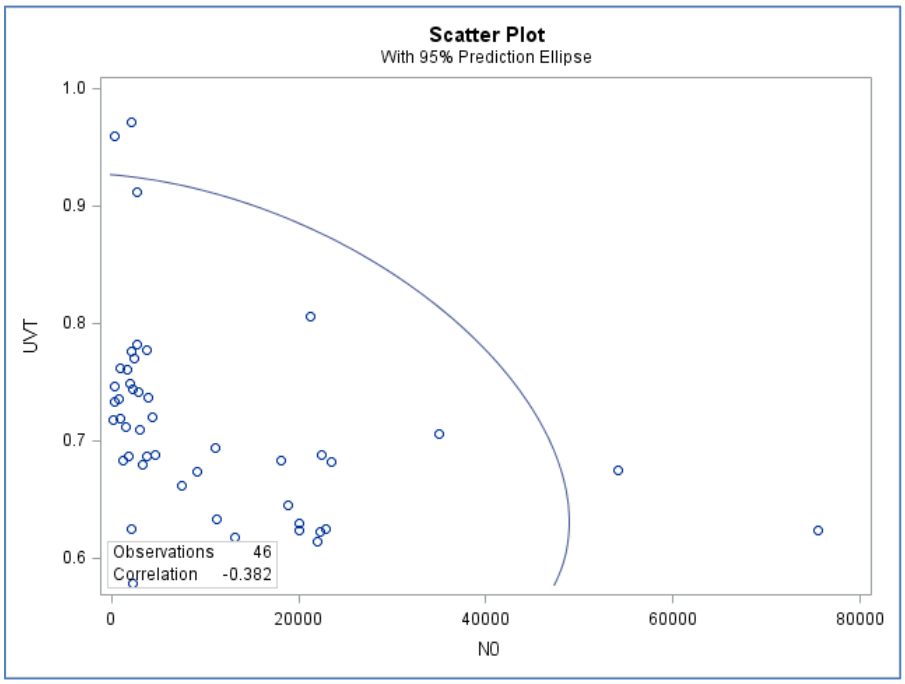

Figure 22. Scatter plot of UVT (%) vs. N_0 (CFU/100mL), where Corr = -0.382, p-value = 0.0088.

Figure 22 displays a strong negative correlation between UVT and N_0. Although it is not clear what could be the cause for this relationship, one hypothesis is that bacteria in the water could contribute to absorbance of light; therefore, water with a higher concentration of bacteria (N_0) would have a lower UVT.

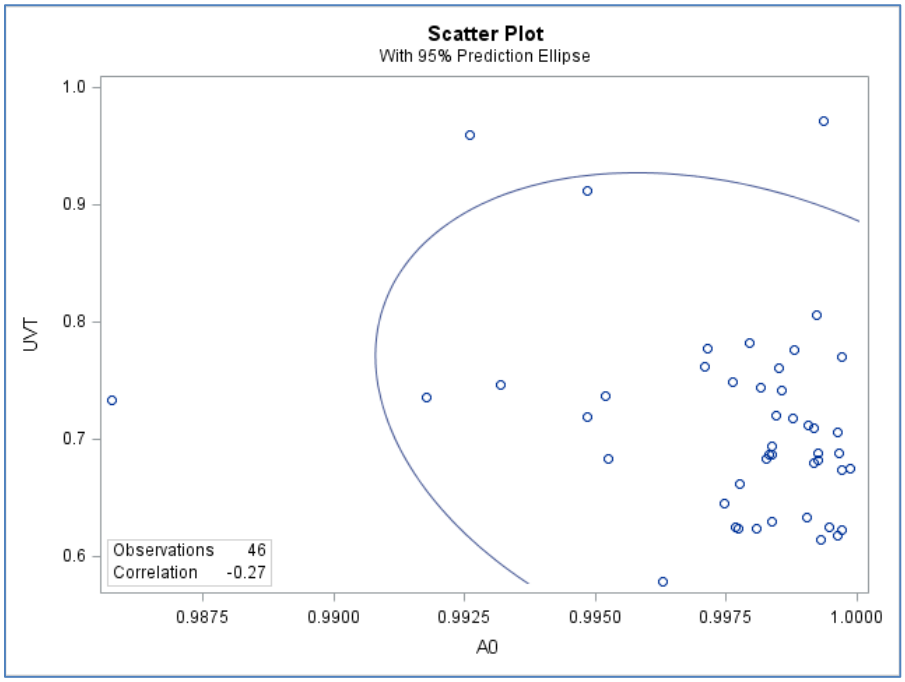

Figure 23. Scatter plot of A_0 (CFU/100mL) vs. UVT (%), where Corr = -0.270, p-value = 0.0698.

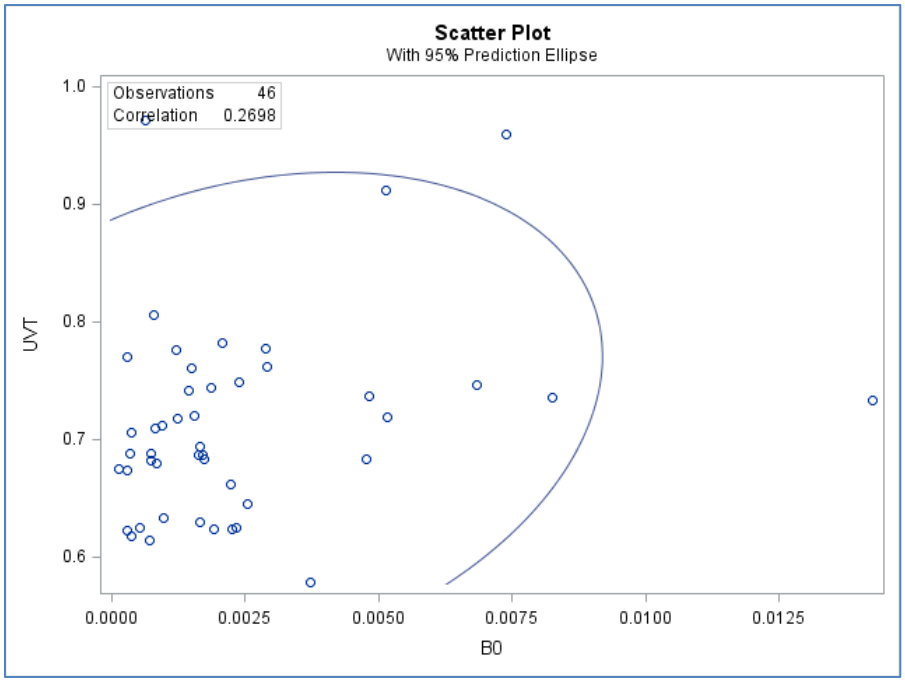

Figure 24. Scatter plot of B_0 (CFU/100mL) vs. UVT (%), where Corr = 0.270, p-value = 0.0698.

Figures 23 and 24 illustrate the correlations of A_0 and B_0 to UVT. The correlations indicate that, just like N_0, A_0 is negatively correlated to UVT. On the other hand, B_0 appears to be positively correlated to UVT. The latter correlation would contradict the hypothesis that higher bacterial concentrations in the water could contribute to lower UVT. If this hypothesis is true, it cannot be physically possible that only the susceptible sub-population (A_0) contributes to lower UVT in the water, while the persistent sub-population (B_0) contributes to higher UVT. However, because of the negative correlation between B_0 and A_0 in the modified PPES model (see Figure 25) this relationship would appear to happen.

To reiterate, it is not that A_0 contributes to lower UVT and conversely B_0 to higher UVT, but rather that this correlation is a consequence of the assumptions of the PPES model (see Equations 9 and10).

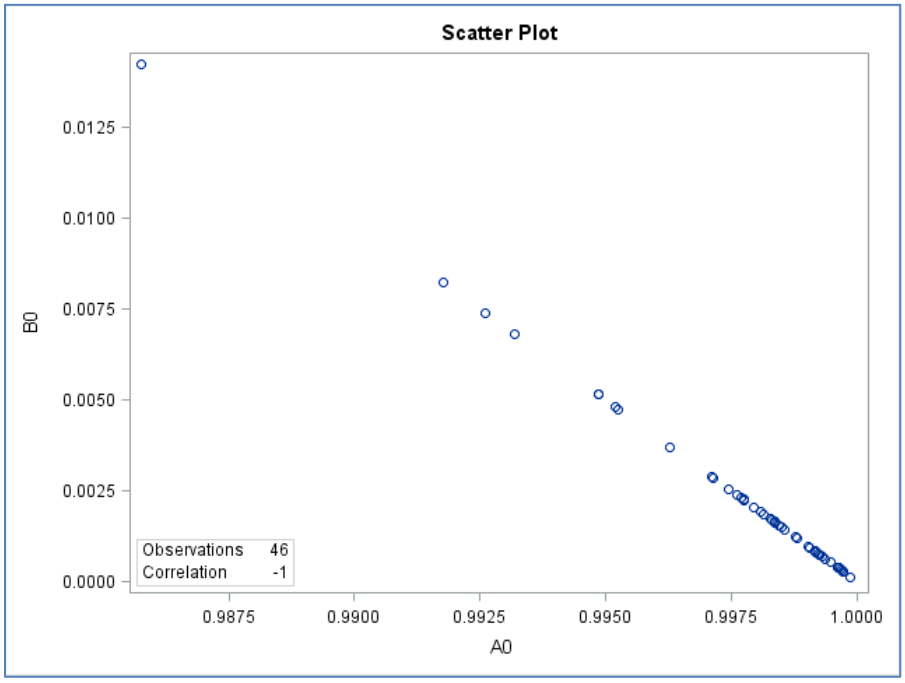

Figure 25. Scatter plot of A_0 (CFU/100 mL) vs. B_0 UVT (CFU/100 mL) where Corr = -1.00, p-value < 0.0001.

4.3.4 Correlation between $N_0 - A_0$ and $N_0 - B_0$

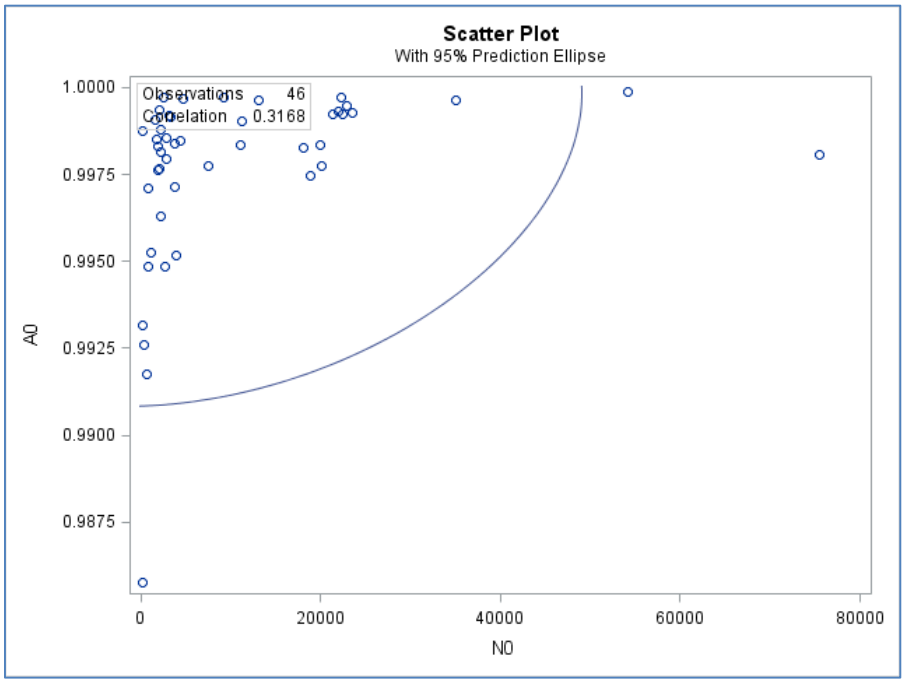

Figure 26. Scatter plot of N_0 (CFU/100mL) vs.A_0 (CFU/100mL), where Corr = 0.317, p-value = 0.0319.

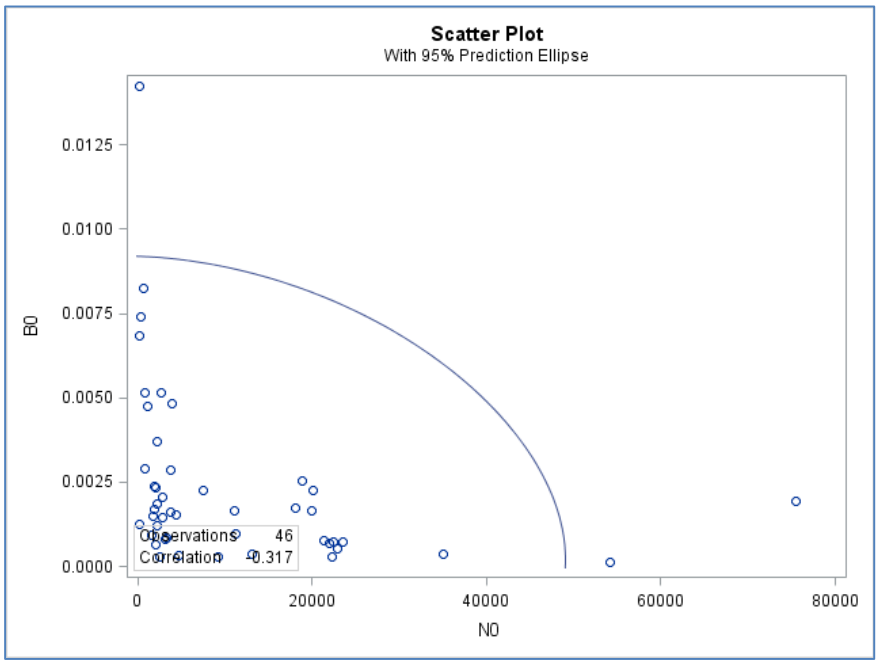

Figure 27. Scatter plot of N_0 (CFU/100mL) vs. B_0 (CFU/100mL), where Corr = -0.317, p-value = 0.0319.

Figures 26 and 27 display moderately strong positive and negative correlations between $A_0 - N_0$ and $B_0 - N_0$ respectively. The observed correlations are explained by the negative correlation between A_0 and B_0 (See Figure 25). Additionally, A_0 appears positively correlated to N_0 because all regressions of the modified PPES model yielded a higher values for sub-population A_0, and lower values for sub-population B_0. This is consistent with the observed UV dose-response of *E. coli*, where a bigger fraction of organisms is inactivated with lower doses (5 – 15 mJ/cm^2), and a smaller fraction is inactivated with high higher dose (> 15 mJ/cm^2).

4.3.5 Correlation between c - k_A

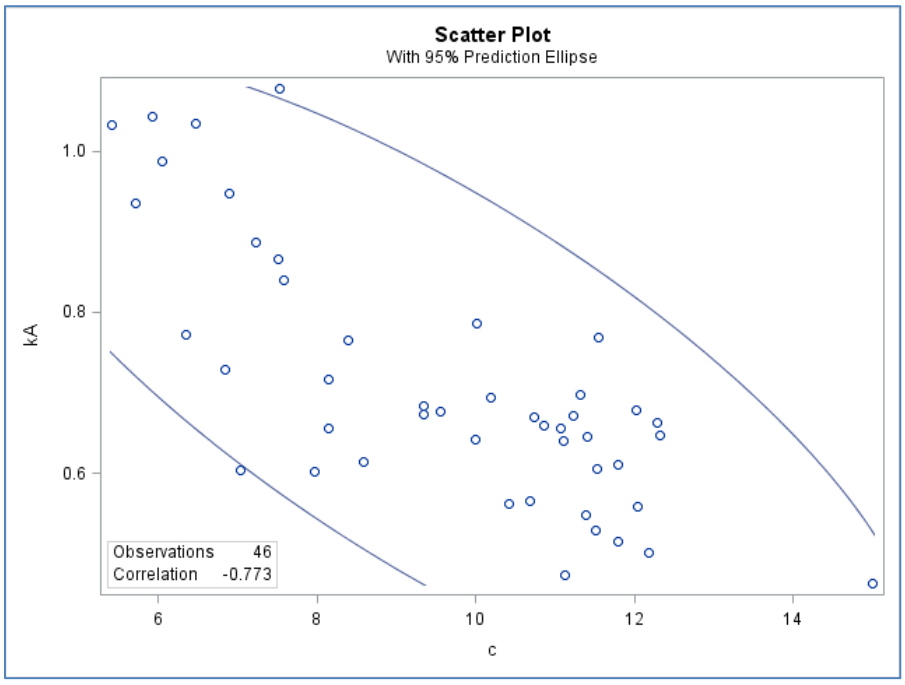

Figure 28. Scatter plot of k_A vs. c (mJ/cm^2), where Corr = -0.773, p-value < 0.0001.

Figure 28 show a strong negative correlation between the k_A and c. This correlation can be imagined as the higher the value of k_A, the longer the tail appears in the dose-response curve. The reason is that a higher value of k_A means that the susceptible sub-population (A_0) is inactivated with a lower dose(s), and as a consequence c is also lower, being that c is the dose at which the persistent sub-population (B_0) remains.

4.3.6 Correlation between N_0 – c, A_0 – c, and B_0 – c

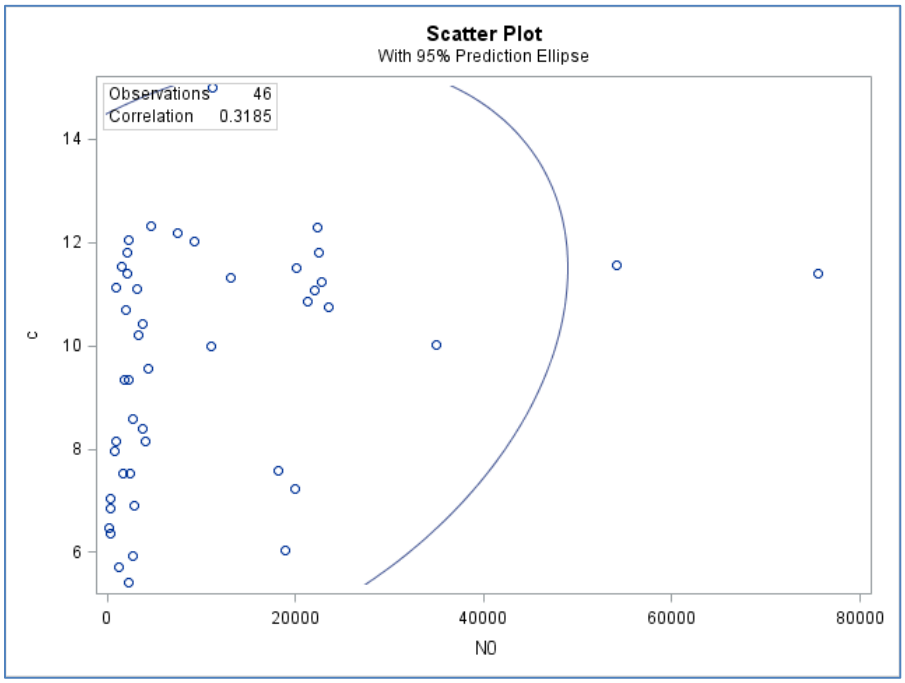

Figure 29. Scatter plot of c (mJ/cm^2) vs. N_0 (CFU/100mL), where Corr = 0.319, p-value = 0.031.

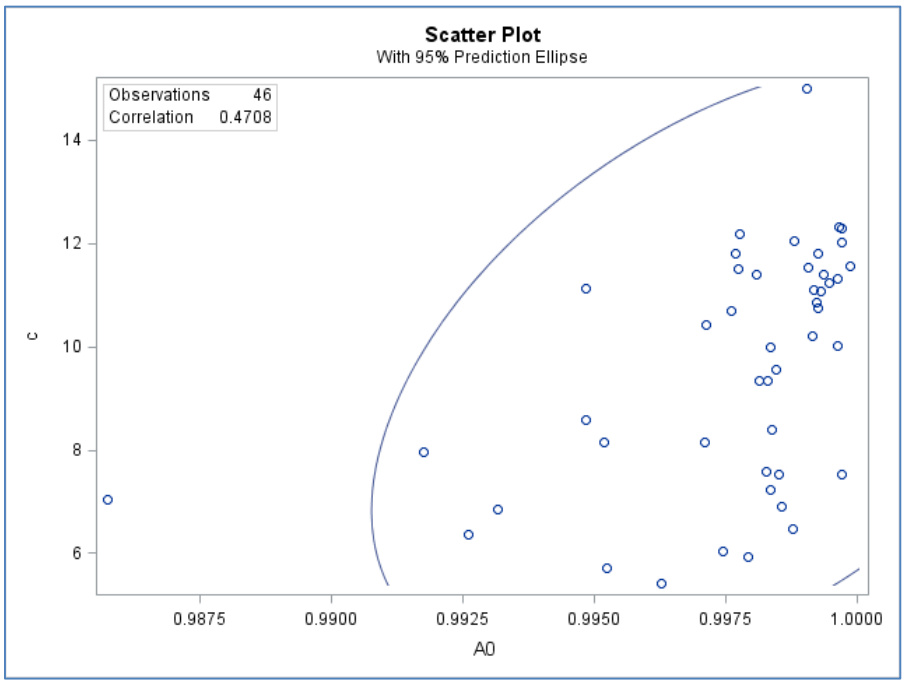

Figure 30. Scatter plot of c (mJ/cm^2) vs. A_0 (CFU/100mL), where Corr = 0.471, p-value = 0.001.

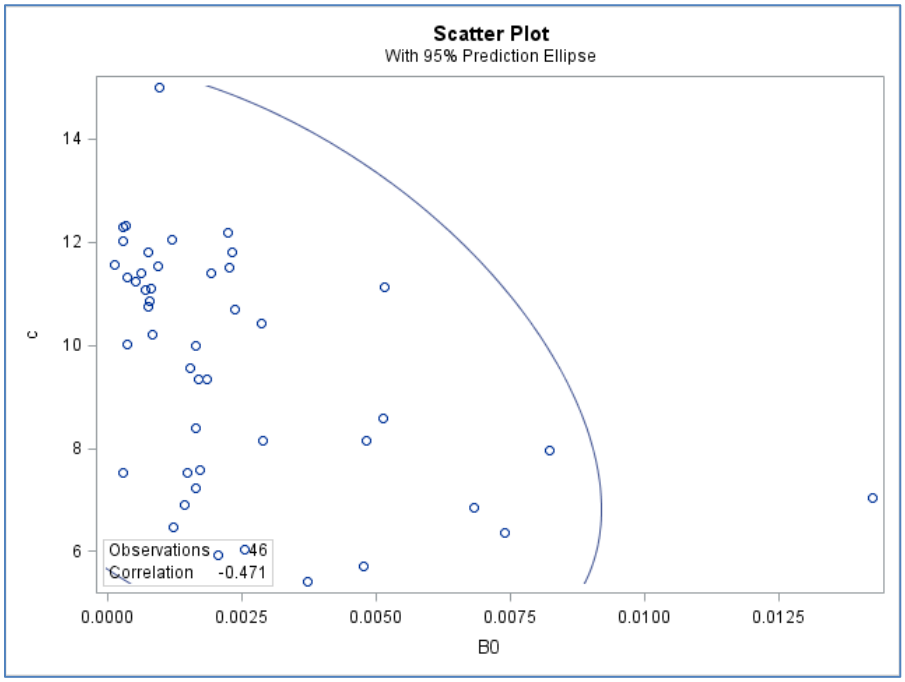

Figure 31. Scatter plot of c (mJ/cm^2) vs. B_0 (CFU/100mL), where Corr = -0.471, p-value = 0.001.

Figures 29, 30, and 31, illustrate moderately strong correlations of N_0, A_0, B_0, to c. Figures 30 and 31 show a positive correlation between A_0 – c, and a negative correlation between B_0 – c respectively. It has been stated that c is the dose at which the persistent sub-population (B_0) remains after inactivation of the susceptible sub-population (A_0) has taken place; so it follows that a lower value of A_0 yields lower values for c, and conversely lower values of B_0 yield higher values of c. In other words, when the tail appears longer, the sub-population A_0 was inactivated with a lower dose (c), leaving a higher concentration of susceptible sub-population (B_0).

The correlation between N_0 – c (Figure 29), is positive. It was mentioned in section 4.3.4 that from experiments, a bigger fraction of organisms are inactivated with lower doses, and a smaller fraction is inactivated with high higher dose. That is, A_0 is higher than B_0, therefore, if most of population N_0 is composed by A_0, and there is a positive correlation between A_0 and c, it follows that N_0 and c would also display a positive correlation.

All other correlation scatter plots indicating the non-significant correlations are presented in Appendix B.

4.4 Ambient Biodosimetry Results

4.4.1 Non-disinfection season

AB experiments were performed during the disinfection season and the non-disinfection season. The experiments performed during the non-disinfection season allowed for alteration of operating conditions. The following results were obtained from experiments performed during the non-disinfection season. For these experiments, a fixed flow rate was diverted to the UV system from the secondary clarifiers and sand filters. Samples were collected at several locations (I, II, III, as defined in Figure 11 for each flow condition.

Table 2. AB flow conditions for experiment executed on 3/1/2013

Flow Condition (Q)	Open Channels	Banks in operation per channel	Sample locations, per operating condition, per channel
1	1,2,3,4,5,6,7	A & B	I, II, III
2	1,2,3,4,5	A & B	I, II, III
3	1,2,3	A & B	I, II, III

The inactivation accomplished by the Belmont UV system on 3/1/2013 is illustrated on Figures 31, 32, and 33. Each graph corresponds to a flow condition. The arrows pointing down included in some of the plots indicate concentrations of *E. coli* obtained below the limit of detection. Similarly, the arrows pointing up indicate concentrations of *E. coli* too numerous to count (TNTC) per plate. Specifically, if the membrane developed more than 100 colonies per volume filtered, it was assigned 100 colonies, and then calculated the equivalent colonies per 100 mL. For example, if 100 colonies were obtained for a volume of 400 mL, the equivalent colonies per 100 mL is:

$$Colonies\ per\ 100\ mL = \frac{100\ col}{400\ mL} \times 100\ mL \qquad \text{Eq. 11}$$

This calculation was used across all resulting numbers of colonies, as it is the convention to express the colony forming unit per 100 mL of sample. The legend in parenthesis next to each arrow shows the volume filtered. The flow rate at the time of collection was Q = 106.7 MGD, UVT = 76.6%, and the dose by PLC was 32.62 mJ/cm^2.

Figures 32 through Figure 36 (and others included in Appendix C), indicate that the UV reactor at Belmont WWTP consistently complies with NPDES limits. As previously demonstrated in the results of UV dose-response experiments, the necessary dose to properly inactivate *E. coli* to

comply with the permit is about 15 mJ/cm^2. By inspecting the measured concentrations of the surviving *E. coli* per channel, per flow condition, the majority of the cases it was below 20 cfu/100 mL, except in a few cases were contamination and/or other sampling errors are suspected to have occurred. For instance, during the transportation of the coolers to the laboratory a few times leakage of one or more samples occurred inside the cooler. Another possible, but less likely occurrence could have been contact between the glove and the sample when it was poured from the bucket into the whirl pack.

As evidenced by Figures 32, 33, and 34 compliance with permit limits was accomplished in all samples tested. Moreover, it is noted that compliance was achieved in the samples collected at location II (after bank A). These and other results (shown in Appendix C) suggest that the Belmont UV system is overdesigned, as it is clearly capable of achieving compliance with just a portion of the existing hardware. This implies that the Belmont UV system can be safely and reliably operated with a portion of its hardware.

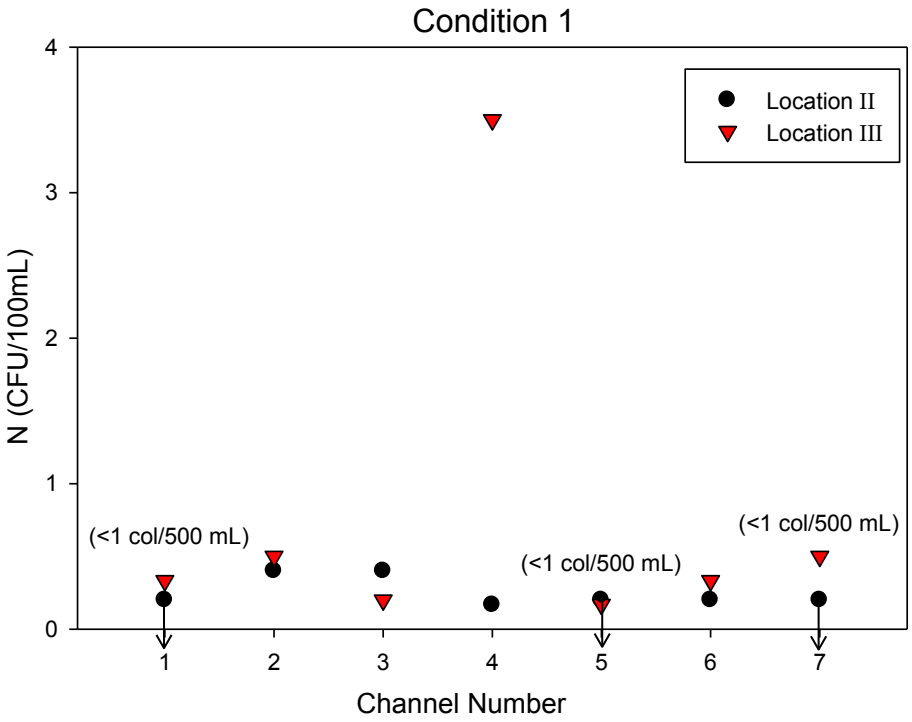

Figure 32. AB Experiment performed on 3/1/13. *E. coli* concentrations per channel for condition 1.

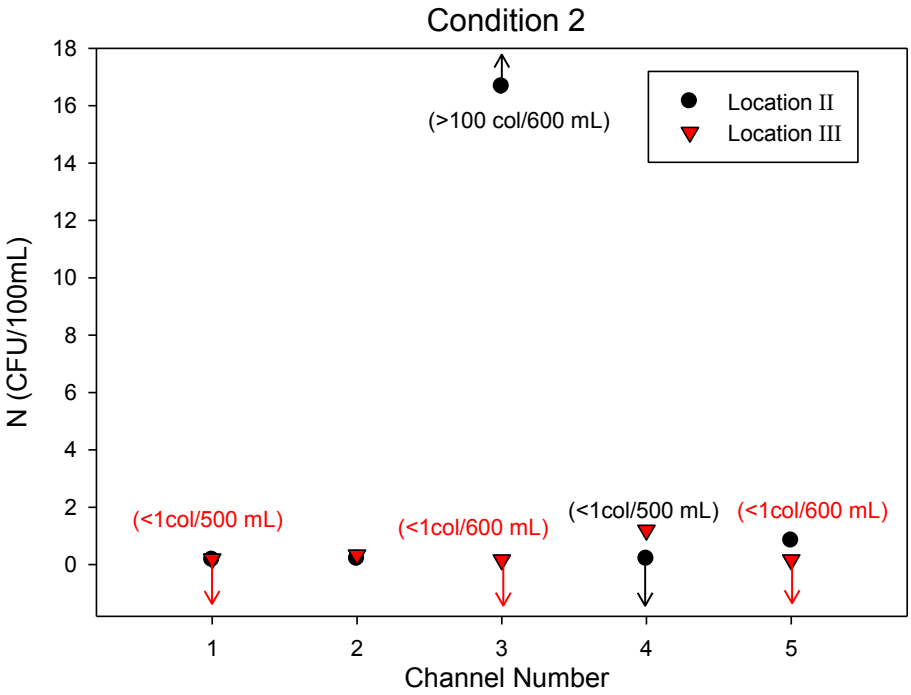

Figure 33. AB Experiment performed on 3/1/13. *E. coli* concentrations per channel for condition 2.

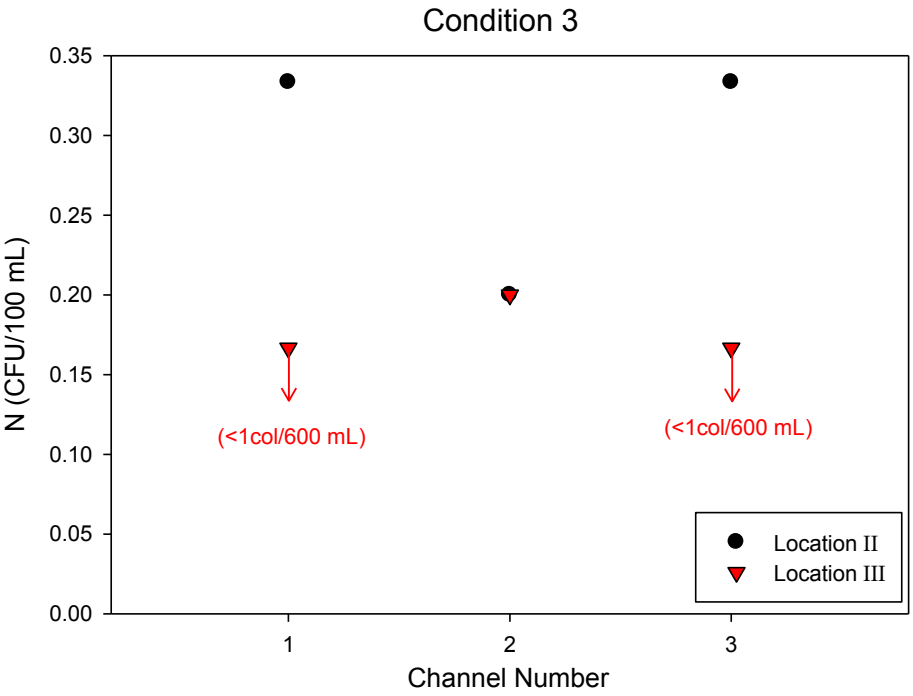

Figure 34. AB Experiment performed on 3/1/13. *E. coli* concentrations per channel for condition 3.

Figures 35 and 36 are the compilation of the inactivation achieved at each location. These figures show the performance of the reactor in relation to the discharge permit limitations of *E. coli* concentrations. The permit limits are illustrated by the red and green lines, which are maximum daily (235 CFU/100 mL) and monthly geometric mean (125 CFU/100 mL) respectively.

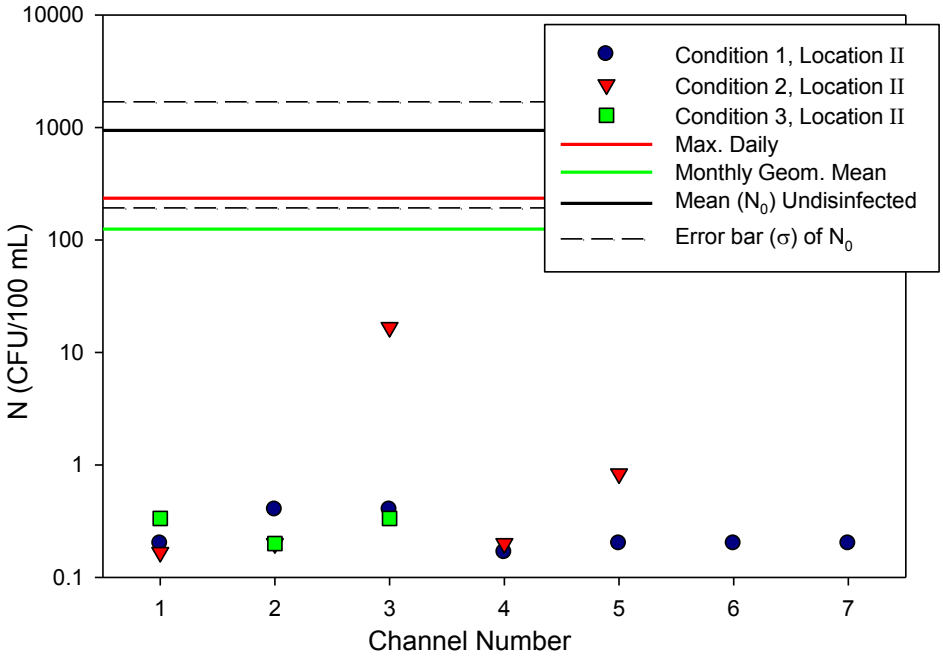

Figure 35. AB Experiment performed on 3/1/13. *E. coli* concentrations per channel, for location II for each of three flow conditions.

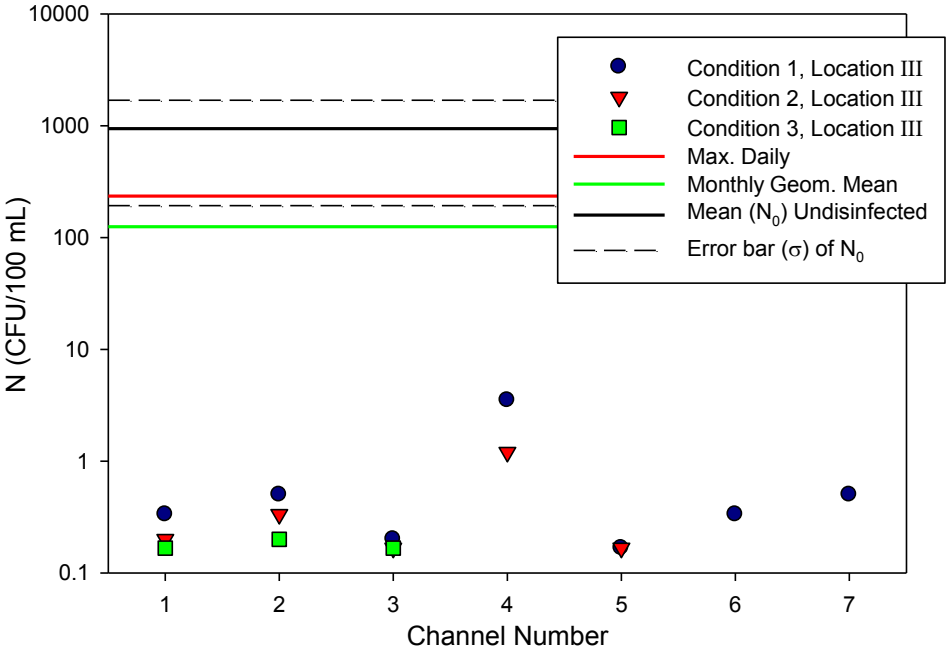

Figure 36. AB Experiment performed on 3/1/13. *E. coli* concentrations per channel, for location III for each of three flow conditions.

Figures 35 and 36 illustrate that the reactor reliably achieves inactivation of *E. coli* well below the permit limits shown. It is noted that channel number 4 appears to have a higher concentration of surviving *E. coli* at location III (downstream of bank B) than at location II (downstream of bank A). It is unlikely that the bacterial population grew from the moment it exited bank A and while being exposed to UV in bank B. There is no clear explanation for this behavior other than the possible contamination of the sample. This also appeared in the results for the experiment performed on 12/13/13.

Figures 37 through 41, present the results non-disinfection season experiment performed on 12/5/13. The flow conditions tested are indicated in Table 3.

Table 3. AB flow conditions for experiment executed on 12/5/2013

Flow Condition (Q)	Open Channels	Banks in operation per channel	Sample locations, per operating condition, per channel
1	2,3,4,5,6,7	A & B	I, II, III
2	5, 6, 7	A & B	I, II, III
3	6, 7	A & B	I, II, III

The flow rate at the time of collection was 50.80 MGD, UVT was recorded at 68.2%, and the dose by the PLC was recorded at the just before sample collection as 165.53 mJ/cm^2, and at the end of sample collection 91.33 mJ/cm^2.

Figures 37, 38, and 39 present the results for conditions 1, 2, and 3 respectively. Although these results are similar to the results of experiment 3/1/13, there is a notable difference in the overall performance of the UV reactor; on 3/1/13 the reactor achieved higher inactivation levels than on 12/5/13.

There is notable change in inactivation from condition 1 to condition 3. The concentrations of surviving *E. coli* in condition 1 were roughly within the range 0.2 – 24 cfu/100 mL, in condition 2 they were in the range of 0.3 – 3 cfu/100 mL, and in condition 3 they were within 0.3 – 100 cfu/100 mL. In other words, as a higher flow rate is imposed in the channels less inactivation is achieved. Yet, all inactivation observed complied with the NPDES effluent limits.

Conditions 1 and 3 (Figures 37 and 38), display higher concentrations of *E. coli* at location III, in channels 2, 3, 6, and 7 which could be attributed to errors in sampling.

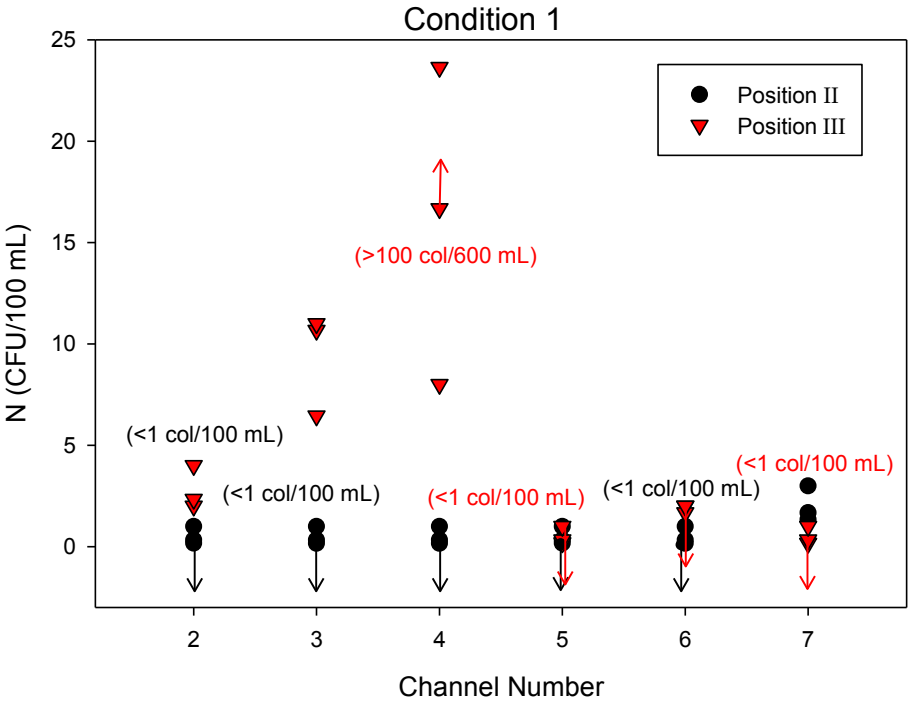

Figure 37. AB Experiment performed on 12/5/13. *E. coli* concentrations per channel for condition 1.

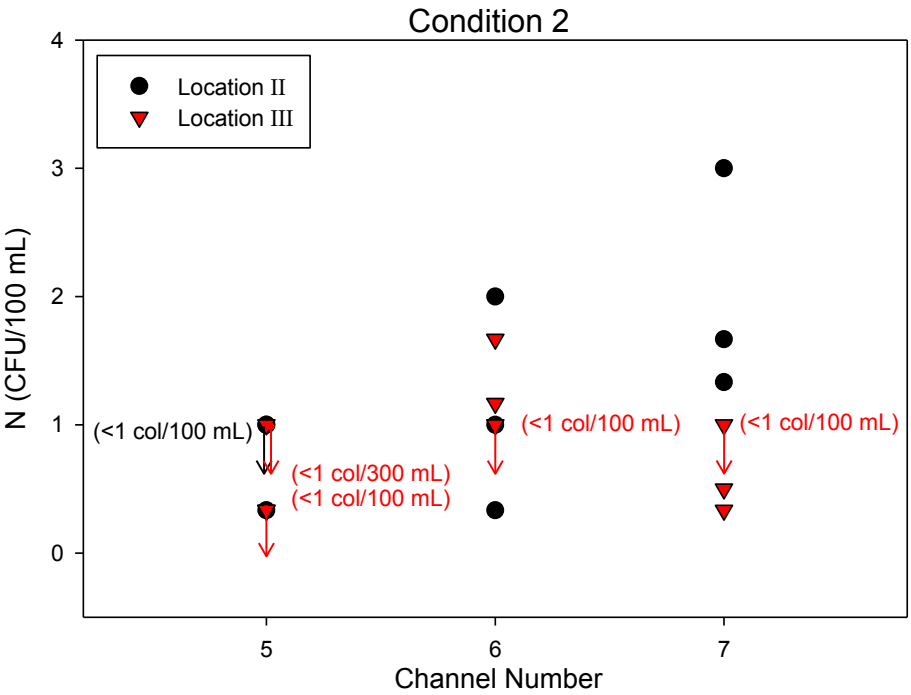

Figure 38. AB Experiment performed on 12/5/13. *E. coli* concentrations per channel for condition 2.

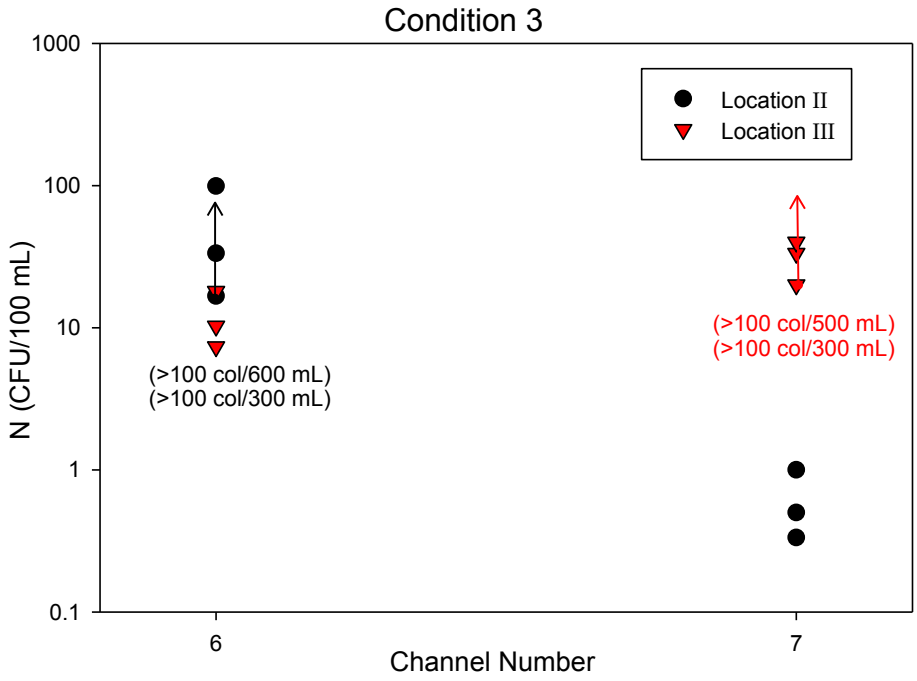

Figure 39. AB Experiment performed on 12/5/13. *E. coli* concentrations per channel for condition 3.

Just like it was presented for experiment 3/1/13, Figures 40 and 41 are the compilations of the achieved in each location. These figures illustrate that the reactor performed up to the standards, even in condition 3 where all the available flow was being diverted to only two channels.

Despite the sampling errors that potentially occurred during this experiment, there is evidence that the UV reactor at Belmont reliably performs to meet the disinfection criteria necessary for compliance.

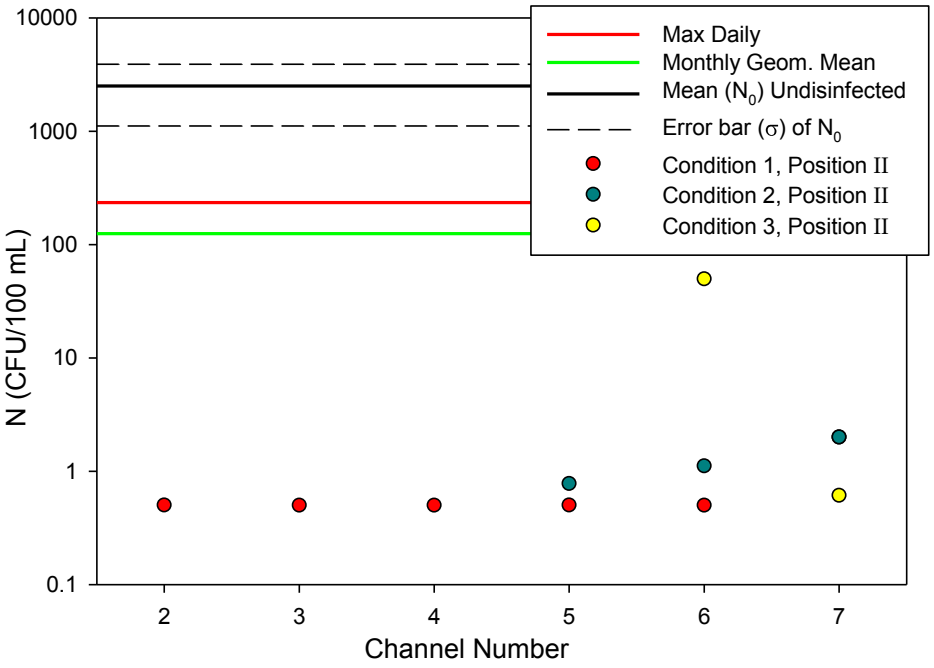

Figure 40. AB Experiment performed on 12/5/13. *E. coli* concentrations per channel, for location II for each of three flow conditions.

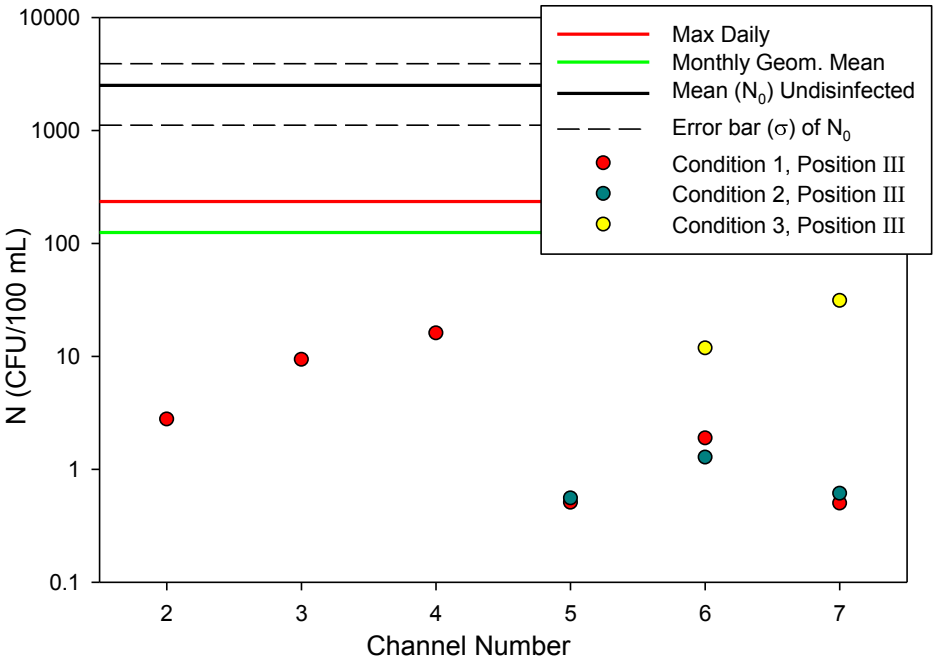

Figure 41. AB Experiment performed on 12/5/13. *E. coli* concentrations per channel, for location III for each of three flow conditions.

4.4.2 Disinfection season

The flow conditions for these experiments represented the condition of normal plant operations because during this time the Belmont WWTP was required to comply with its NPDES permit. No changes in flow condition were allowed. *E. coli* concentrations were measured by sampling at location I, and downstream of each bank in operation (locations II and/or III), for each channel in operation.

The results of five AB experiments performed during the disinfection season are presented. The first four experiments presented (Figures 43, 44, 45, and 46) were collected when the UV system was being operated with the following operation scheme: one bank of lamps was in operation in each channel. Bank A was being operated in channels 2, 3, 4, 5 and 7. Bank B was being operated in channels 1 and 6. This operational scheme is illustrated in Figure 42.

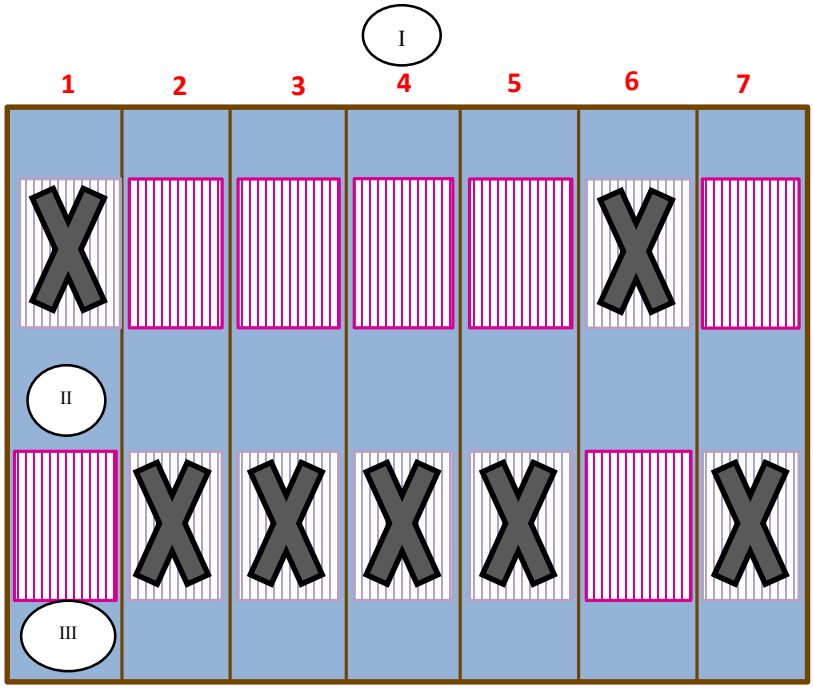

Figure 42. Schematic of the UV reactor at Belmont WWTP illustrating the operation scheme for AB experiment in Figures 43, 44, 45, and 46. The banks that are not crossed out represent the operating bank of lamps at the time of collection.

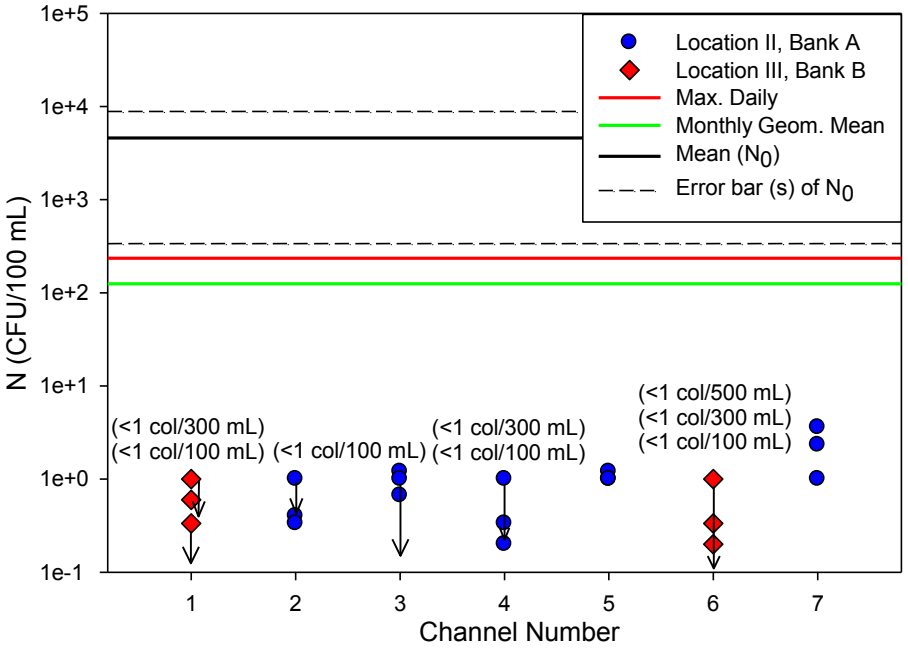

Figure 43. AB Experiment performed on 7/11/13.

Flow rate at the time of collection of experiments 7/11/13 was Q = 69.5 MGD, UVT = 71.4%, and PLC Dose = 36.4 mJ/cm^2.

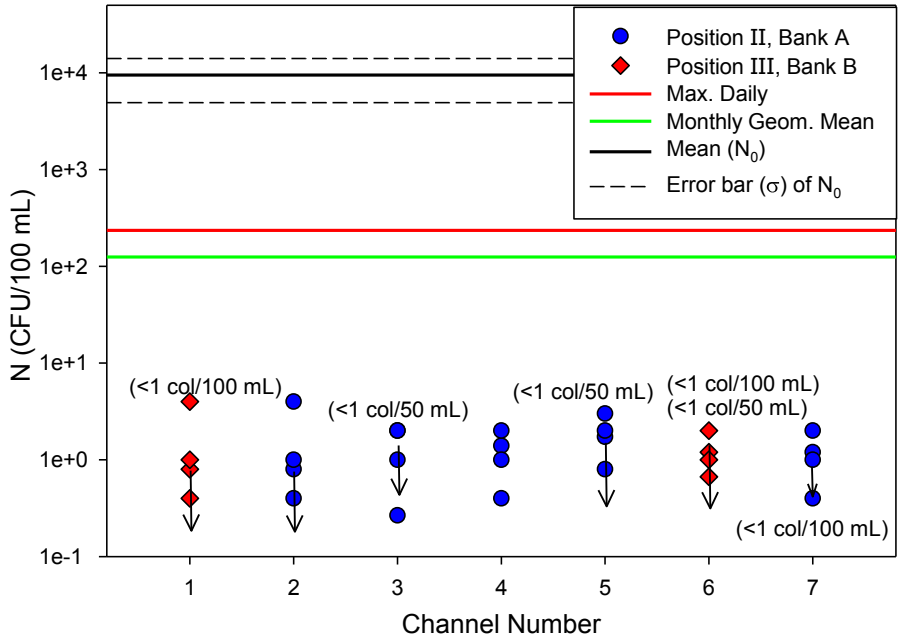

Figure 44. AB Experiment performed on 7/23/13.

Flow rate at the time of collection of experiments 7/23/13 was Q = 67.6 MGD, UVT = 70.3%, and PLC Dose = 35.62 mJ/cm^2.

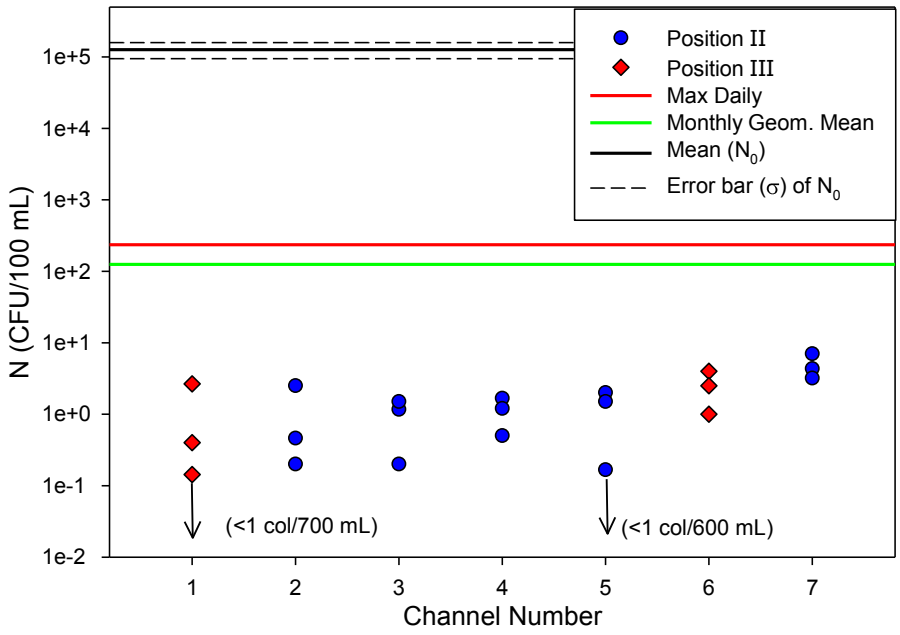

Figure 45. AB Experiment performed on 8/6/13.

Flow rate at the time of collection of experiments 8/6/13 was Q = 47.7 MGD, UVT = 68.9%, and PLC Dose = 49.38 mJ/cm^2.

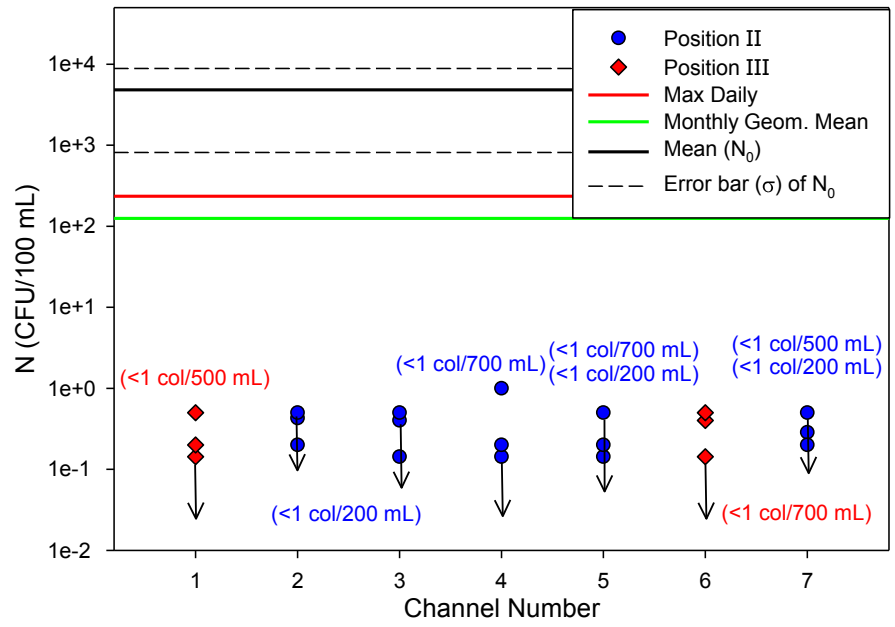

Figure 46. AB Experiment performed on 10/24/13.

Flow rate at the time of collection of experiments 10/24/13 was Q = 58 MGD, UVT = 72.4%, and PLC Dose = 48.16 mJ/cm^2.

Figure 50 illustrates AB experiment performed on 9/19/13. This day the UV reactor had both banks A and B in operation in all seven channels. Flow rate at the time of collection of experiments 9/19/13 was Q = 115 MGD, UVT = 63.2%, and PLC Dose = 41.29 mJ/cm^2.

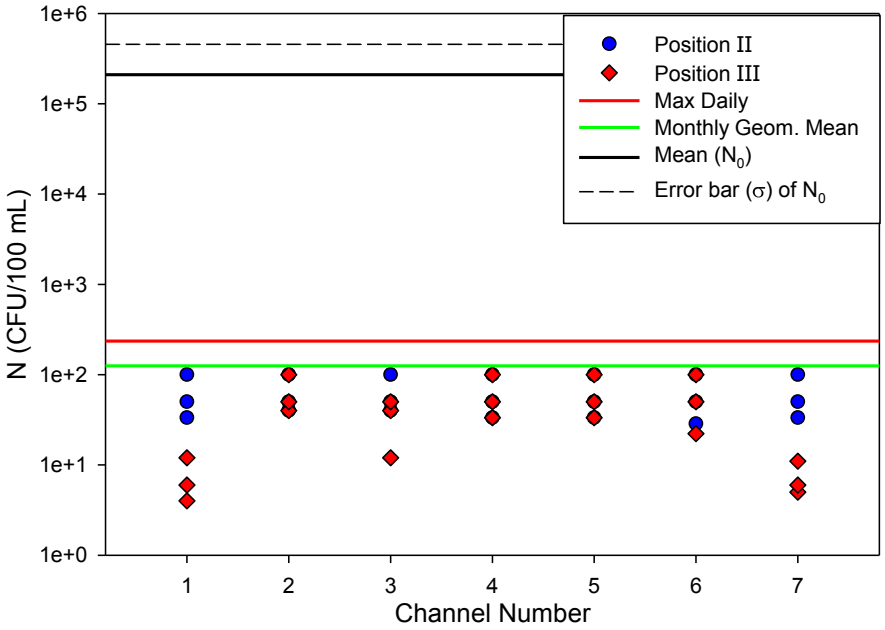

Figure 47. AB Experiment performed on 9/19/13

The experiment illustrated in Figure 47 was performed during a rain event when the precipitation was 1.53 in. This experiment yielded the highest surviving *E. coli* concentrations of all AB experiments performed. Because the y-axis in Figure 47 is in logarithmic scale, it appears as if the discharge permit limits were exceed, but this is in fact not the case with the highest concentrations being 100 cfu/100 mL. While this is close to the monthly geometric mean limit of 125 cfu/100 mL, it does not exceed the daily maximum limit of 235 cfu/100 mL.

All the AB experiments shown and others included in Appendix C performed during the disinfection season showed comparable results, with the highest concentration of surviving *E. coli* of 100 cfu/100 mL measured in experiment 9/19/13 (Figure 47).

The motivation for operating one bank during the AB experiments illustrated by Figures 43, 44, 45, and 46 is not clear; however, these results further demonstrate that the UV system at Belmont WWTP is capable to reliably comply with the NPDES permit with only a portion its hardware.

These findings also suggests that this UV system appears to be overdesigned because it has been designed to meet recommended standards that are not do not take into account contemporary knowledge of UV disinfection reactors. This means that the system can be operated using a portion of its hardware, whether that is operating one bank of lamps at full power, or both banks with only a portion of its power.

4.4.3 Correlation between $Log_{10}(N/N_0)$ and product UVT · θ (hydraulic detention time) of AB experiments

Figure 48 illustrates the relationship between the inactivation (presented in the form $log_{10}(N/N_0)$)measured in all AB experiments and the product of UVT and hydraulic detention time (θ) in seconds. The inactivation responses presented in Figure 48 correspond to those of the final effluent, per channel. For example, if in a given channel banks A and B were operating, the inactivation achieved downstream of bank B (location III) is presented.

The hydraulic detention time (θ) presented in Figure 48, corresponds to the time in seconds the water was exposed to UV radiation in each the channel. For example, if banks A and B were operating in a given channel, the detention time corresponds to the time of exposure to UV by both banks of lamps.

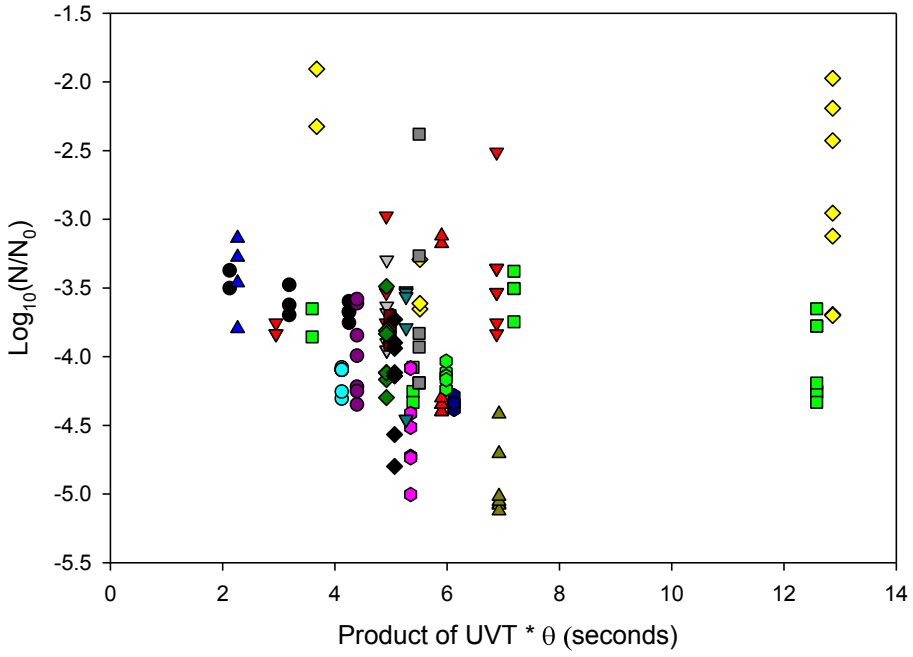

Figure 48. Log_{10} inactivation vs. product of UVT and θ corresponding for AB experiments.

In general terms, the inactivation response should increase as UVT increases, because of increased penetration of UV radiation through water, resulting in greater microbial exposure. Similarly, an increase in (mean) hydraulic detention time should imply greater exposure to UV radiation. Following this logic, it was expected that the inactivation response would tend to increase with the product of these two parameters.

The purpose of plotting the parameters shown in Figure 48 was to examine the influence the UVT and mean hydraulic detention time (θ) on the inactivation response achieved in each channel. The data presented in Figure 48 do not exhibit the expected trend, and furthermore it demonstrates that the inactivation response achieved by the reactor was highly variable. For example, for measurements corresponding to $UVT \cdot \theta \approx 7$ s, the inactivation response varied from roughly 2.5 – 5.1 $\log_{10}$ units. These results indicate that additional factors contribute to variability of the inactivation response, and that these factors need to be investigated.

CHAPTER 5. CONCLUSIONS

UV dose-response experiments indicate that reliable compliance with the NPDES limitations can be achieved with a substantially lower dose than the recommended dose(s) by guidelines, such as the *Ten State Standards*. According to the observed dose-response behavior from the collimated beam experiments, a UV_{254} dose of 15 mJ/cm^2 is sufficient to reach an inactivation that surpasses the required limits.

The piece-wise regression fit of the PPES model for UV dose-response curves obtained from collimated beam experiments, suggest that accurate predictions can be made of the inactivation of the ambient *E. coli*, if the a dose can be guaranteed to be properly delivered, and the values of undisinfected populations N_0 are known. The results of these regression analyses also illustrated variability that is inherent in the UV_{254} inactivation response of *E. coli*.

Additionally, correlation relationships for a total of 49 UV dose-response experiments yielded that there are statistically significant correlations between:

- **Q – UVT** (Corr = 0.454, *p*-value = 0.0015)
- **Q – TSS** (Corr = 0.503, *p*-value = 0.0004)
- **Q – Pec** (Corr = 0.313, *p*-value = 0.0342)
- **N_0 – UVT** (Corr = -0.382, *p*-value = 0.0088)
- **TSS – Prec** (Corr = 0.555, *p*-value < 0.0001)
- **k_A – c** (Corr = -0.773, *p*-value < 0.0001)
- **c – A_0** (Corr = 0.471, *p*-value = 0.001)
- **c – B_0** (Corr = -0.471, *p*-value = 0.001)

The analysis also showed that there are moderately strong correlations between:

- **N_0 – A_0** (Corr = 0.317, *p*-value = 0.0319)
- **N_0 – B_0** (Corr = -0.317, *p*-value = 0.0319)
- **c – B_0** (Corr = -0.2681, *p*-value= 0.0626)

- **UVT – A_0** (Corr = -0.270, *p*-value = 0.0698)
- **UVT – B_0** (Corr = 0.270, *p*-value = 0.0698)

Ambient Biodosimetry results demonstrate that because the UV reactor system at the Belmont WWTP was designed to conform to the current guidelines, it satisfactorily and consistently performs to reach *E. coli* inactivation levels that are well below the NPDES limits using only a fraction of the available hardware. This implies that an improved understanding of variability in performance of this system (and other systems) may allow for easing of the design criteria, therefore improving and optimizing system performance. Such an optimization effort may allow for improvement in process reliability, and decreases in capital and operating costs of UV wastewater disinfection systems.

REFERENCES

REFERENCES

Blatchley, E. R. (1997). Numerical modelling of UV intensity: Application to collimated-beam reactors and continuous-flow systems. *Water Research*, 31(9), 2205-2218.

Blatchley, E. R., Bastian, K. C., Duggirala, R. K., Alleman, J. E., Moore, M., & Schuerch, P. (1996). Ultraviolet Irradiation and Chlorination/ Dechlorination for Municipal Wastewater Disinfection: Assessment of Performance Limitations. *Water Environment Research*, 68(2), 194-204.

Blatchley, E. R., Dumoutier, N., Halaby, T. N., Levi, Y., & Laine, J. M. (2001). Bacterial responses to ultraviolet irradiation. *Water Science and Technology*, 43(10), 179-186.

Blatchley, E. R., Shen, C. Y., Naunovic, Z., Lin, L. S., Lyn, D. A., Robinson, J. P., Ragheb, K., Gregori, G., Bergstrom, D. E., Fang, S. Y., Guan, Y. H., Jennings, K., & Gunaratna, N. (2006). Dyed microspheres for quantification of UV dose distributions: Photochemical reactor characterization by Lagrangian actinometry. *Journal of Environmental Engineering-Asce*, 132(11), 1390-1403.

Blatchley, E. R., Shen, C., Scheible, O. K., Robinson, J. P., Ragheb, K., Bergstrom, D. E., & Rokjer, D. (2008). Validation of large-scale, monochromatic UV disinfection systems for drinking water using dyed microspheres. *Water Research*, 42(3), 677-688.

Bolton, J. R., & Linden, K. G. (2003). Standardization of methods for fluence (UV dose) determination in bench-scale UV experiments. *Journal of Environmental Engineering-Asce*, 129(3), 209-215.

Cabaj, A., Sommer, R., & Schoenen, D. (1996). Biodosimetry: Model calculations for u.v. water disinfection devices with regard to dose distributions. *Water Research*, 30(4), 1003-1009.

California Code of Regulations. *Title 22. Div 4. Ch 3*. CA.

Das, T. K. (2002). Evaluating the life cycle environmental performance of chlorine disinfection and ultraviolet technologies. Olympia, WA: Clean Techn Environ Policy, pp. 32-43.

Emerick, R. W. a. T., G. (2012). Ultraviolet Disinfection Guidelines for Drinking Water and Water Reuse. In: Foundation, N. W. R. I. a. W. R., ed, p. 78.

Fisher, R. A. (1938). *Statistical methods for research workers*. Edinburgh: Edinburgh, Oliver and Boyd.

Florida Administrative Code. FL.

G.L.U.M.R.B. (2004). Great Lakes Upper Mississippi River Board of State and Provincial Public Health and Environmental Managers. Recommended Standards for Wastewater Facilities 2004 Edition: Policies for the Design, Review, and Approval of Plans and Specifications for Wastewater Collection and Treatment Facilities. Albany, NY.

Glaze, W. H., Kang, J.-w., & Chapin, D. H. (1987). The Chemistry of Water Treatment Processes Involving Ozone, Hydrogen Peroxide and Ultraviolet Radiation. *The Journal of the International Ozone Association*, 9(4), 335-352.

IDEM, I. D. o. E. M. (2013). State of Indiana Department of Environmental Management Authorization to Discharge Under the National Pollutant Discharge Elimination System. Belmont & Southpor Advanced WWTP. Indianapolis, IN.

IEPA, I. E. P. A. (2013). National Pollutant Discharge Elimination System. MWRDGC Stickney Water Reclamation Plant. Chicago, IL.

Jagger, J. (1967). *Introduction to research in ultra-violet photobiology*. Englewood Cliffs, N.J.: Englewood Cliffs, N.J., Prentice-Hall.

Kruithof, J. C., Kamp, P. C., & Belosevic, M. (2002). UV/H2O2-treatment: the ultimate solution for pesticide control and disinfection. *Innovations in Conventional and Advanced Water Treatment Processes*, 2(1), 113-122.

Lazarova, V., Savoye, P., Janex, M. L., Blatchley, E. R., & Pommepuy, M. (1999). Advanced wastewater disinfection technologies: State of the art and perspectives. *Water Science and Technology*, 40(4-5), 203-213.

Mbonimpa, E. G., Vadheim, B., & Blatchley, E. R. (2012). Continuous- flow solar UVB disinfection reactor for drinking water. *Water Research*, 46(7), 2344-2354.

McGuigan, K. G., Conroy, R. M., Mosler, H. J., du Preez, M., Ubomba-Jaswa, E., & Fernandez-Ibanez, P. (2012). Solar water disinfection (SODIS): A review from bench-top to roof-top. *Journal of Hazardous Materials*, 235, 29-46.

MWRDGC, M. W. R. D. o. G. C. (2013). NPDES Permits Responsiveness Summary Regarding March 9, 2010 Public Hearing. Illinois Environmental Protection Agency, Office of Community Relations.

Naunovic, Z., Lim, S., & Blatchley, E. R. (2008). Investigation of microbial inactivation efficiency of a UV disinfection system employing an excimer lamp. *Water Research*, 42(19), 4838-4846.

Pennell, K. G., Aronson, A. I., & Blatchley, E. R. (2007). Phenotypic persistence and external shielding ultraviolet radiation inactivation kinetic model. *Journal of Applied Microbiology*, 104(4), 1192-1202.

Qualls, R. G., & Johnson, J. D. (1983). Bioassay and dose measurement in UV disinfection. *Applied and Environmental Microbiology*, 45(3), 872.

Santoro, D., Bartrand, T. A., Greene, D. J., Farouk, B., Haas, C. N., Notarnicola, M., & Liberti, L. (2005). Use of CFD for Wastewater Disinfection Process Analysis: E.coli Inactivation with Peroxyacetic Acid (PAA). *ijcre*, 3(1)Schervish, M. (1996). P Values: What They are and What They are Not. *The American Statistician*, 50(3), 203-206.

Severin, B. F., Suidan, M. T., & Engelbrecht, R. S. (1983). Kinetic modeling of U.V. disinfection of water. *Water Research*, 17(11), 1669-1678.

Severin, B. F., Suidan, M. T., & Engelbrecht, R. S. (1984). SERIES-EVENT KINETIC-MODEL FOR CHEMICAL DISINFECTION. *Journal of Environmental Engineering-Asce*, 110(2), 430-439.

Sommer, R., Lhotsky, M., Haider, T., & Cabaj, A. (2000). UV Inactivation, Liquid- Holding Recovery, and Photoreactivation of Escherichia coli O157 and Other Pathogenic Escherichia coli Strains in Water. *Journal of Food Protection®*, 63(8), 1015-1020.

Stigler, S. (2008). Fisher and the 5% level. *CHANCE*, 21(4), 12-12.

USEPA (1976). Disinfection of Wastewater - Task Force Report. In: Agency, U. E. P., ed. Washington, DC.

USEPA (2006a). UV Disinfection Guidance Manual For the Final LT2ESWTR. In: EPA, U. S., ed. Washington, D.C., p. 436.

USEPA (2006b). Method 1103.1: Escherichia coli (E. coli) in Water by Membrane Filtration Using membrane-Thermotolerant Escherichia coli Agar (mTEC). Washington, DC.

UV, T. (2014). Case Studies: Municipal Drinking Water.

Watson, H. E. (1908). A note on the variation of the rate of disinfection with change in the concentration of the disinfectant. *Journal of Hygiene*, 8, 536-542.

Whitby, E. G., & Scheible, K. O. (2004). The History of UV and Wastewater. IUVA, pp. 15-26.

Wols, B. A., Hofman, J., Beerendonk, E. F., Uijttewaal, W. S. J., & van Dijk, J. C. (2011). A Systematic Approach for the Design of UV Reactors Using Computational Fluid Dynamics. *Aiche Journal*, 57(1), 193-207.

Wols, B. A., Hofman-Caris, C. H. M., Harmsen, D. J. H., Beerendonk, E. F., van Dijk, J. C., Chan, P. S., & Blatchley, E. R. (2012). Comparison of CFD, Biodosimetry and Lagrangian Actinometry to Assess UV Reactor Performance. *Ozone-Science & Engineering*, 34(2), 81-91.

Zwiener, C., Weil, L., & Niessner, R. (1995). ATRAZINE AND PARATHION-METHYL REMOVAL BY UV AND UV/O-3 IN DRINKING-WATER TREATMENT. *International Journal of Environmental Analytical Chemistry*, 58(1-4), 247-264.

APPENDCES

Appendix A. UV dose-response and PPES regression

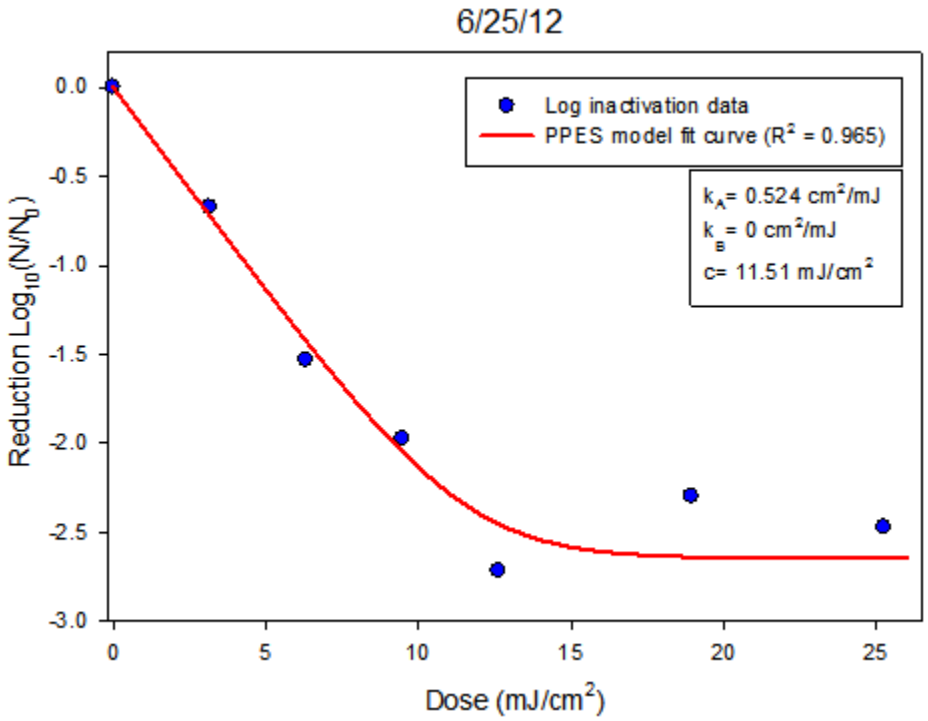

Figure A1. Unfiltered sample

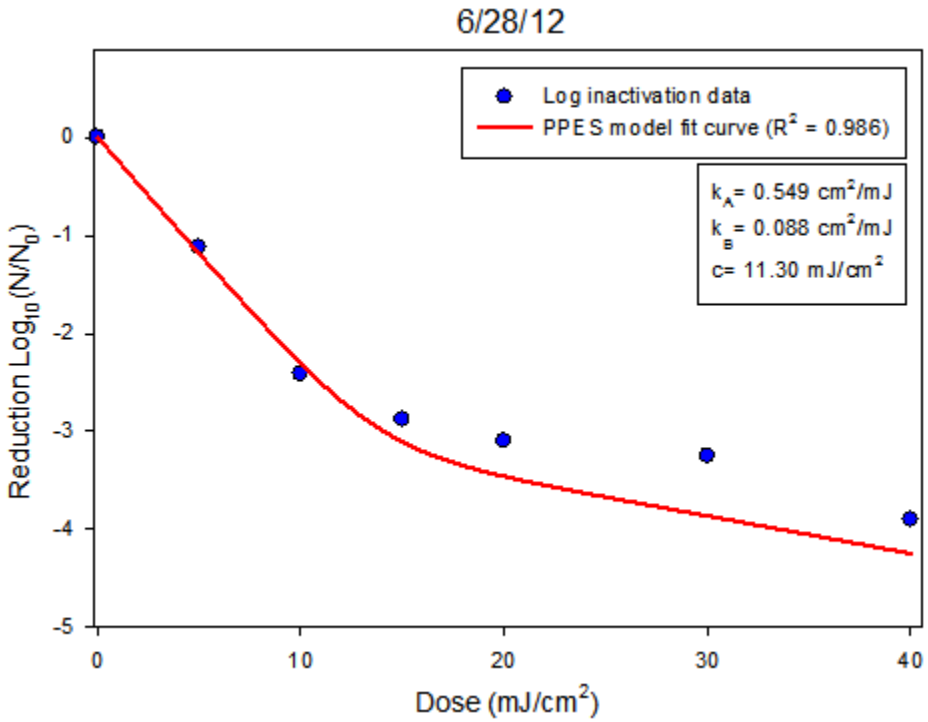

Figure A2. Unfiltered sample

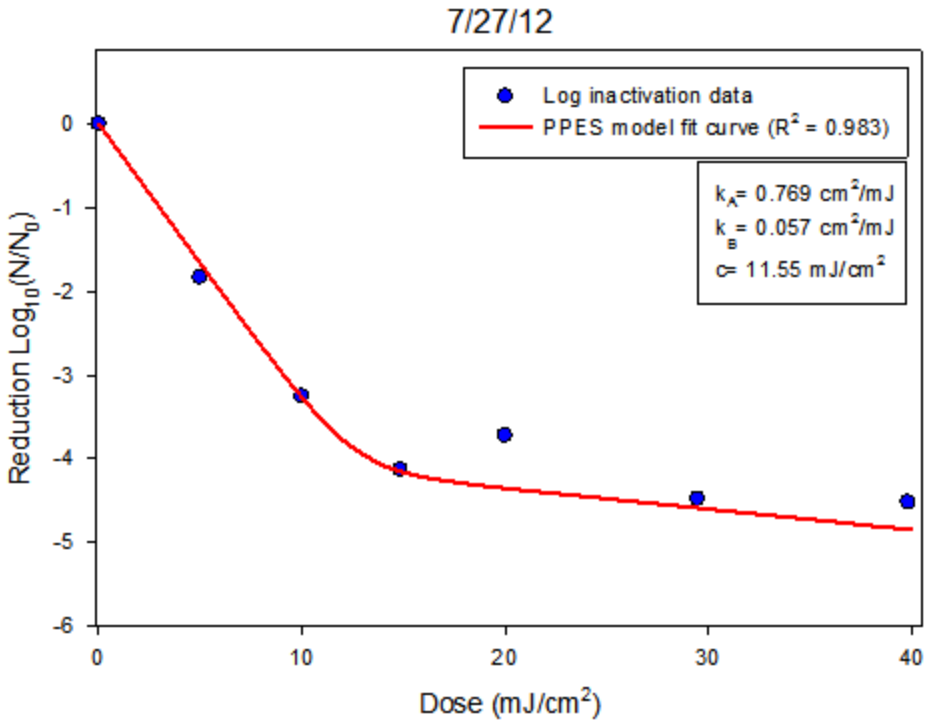

Figure A3. Unfiltered sample

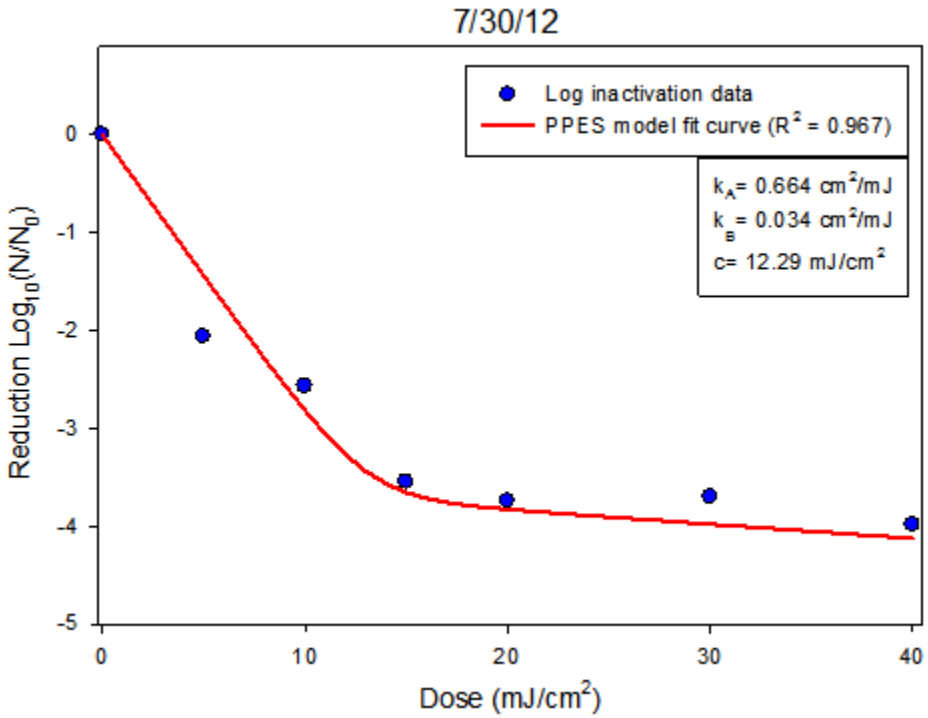

Figure A4. Unfiltered sample

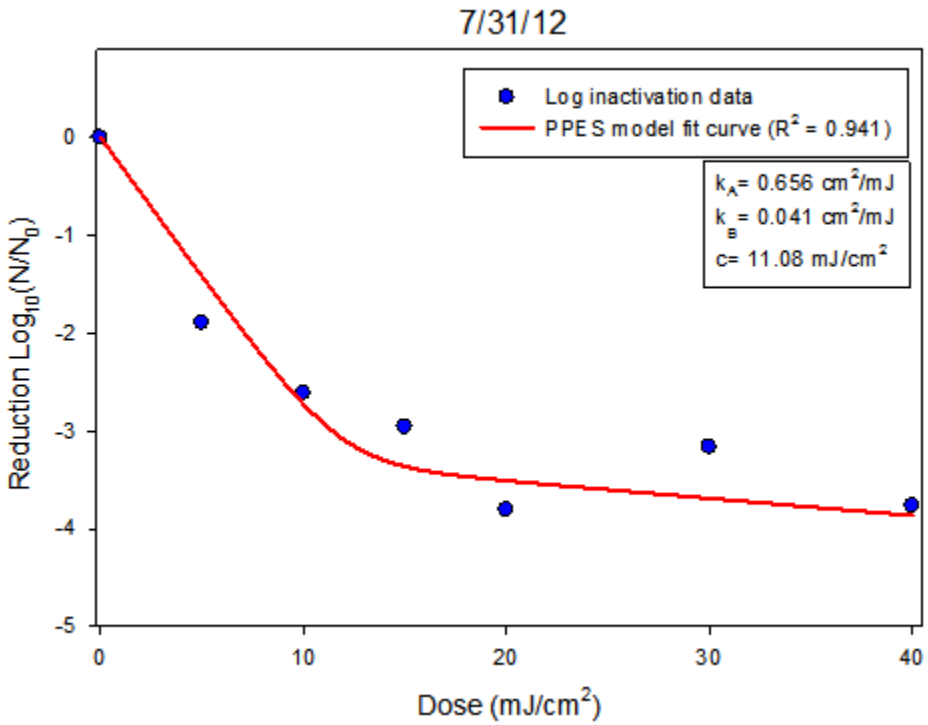

Figure A5. Unfiltered sample

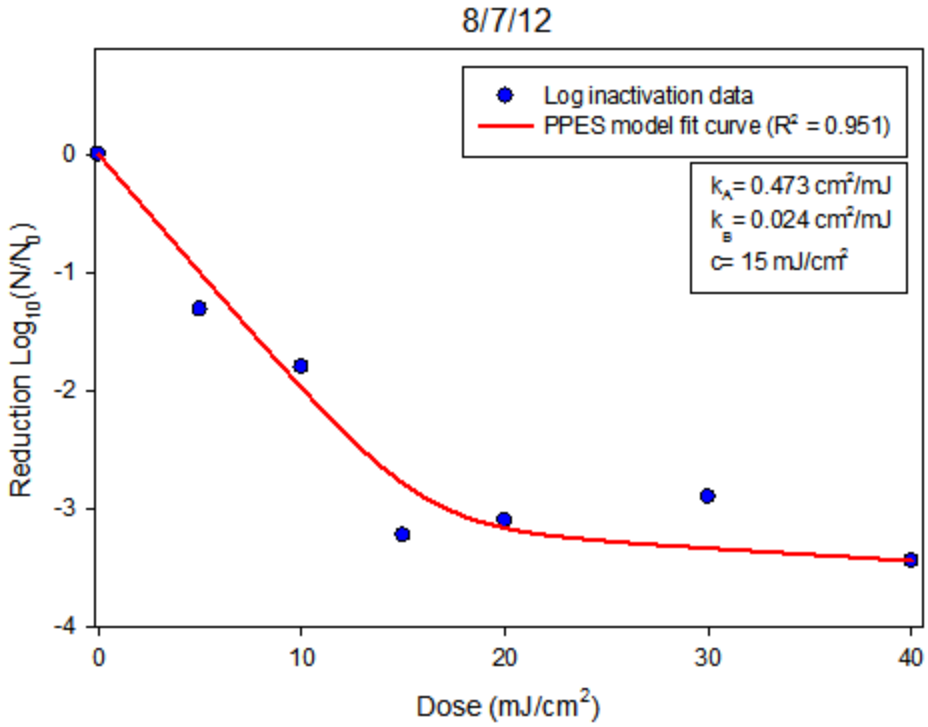

Figure A6. Unfiltered sample

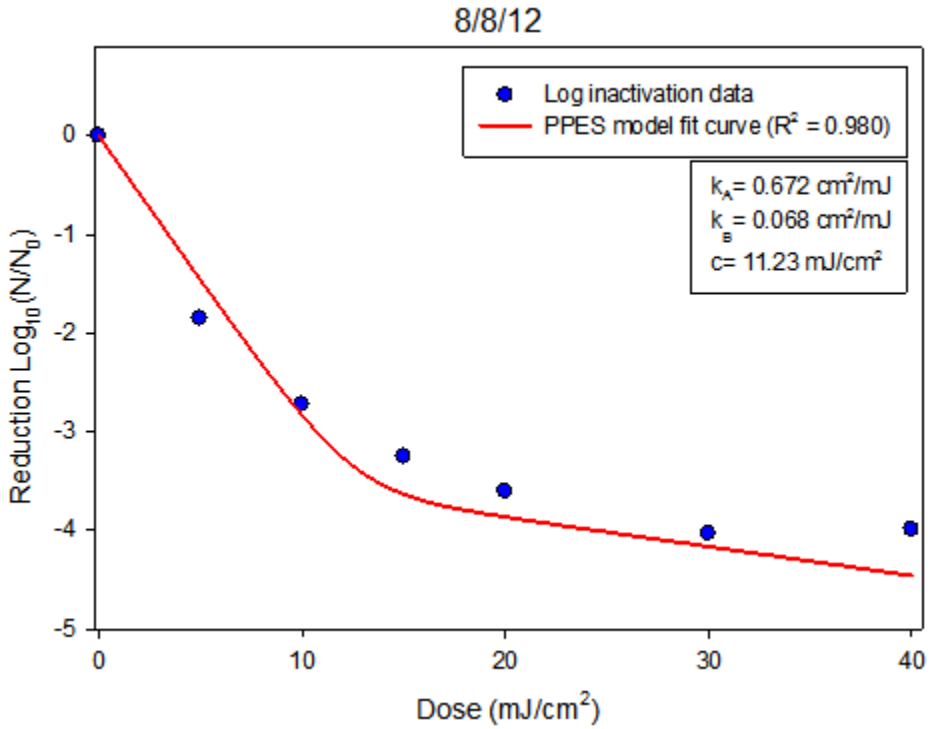

Figure A7. Unfiltered sample

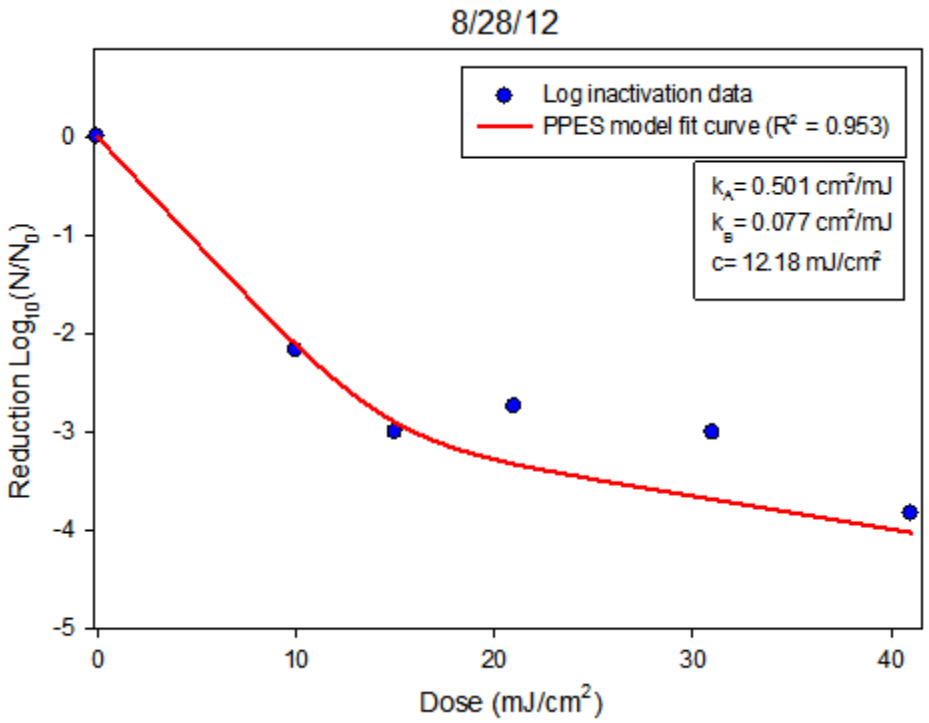

Figure A8. Unfiltered sample

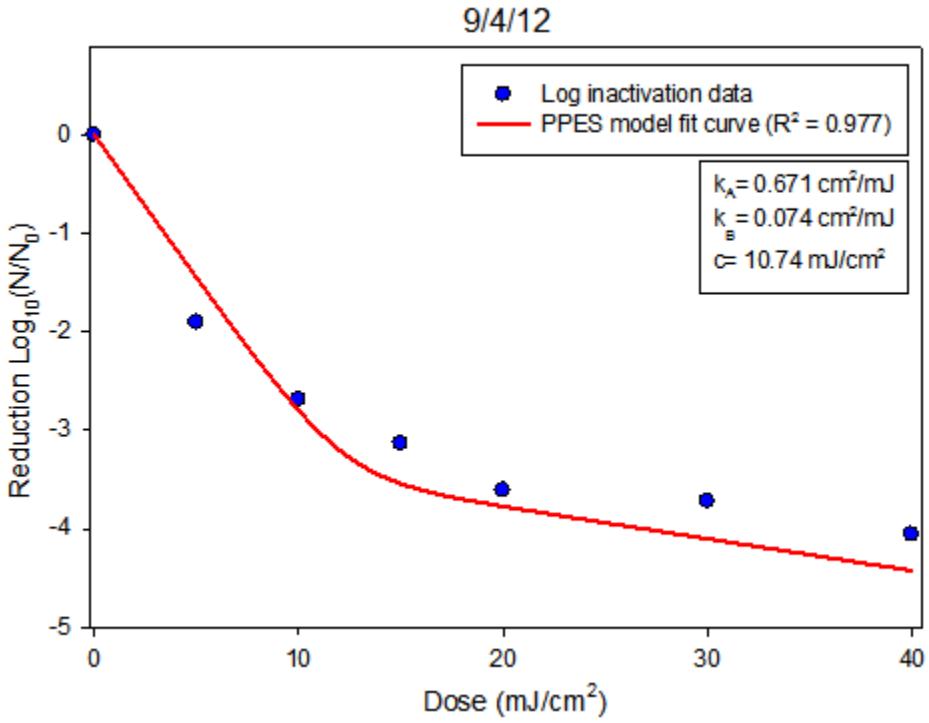

Figure A9. Unfiltered sample

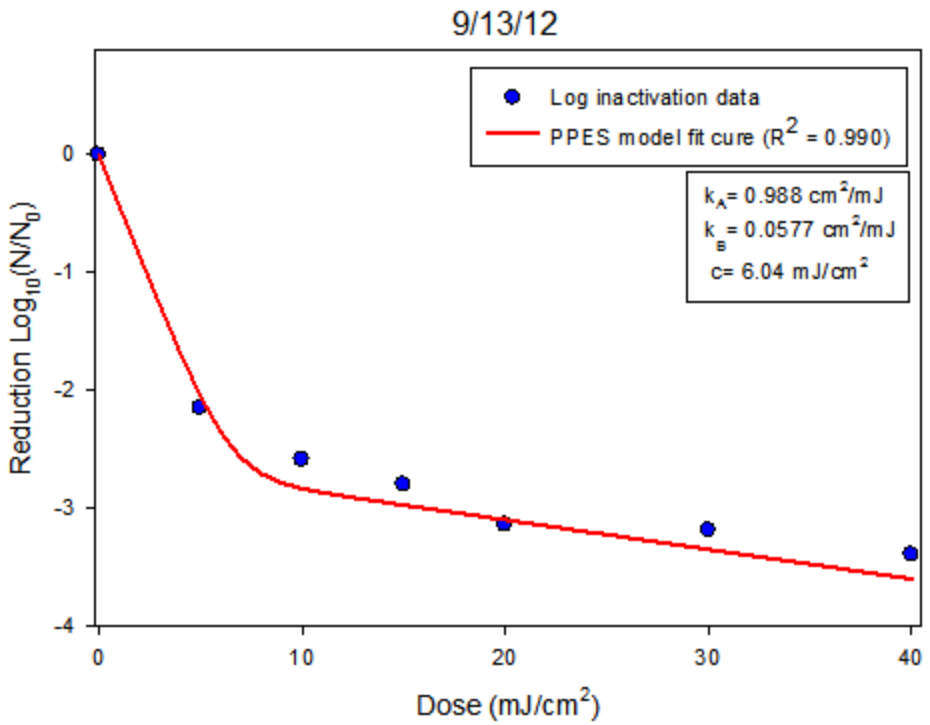

Figure A10. Unfiltered sample

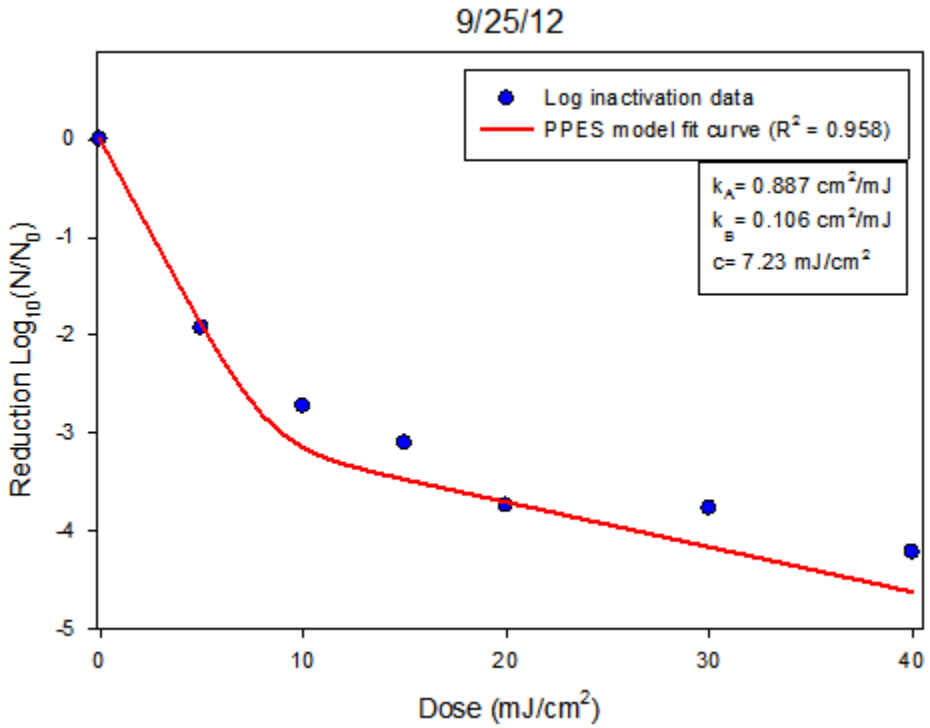

Figure A11. Unfiltered sample

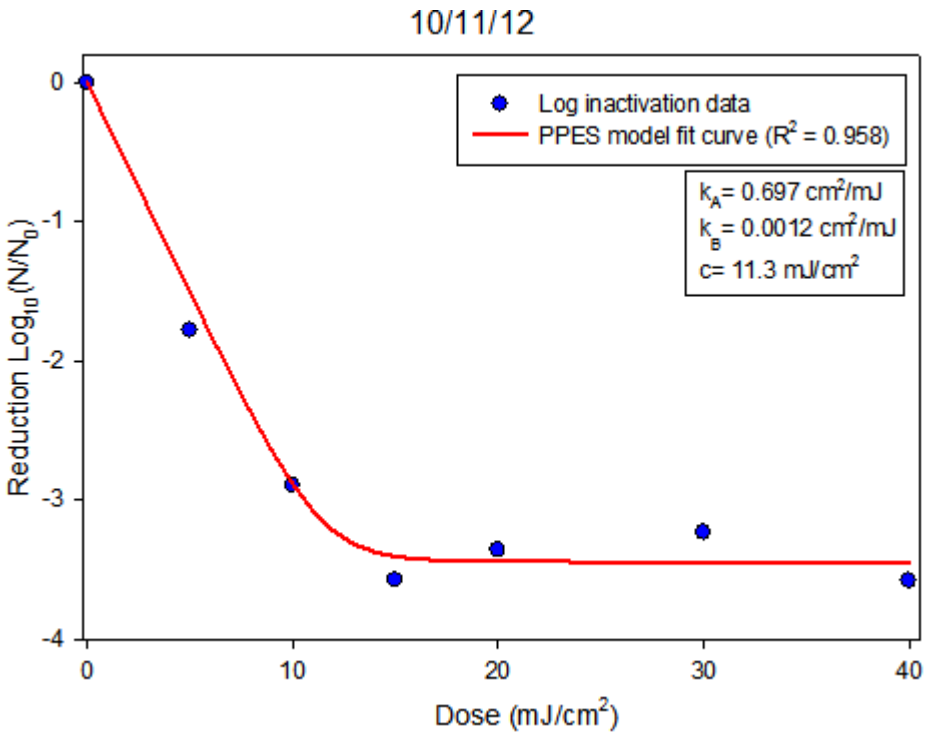

Figure A12. Unfiltered sample

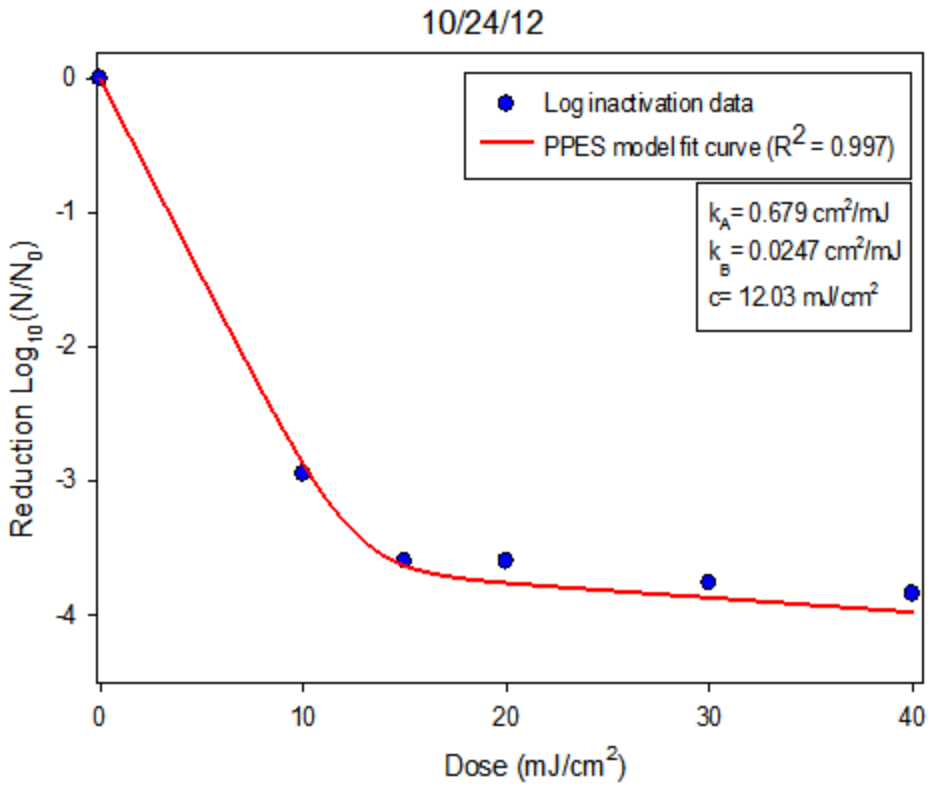

Figure A13. Unfiltered sample

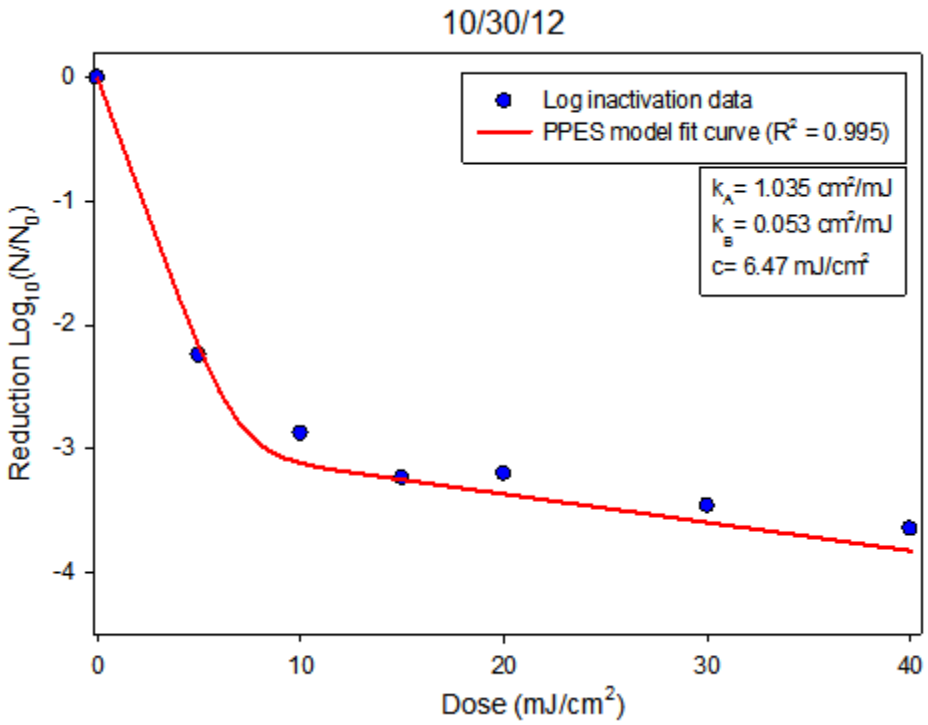

Figure A14. Unfiltered sample

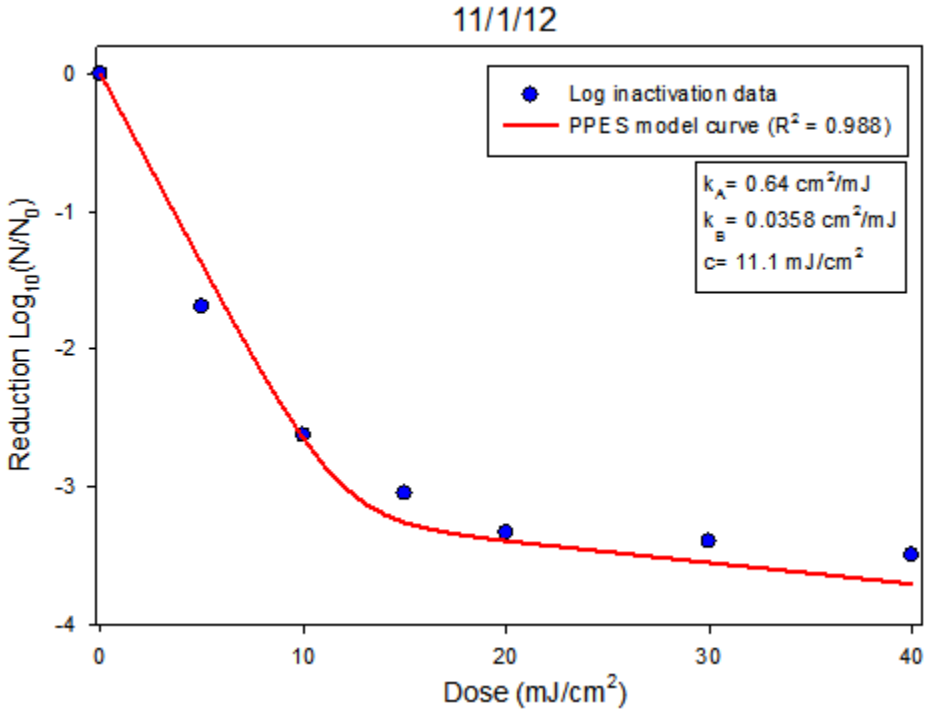

Figure A15. Filtered sample

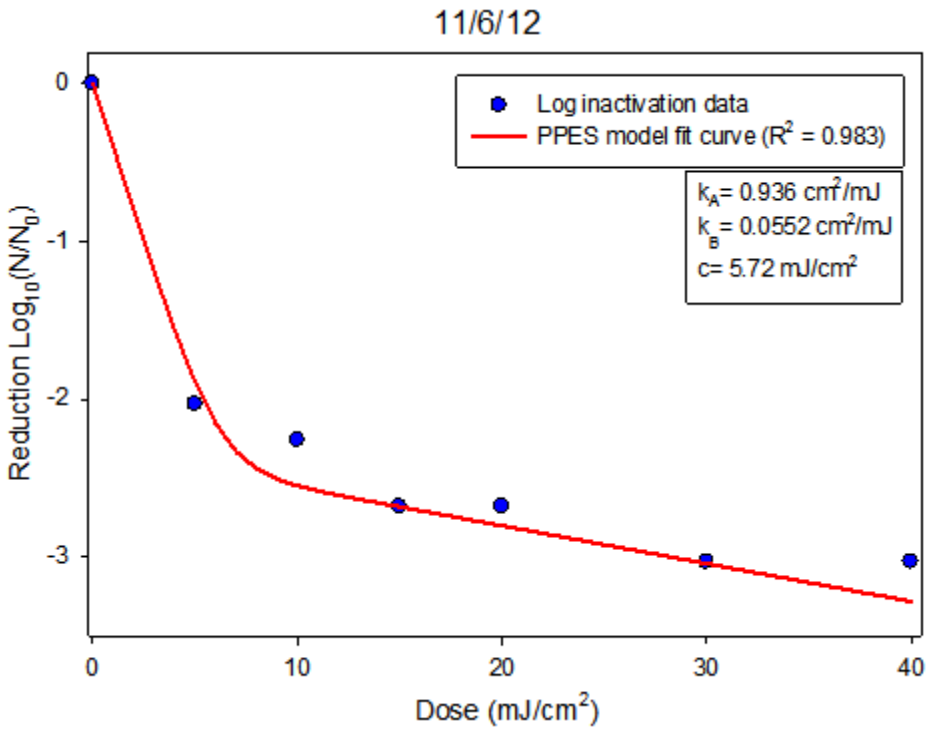

Figure A16. Filtered sample

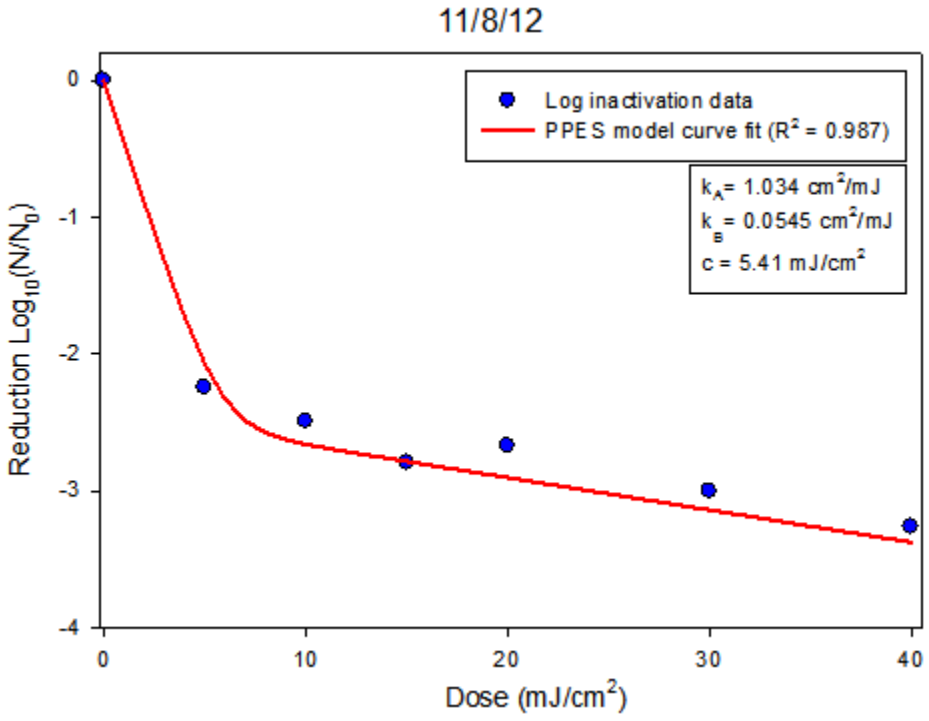

Figure A17. Filtered sample

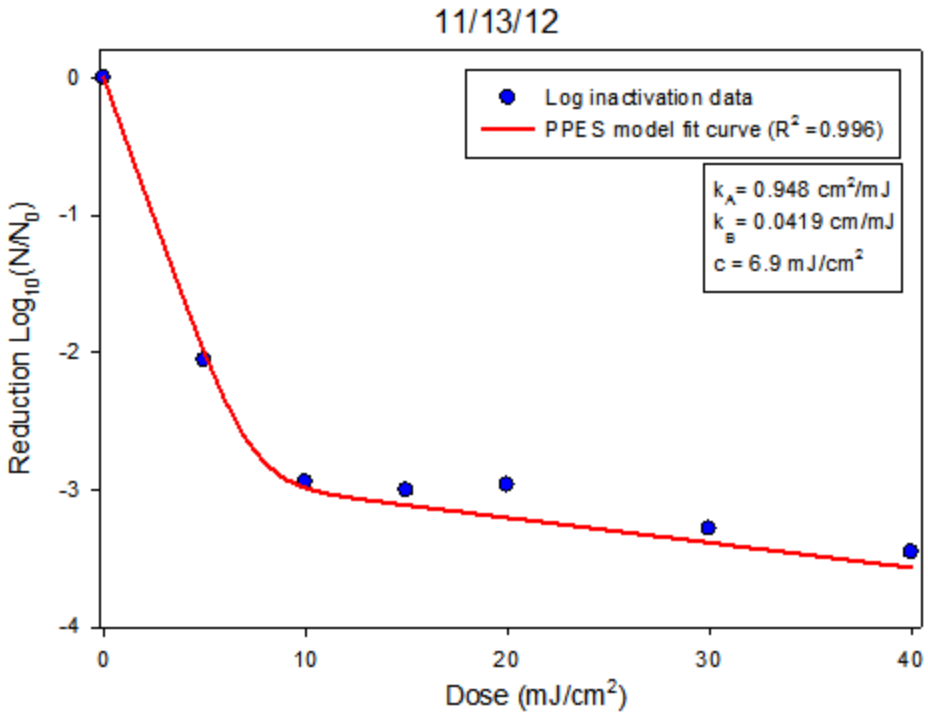

Figure A18. Filtered sample

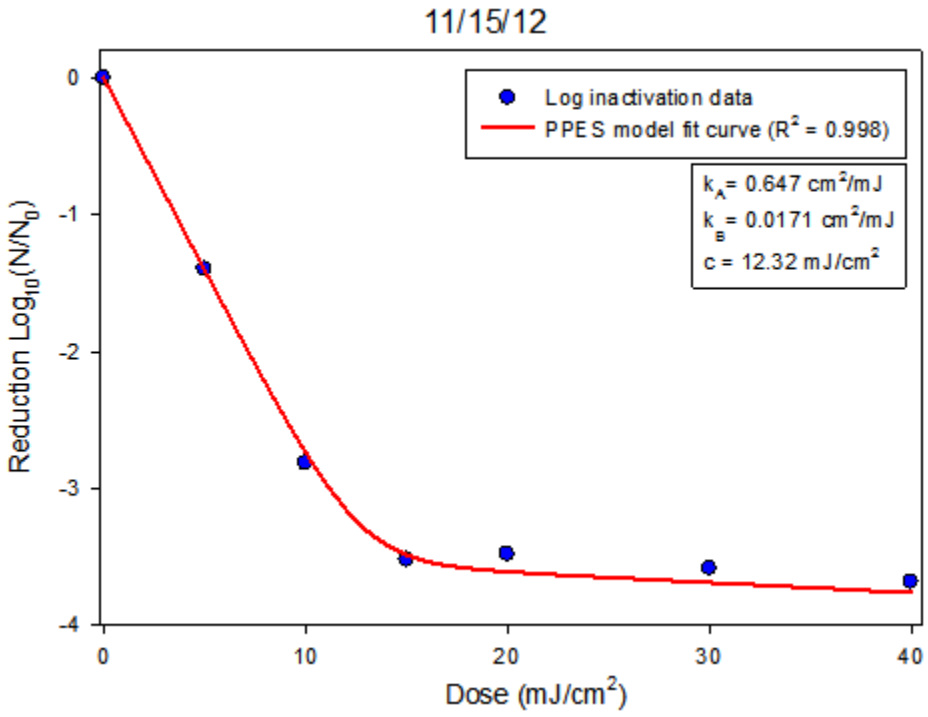

Figure A19. Filtered sample

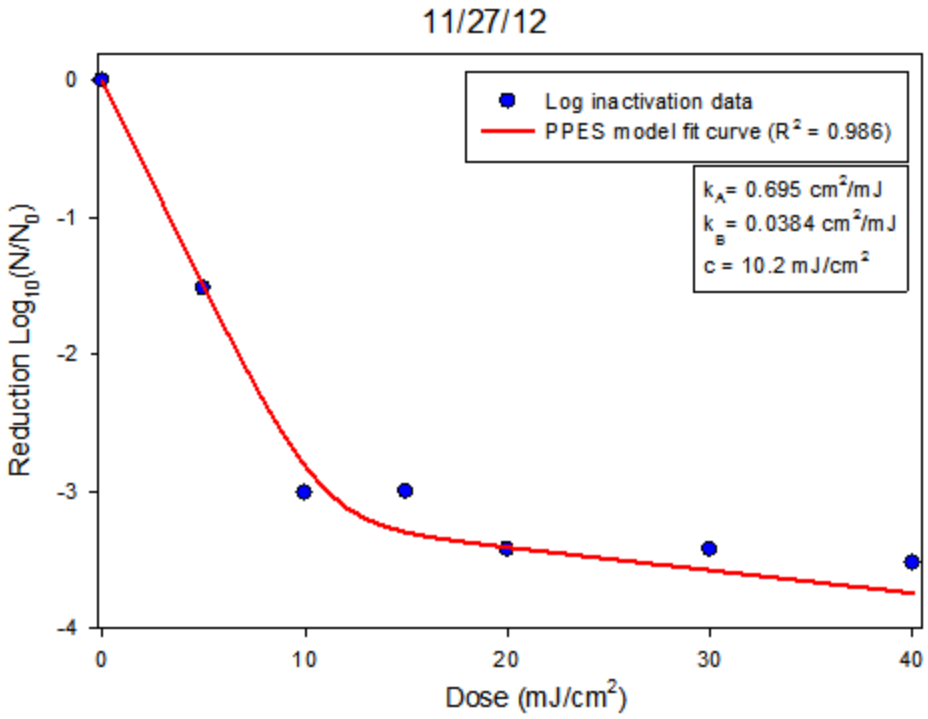

Figure A20. Filtered sample

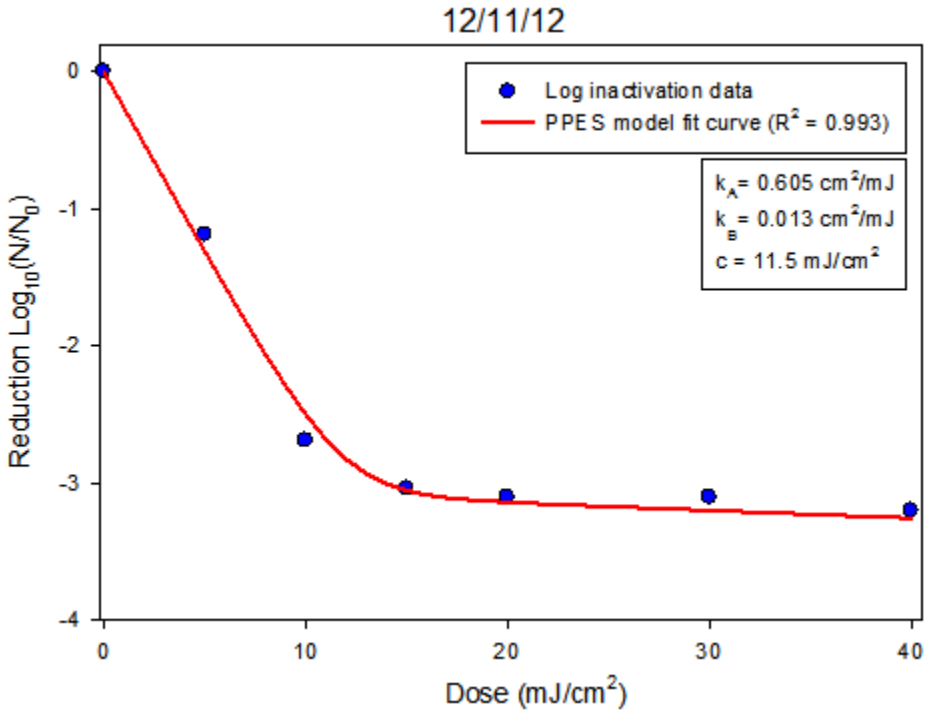

Figure A21. Filtered sample

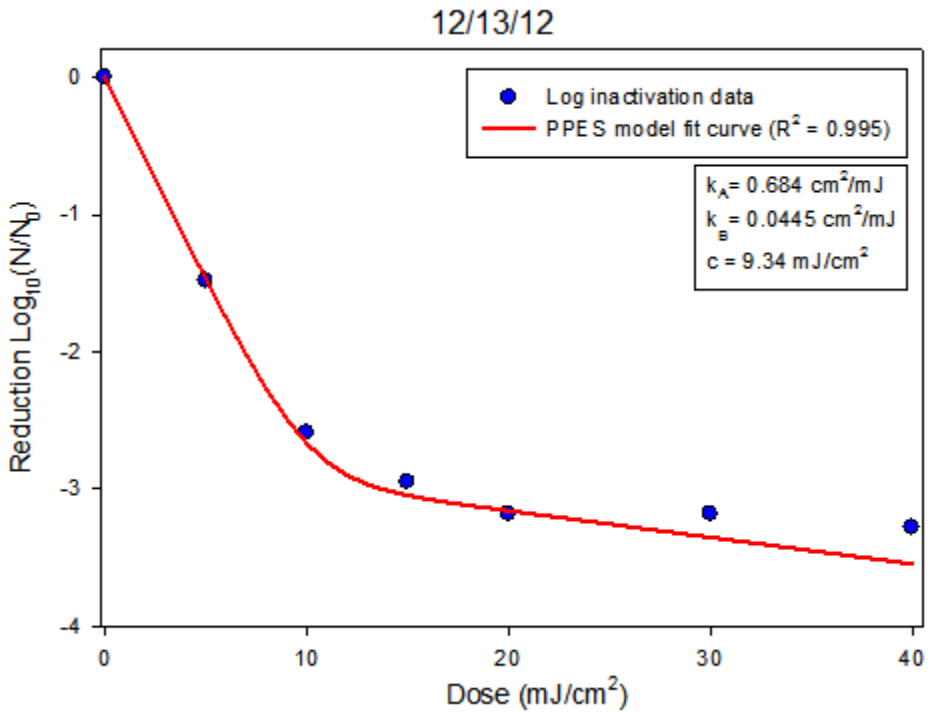

Figure A22. Filtered sample

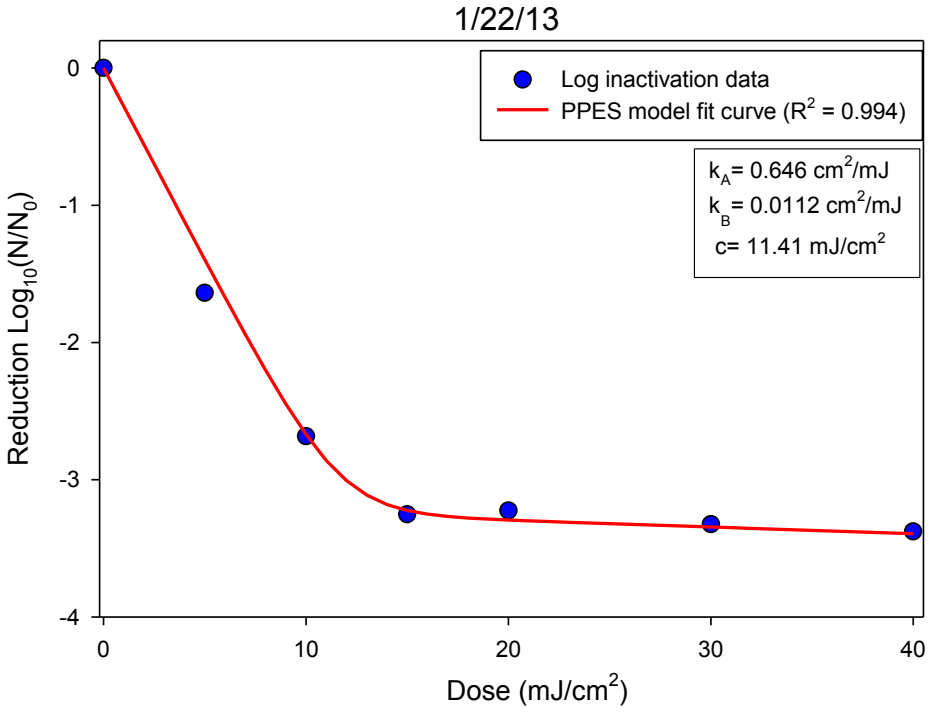

Figure A23. Filtered sample

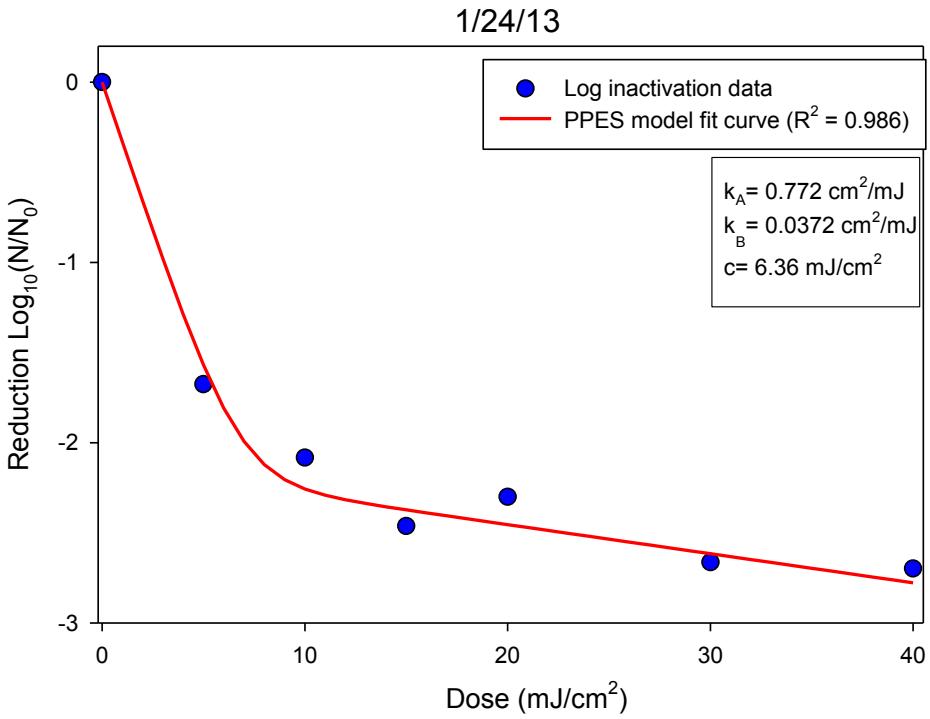

Figure A24. Filtered sample

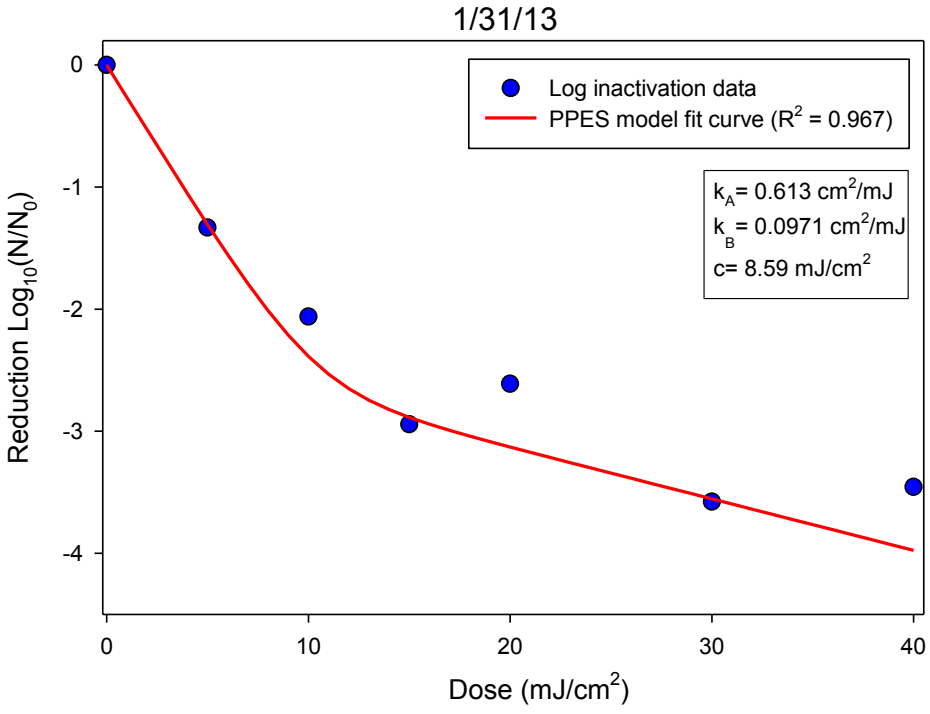

Figure A25. Filtered sample

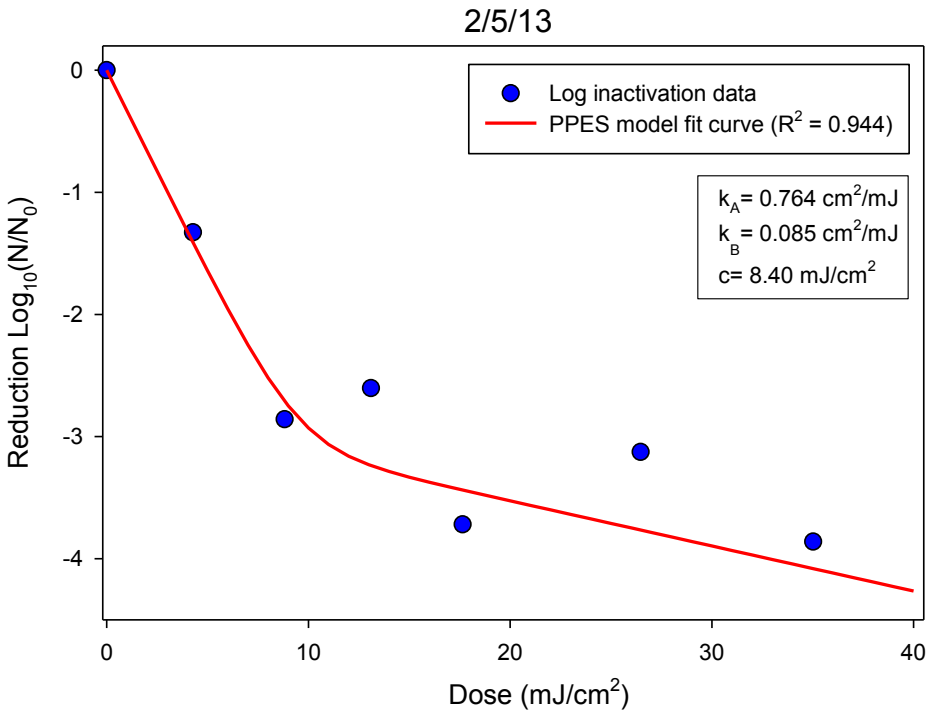

Figure A26. Filtered sample

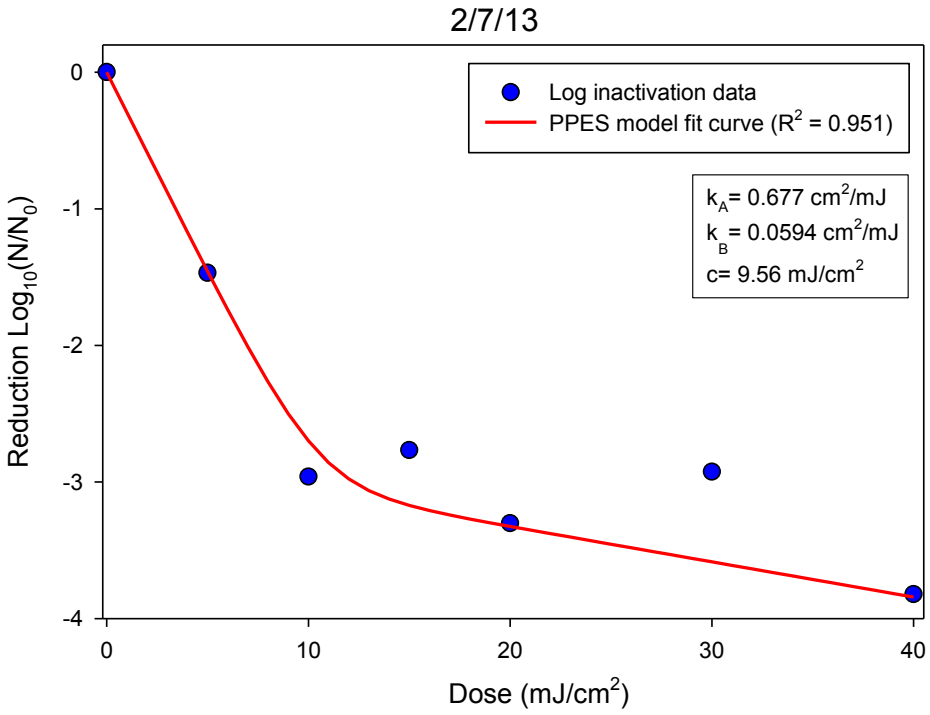

Figure A27. Filtered sample

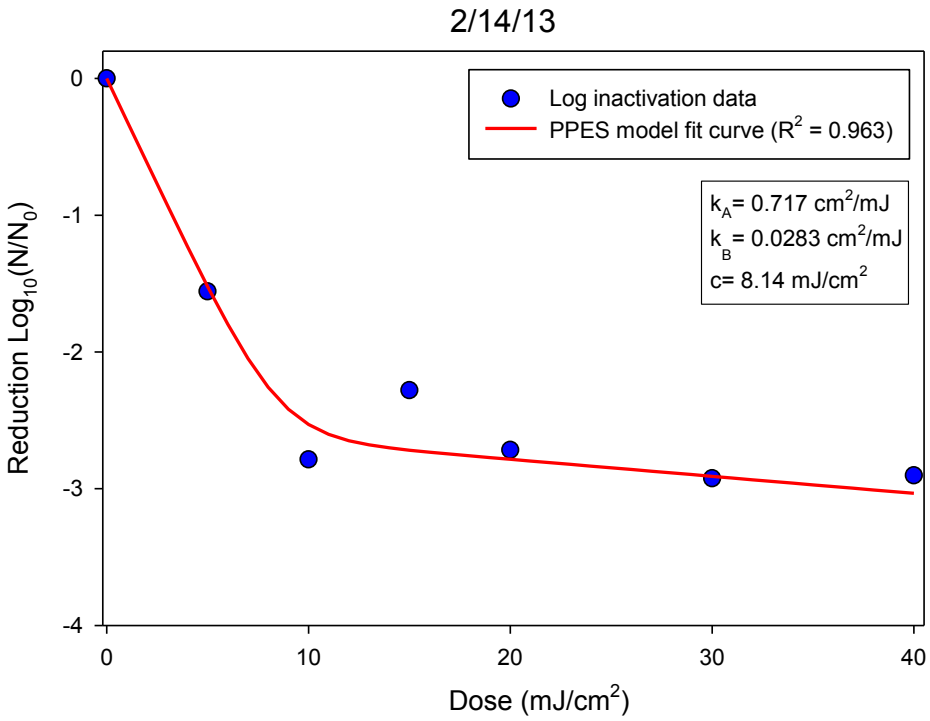

Figure A28. Filtered sample

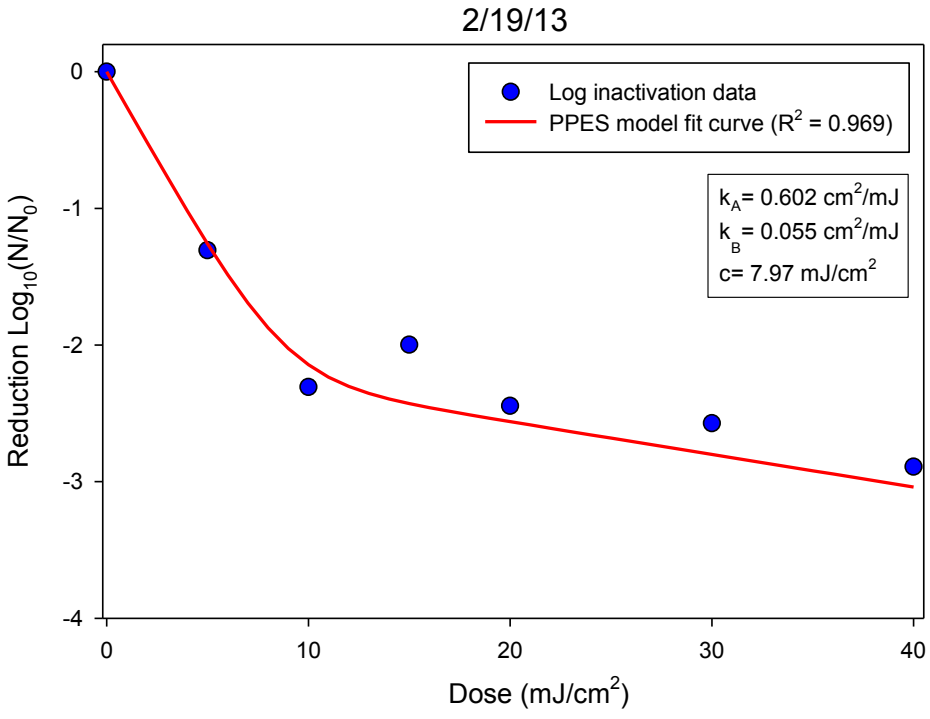

Figure A29. Filtered sample

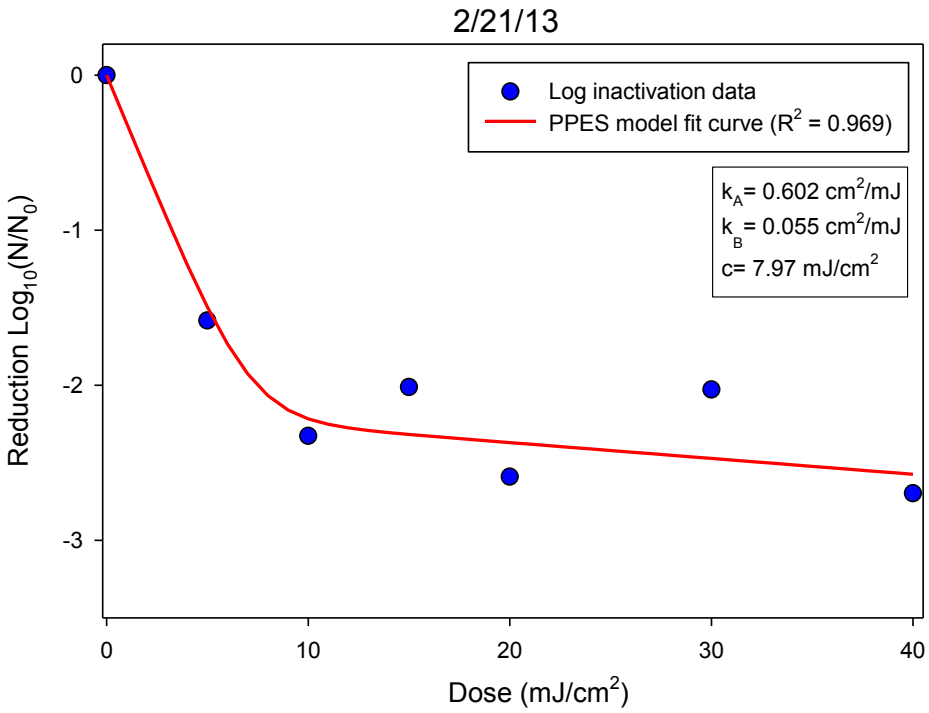

Figure A30. Filtered sample

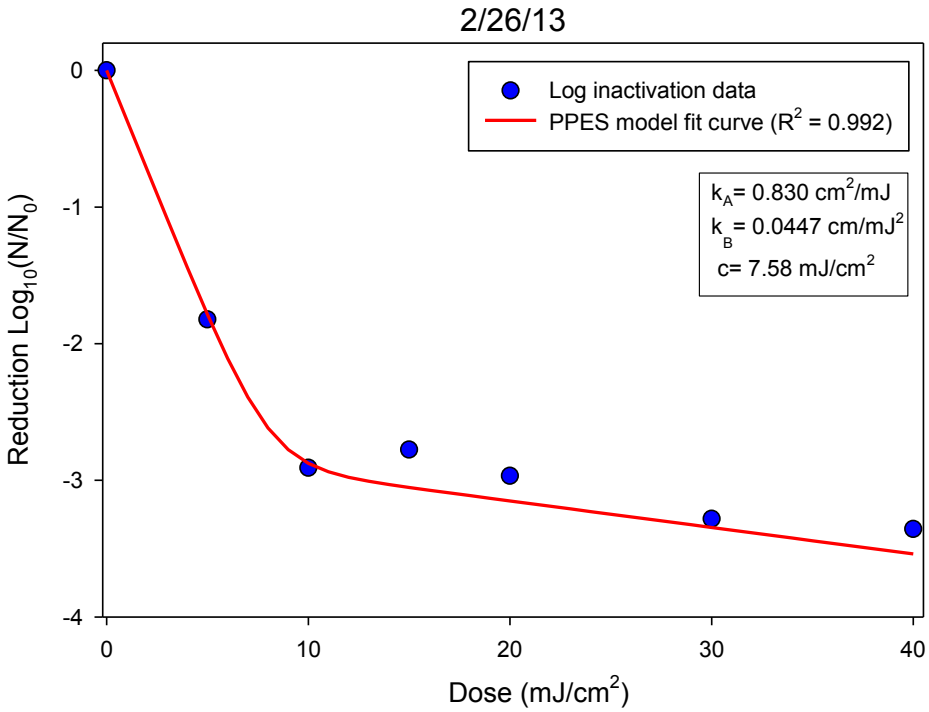

Figure A31. Filtered sample

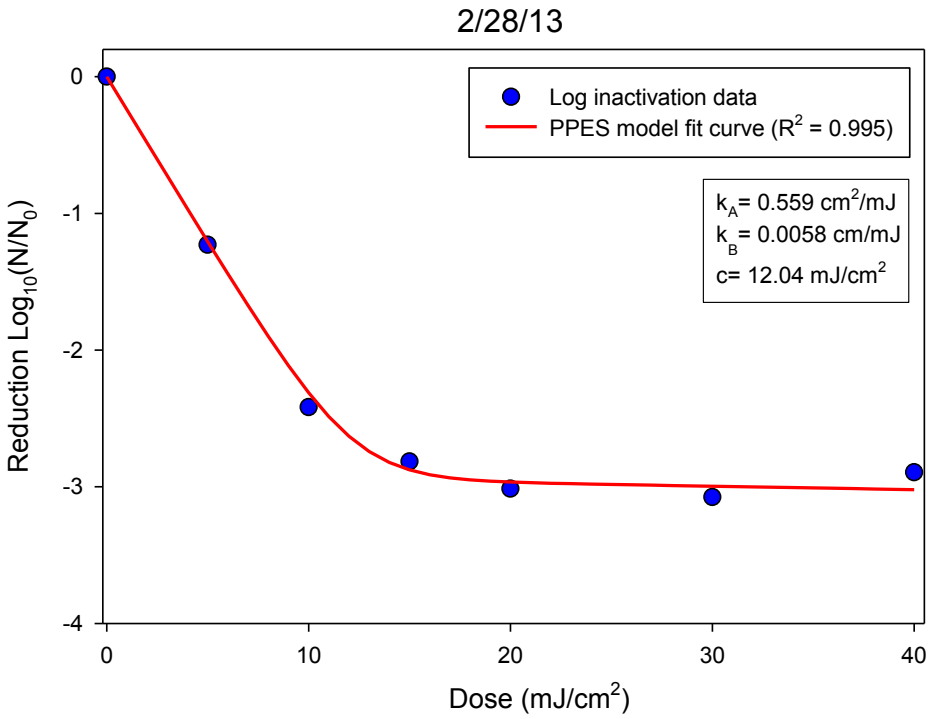

Figure A32. Filtered sample

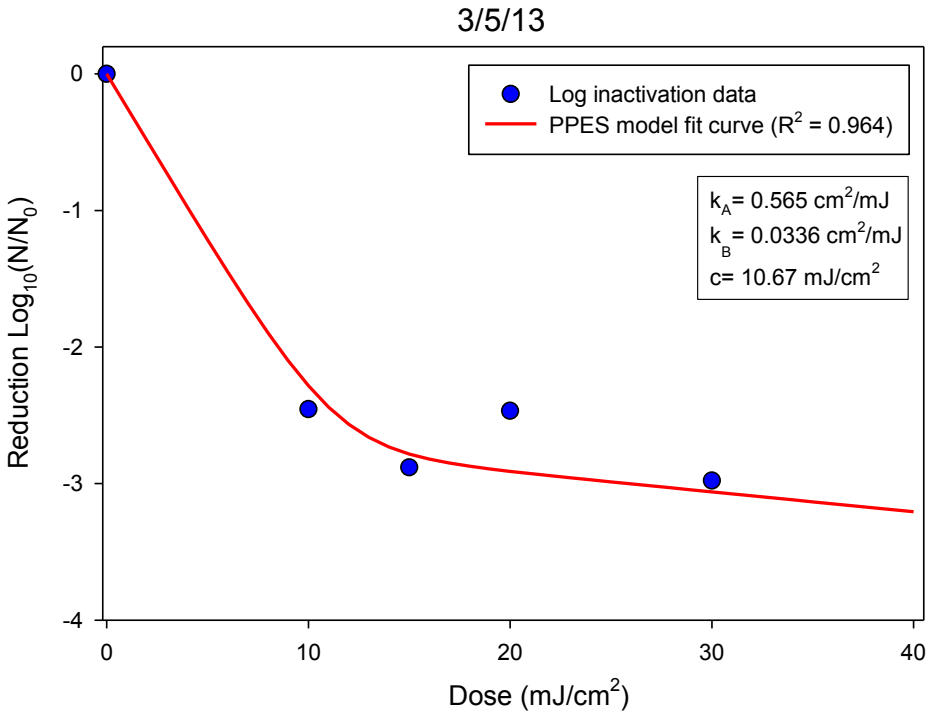

Figure A33. Filtered sample

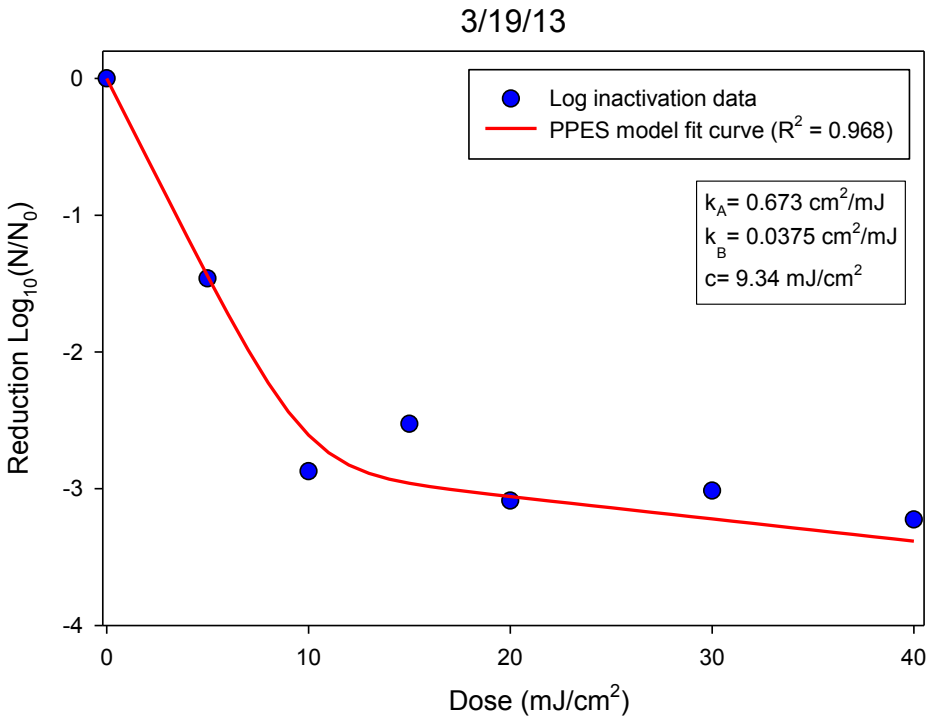

Figure A34. Filtered sample

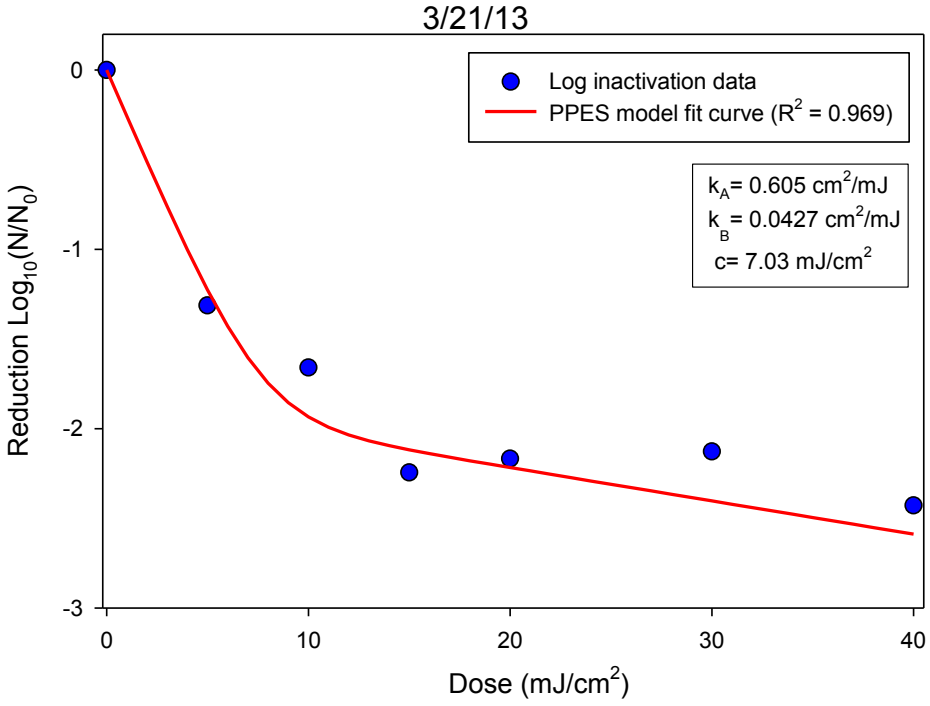

Figure A35. Filtered sample

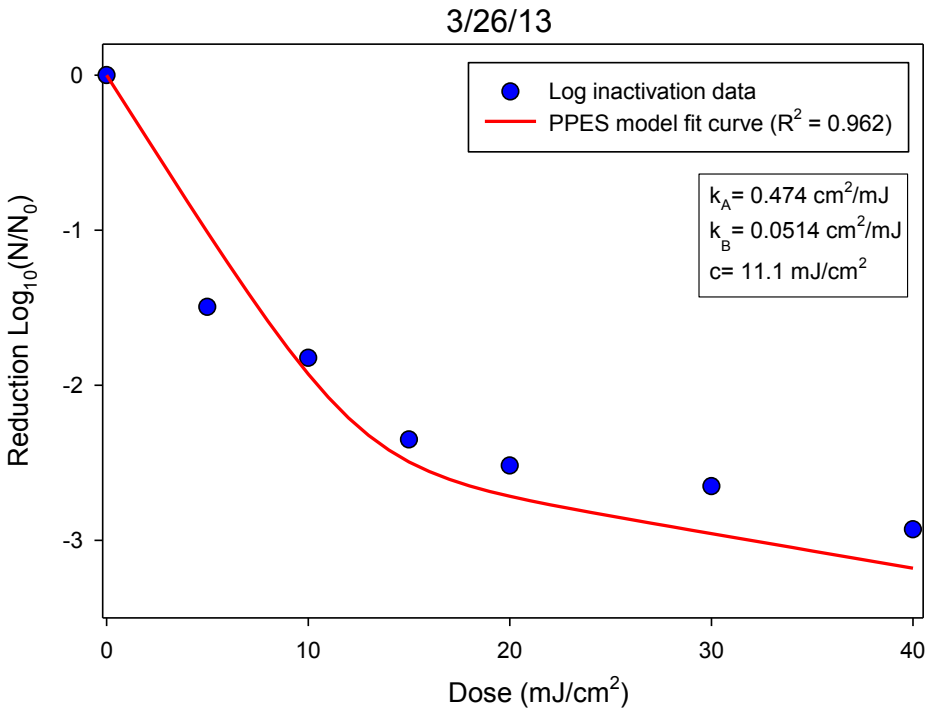

Figure A36. Filtered sample

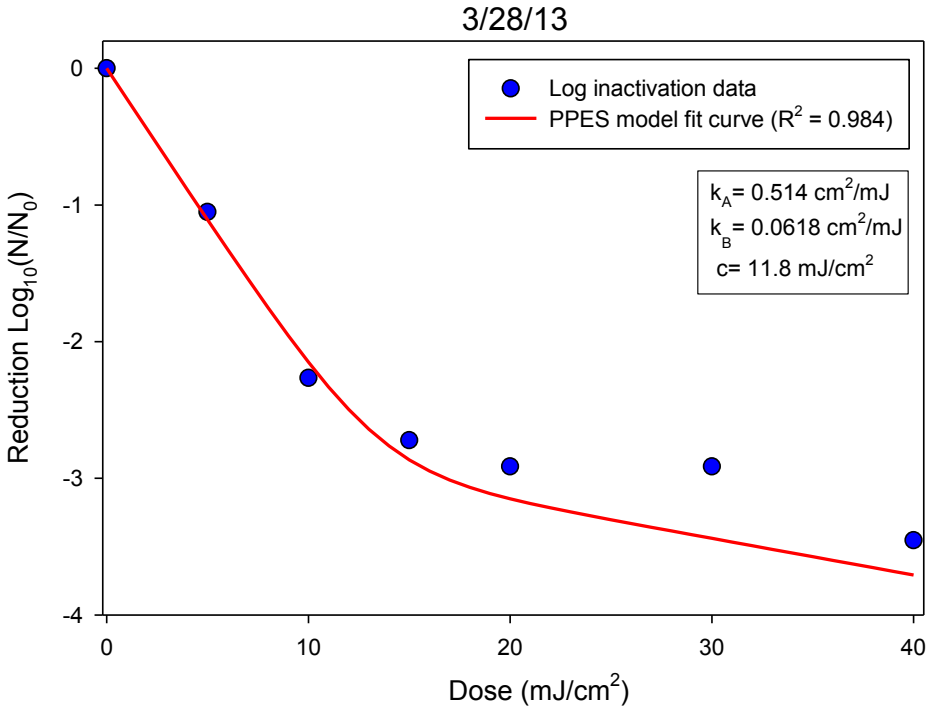

Figure A37. Filtered sample

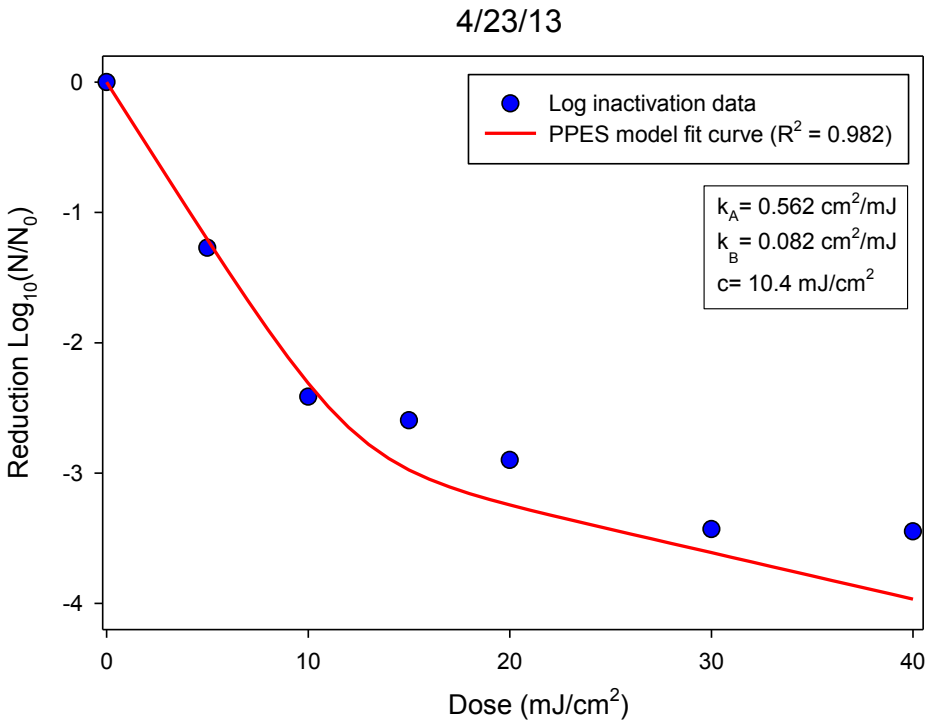

Figure A38. Filtered sample

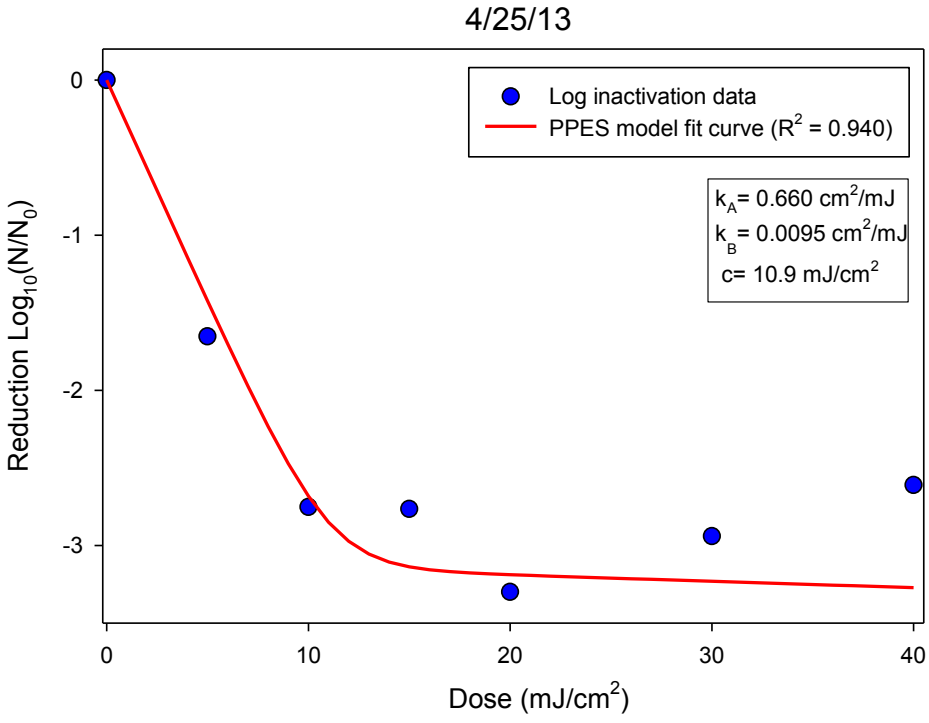

Figure A39. Filtered sample

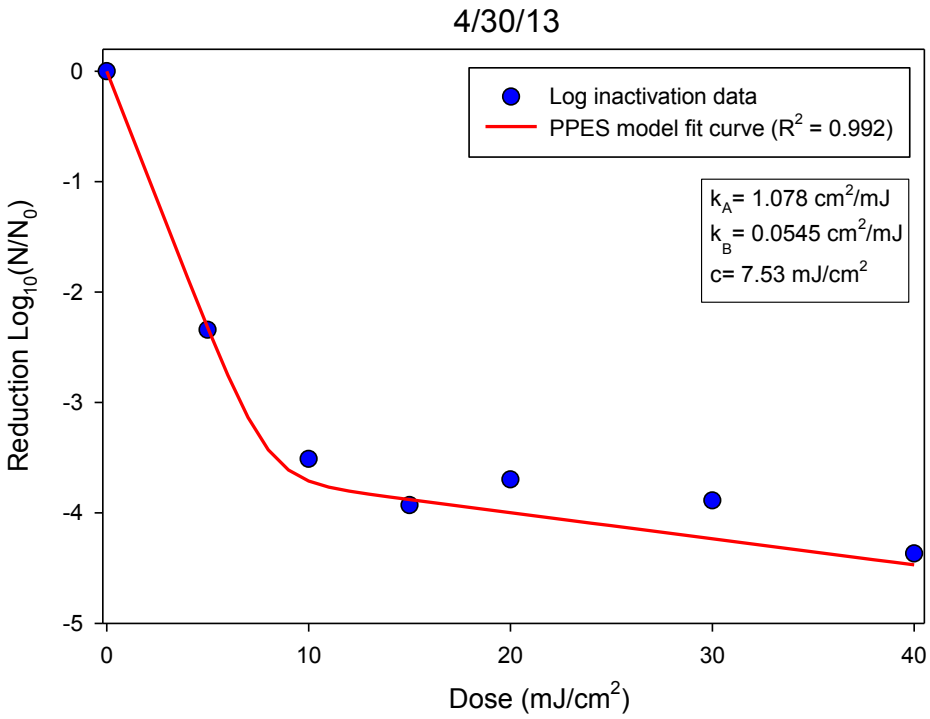

Figure A40. Filtered sample

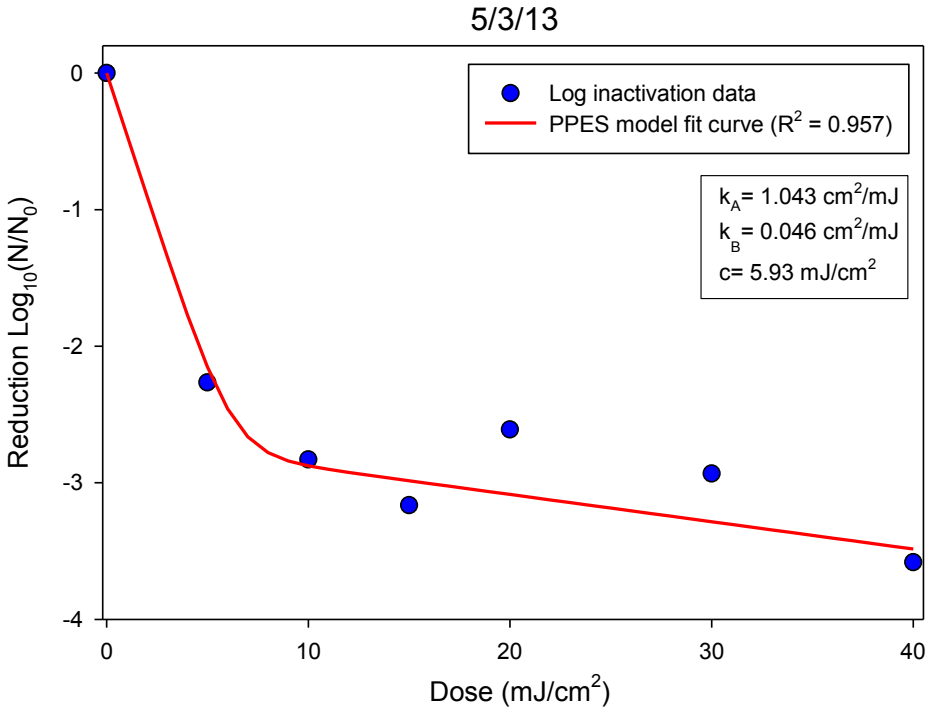

Figure A41. Unfiltered sample

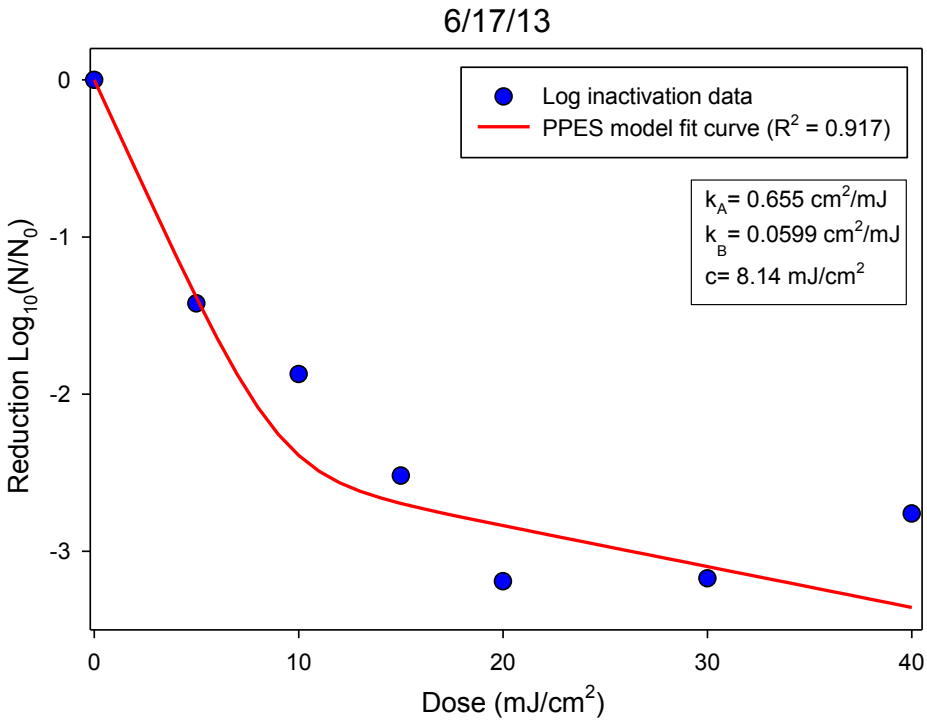

Figure A42. Unfiltered sample

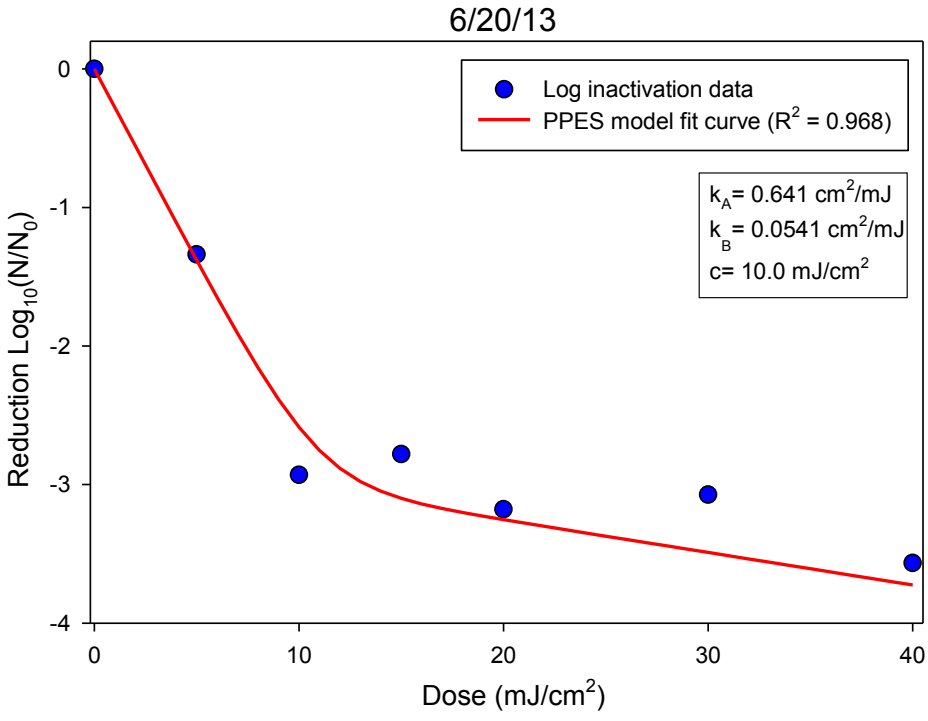

Figure A43. Unfiltered sample

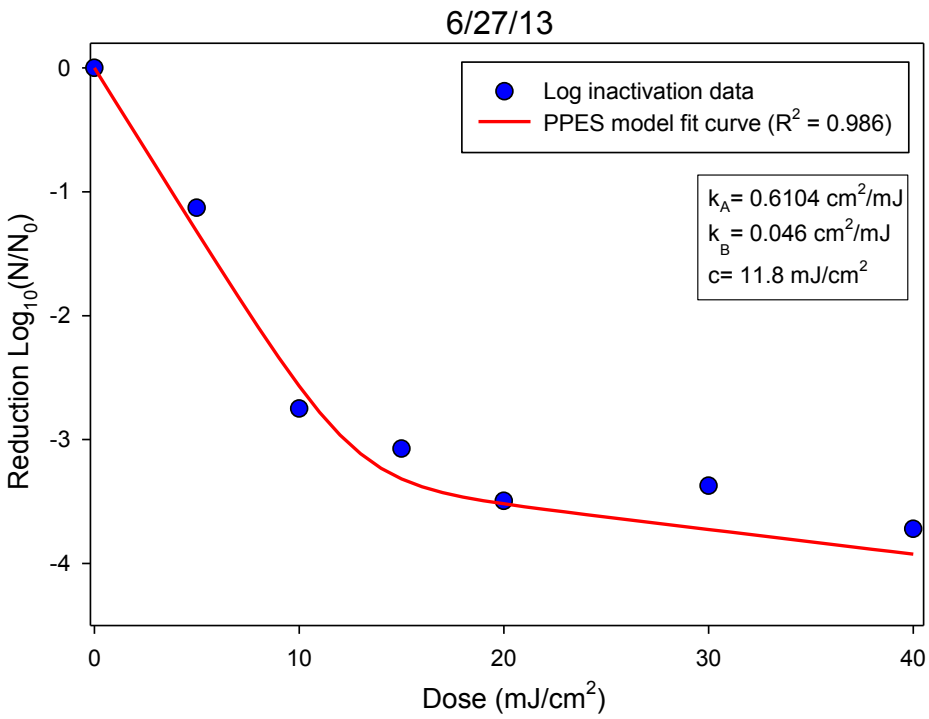

Figure A44. Unfiltered sample

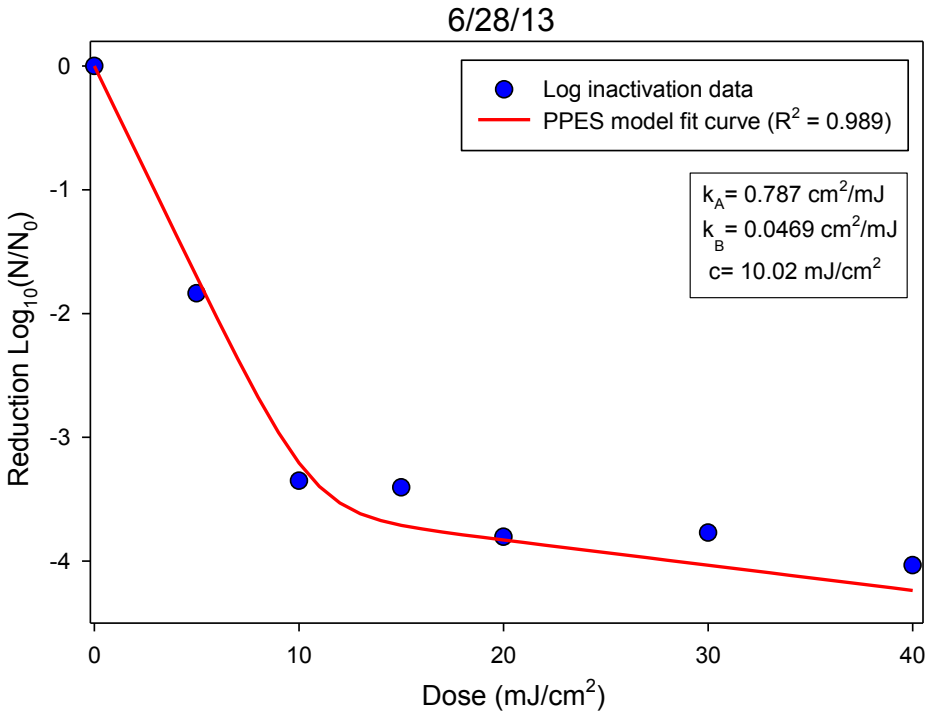

Figure A45. Unfiltered sample

Appendix B. Correlation scatter plots

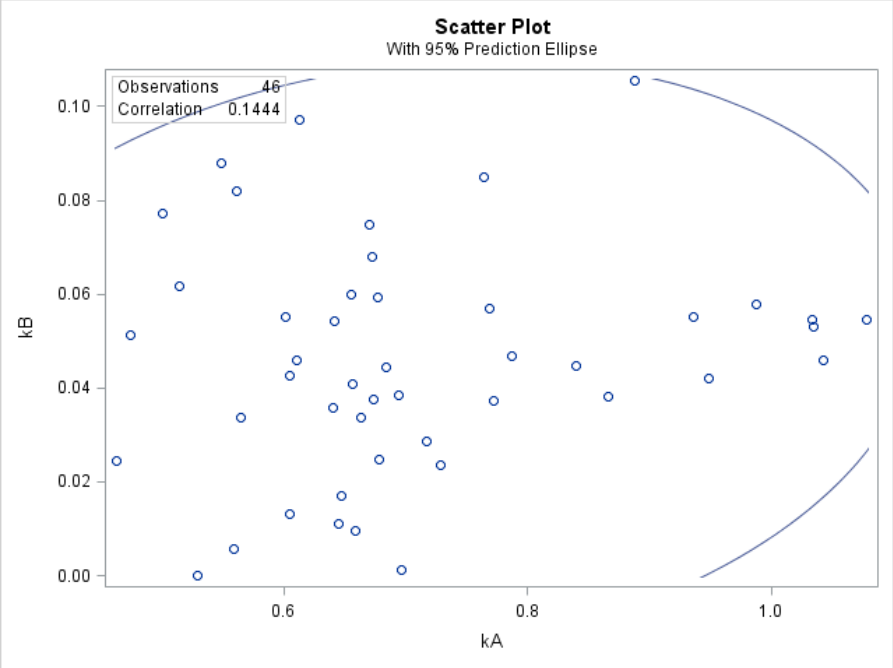

Figure B1. Scatter plot of k_A (cm^2/mJ) vs. k_B (cm^2/mJ)

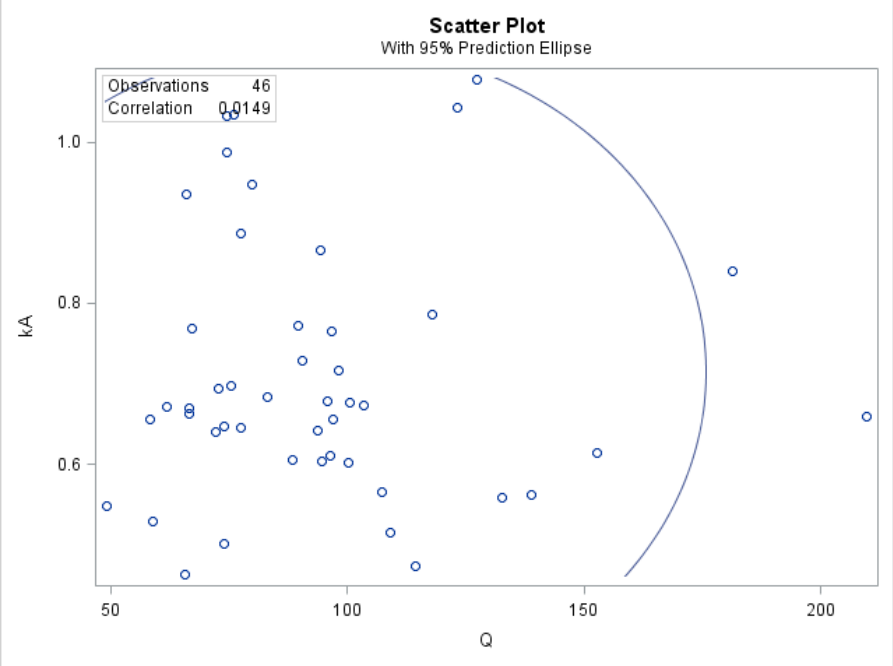

Figure B2. Scatter plot of Q (MGD) vs. k_A (cm^2/mJ)

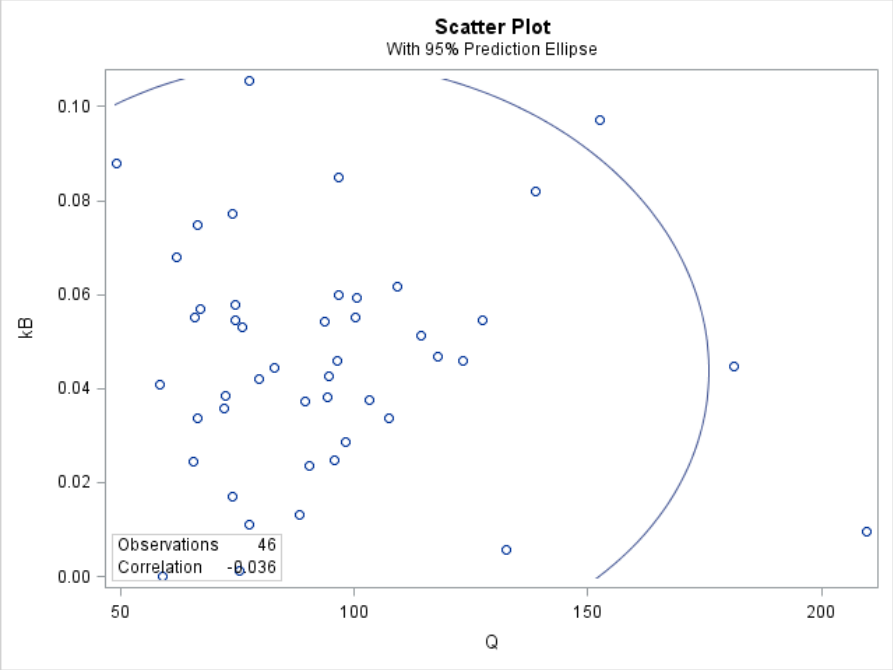

Figure B3. Scatter plot of Q (MGD) vs. k_B (cm^2/mJ)

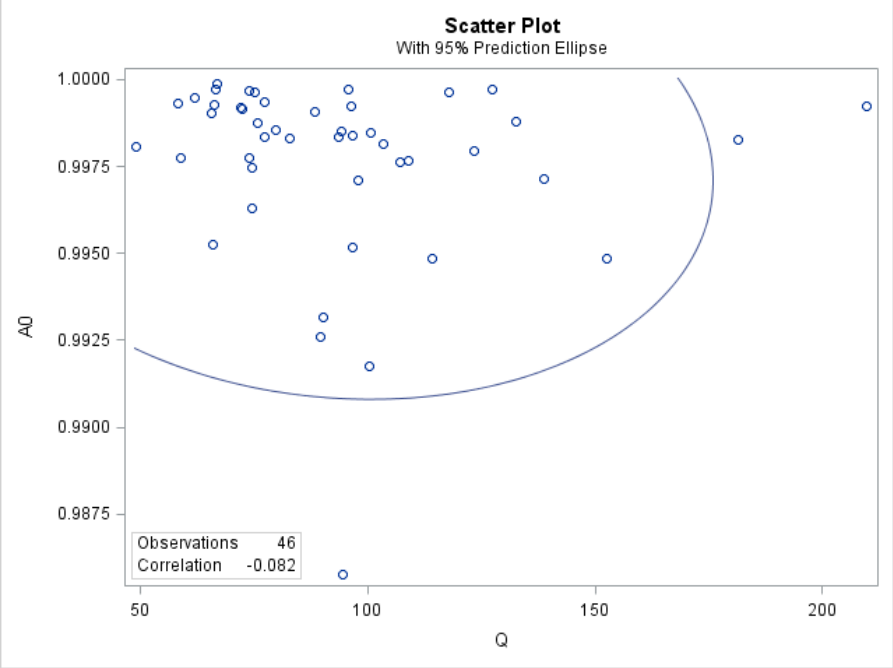

Figure B4. Scatter plot of Q (MGD) vs. A_0 (cfu/100 mL)

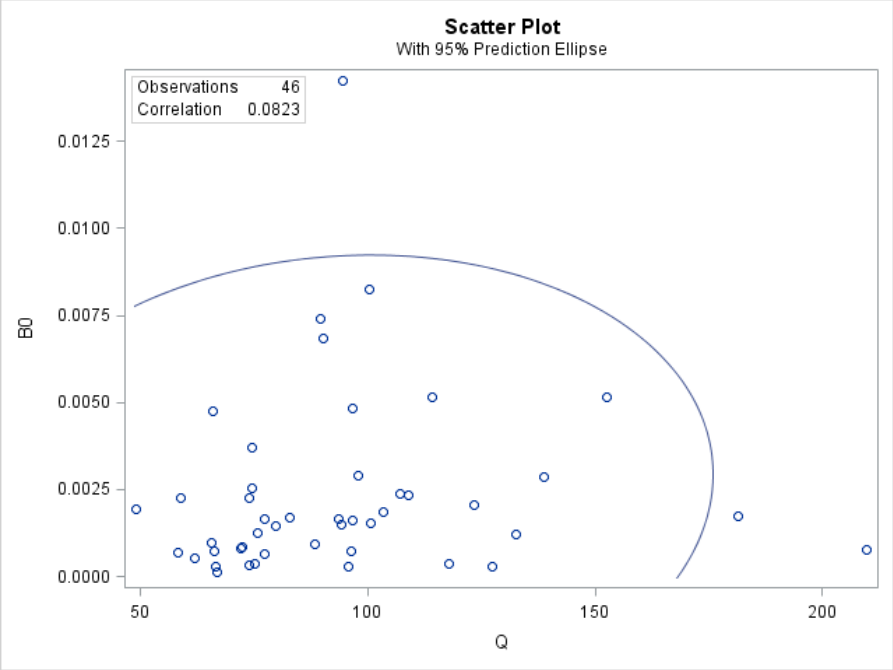

Figure B5. Scatter plot of Q (MGD) vs. B_0 (cfu/100 mL)

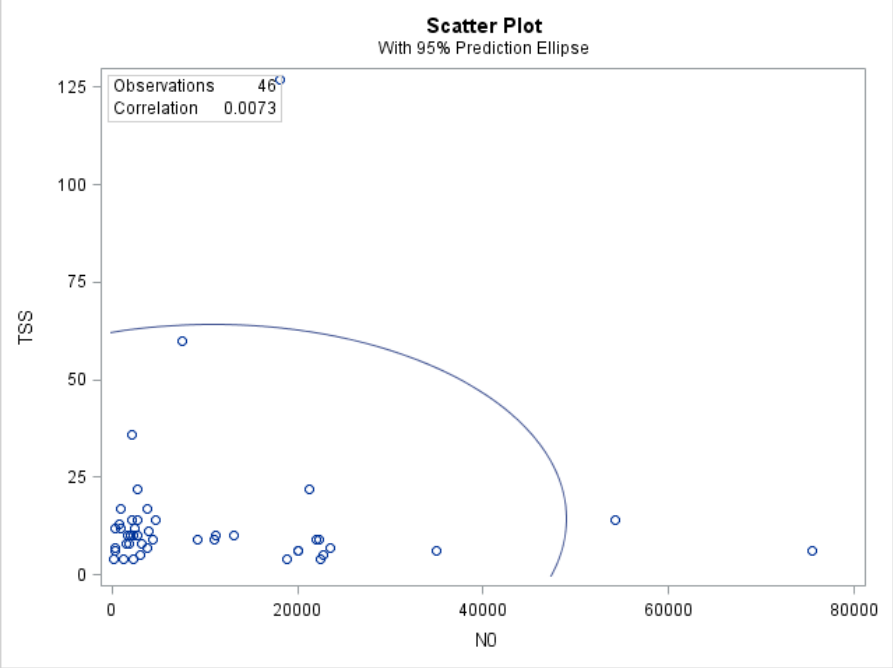

Figure B6. Scatter plot of N_0 (cfu/100 mL) vs. TSS (mg/L)

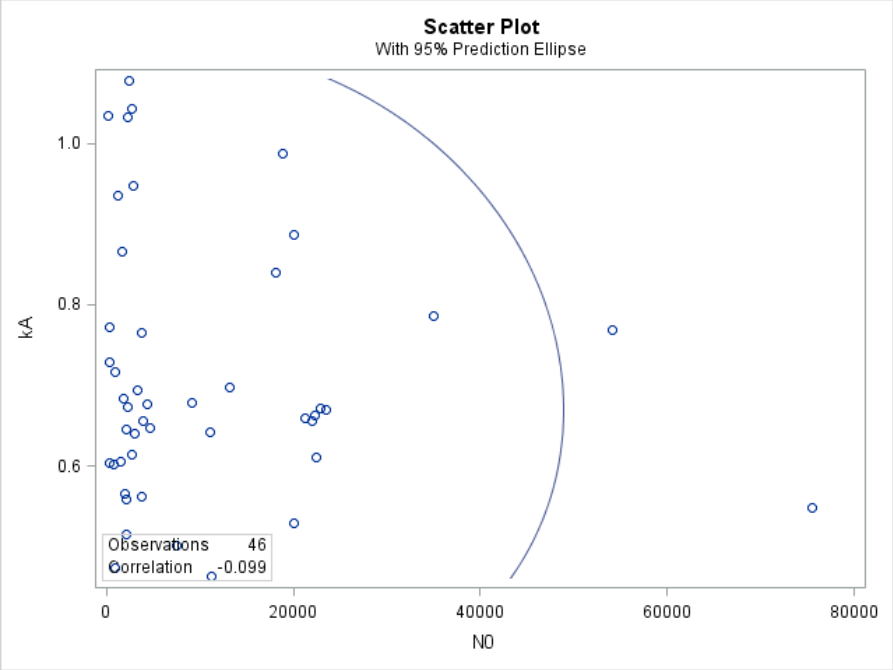

Figure B7. Scatter plot of N_0 (cfu/100 mL) vs. k_A (cm^2/mJ)

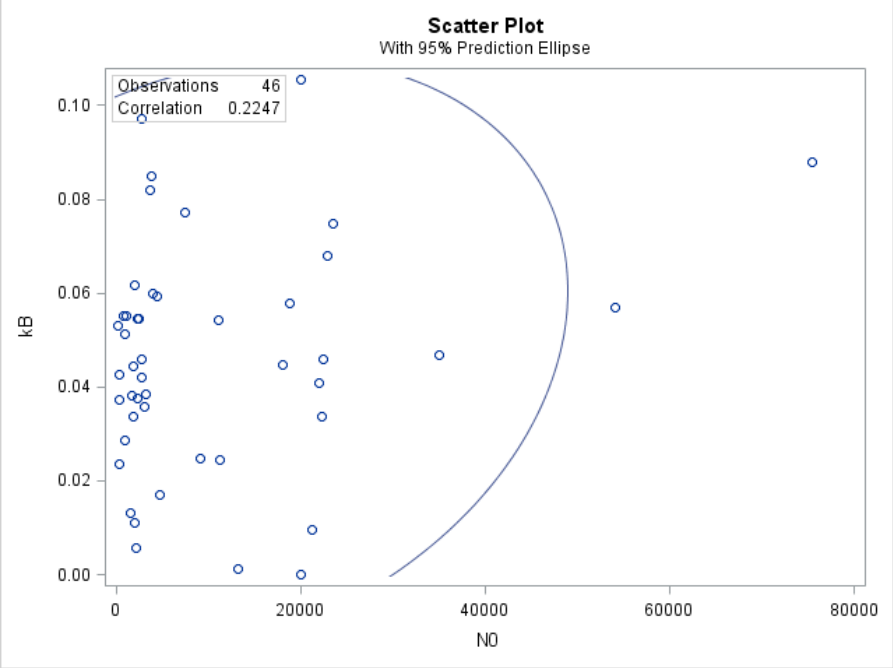

Figure B8. Scatter plot of N_0 (cfu/100 mL) vs. k_B (cm^2/mJ)

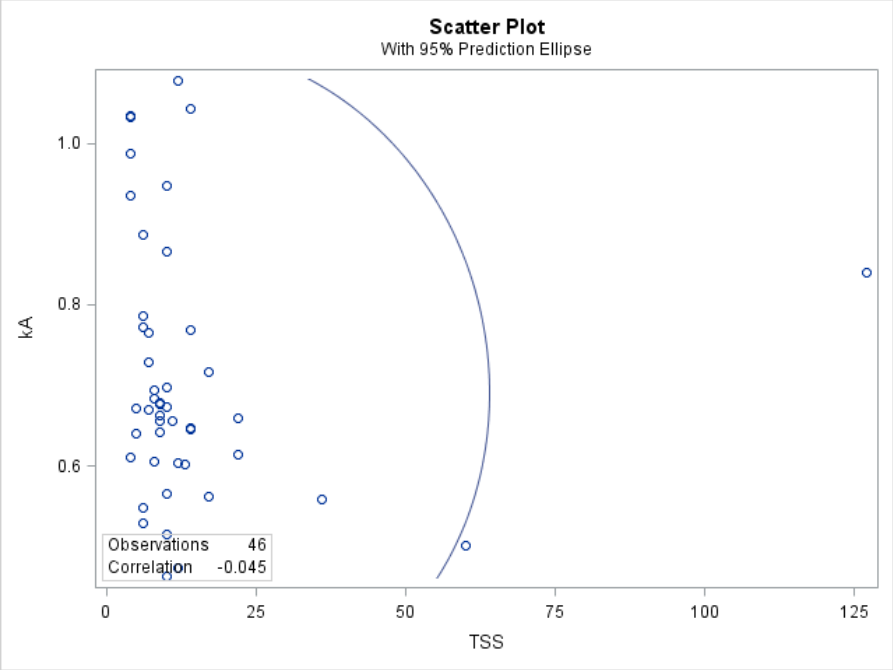

Figure B9. Scatter plot of TSS (mg/L) vs. k_A (cm^2/mJ)

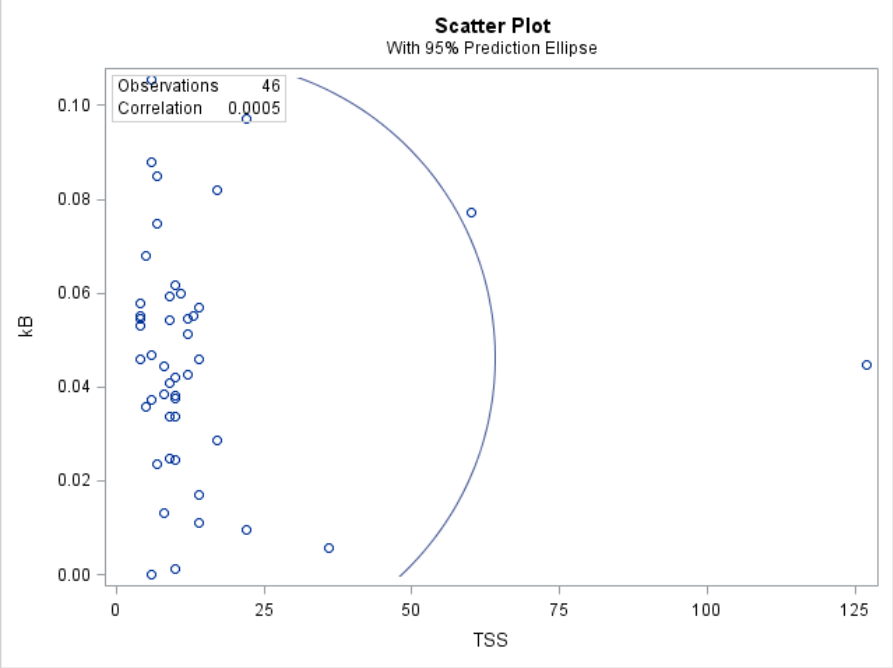

Figure B10. Scatter plot of TSS (mg/L) vs. k_B (cm^2/mJ)

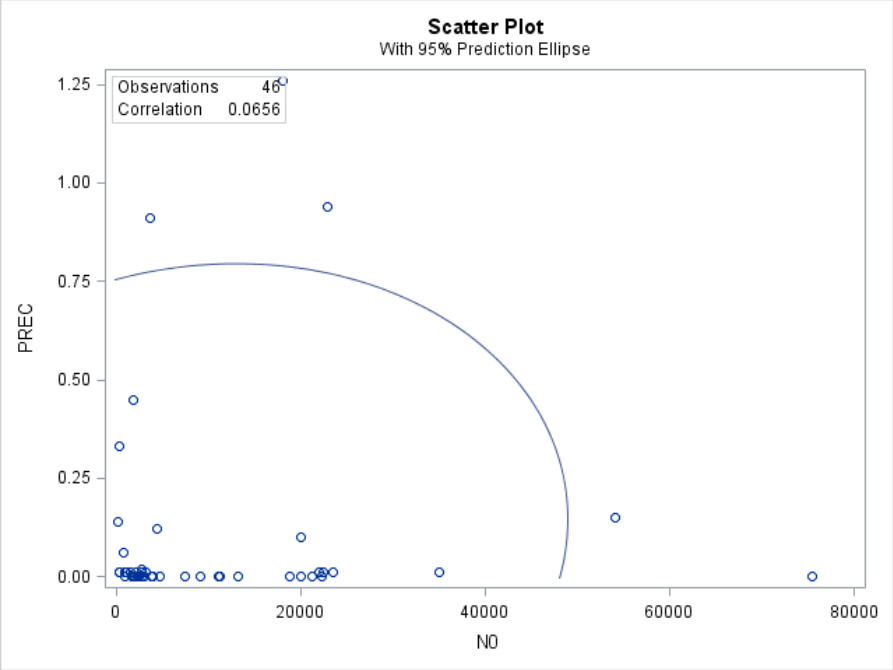

Figure B11. Scatter plot of N_0 (cfu/100 mL) vs. Precipitation (in)

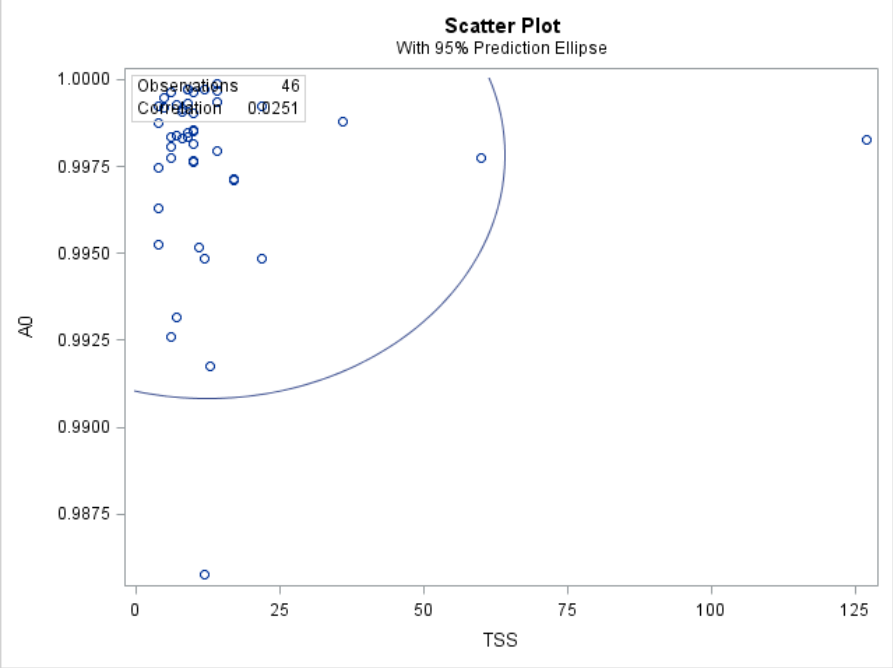

Figure B12. Scatter plot of TSS (mg/L) vs. A_0 (cfu/100 mL)

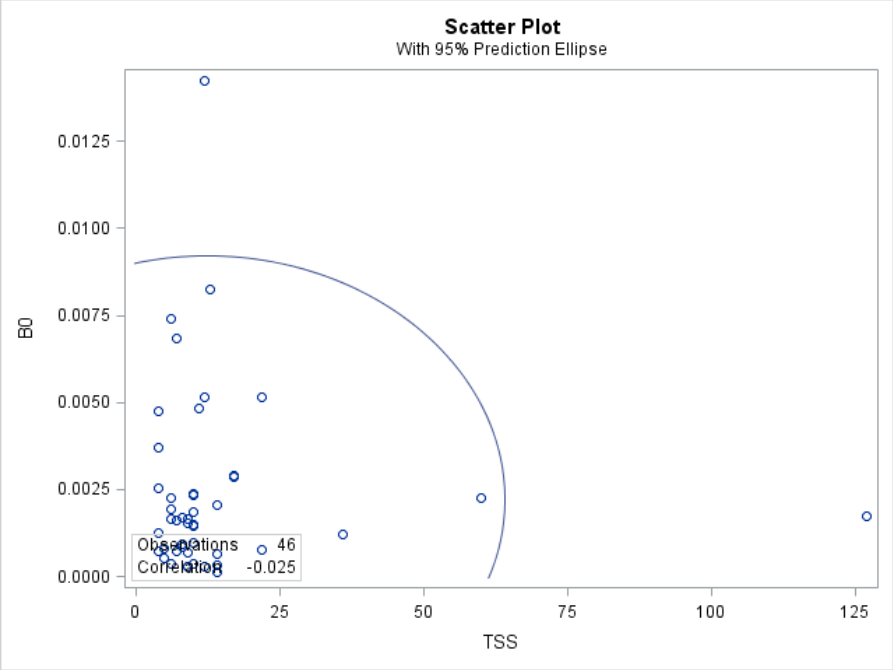

Figure B13. Scatter plot of TSS (mg/L) vs.B_0 (cfu/100 mL)

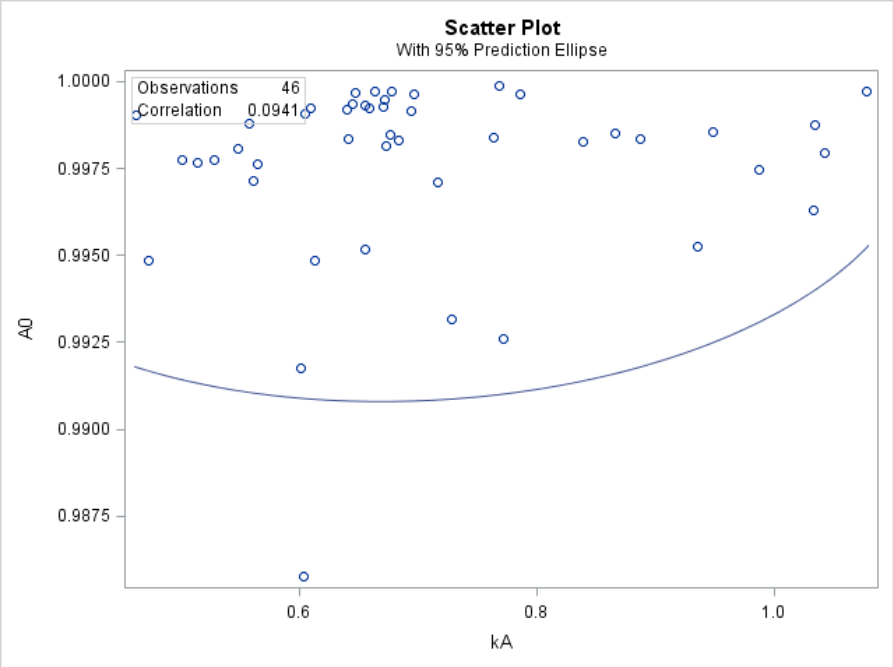

Figure B14. Scatter plot of k_A (cm^2/mJ) vs.A_0 (cfu/100 mL)

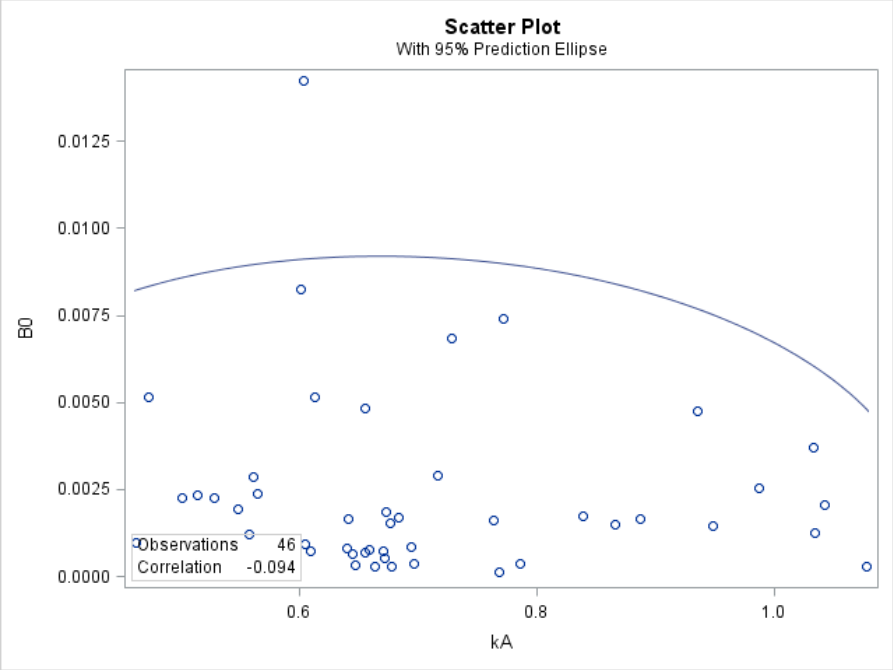

Figure B15. Scatter plot of k_A (cm^2/mJ) vs.B_0 (cfu/100 mL)

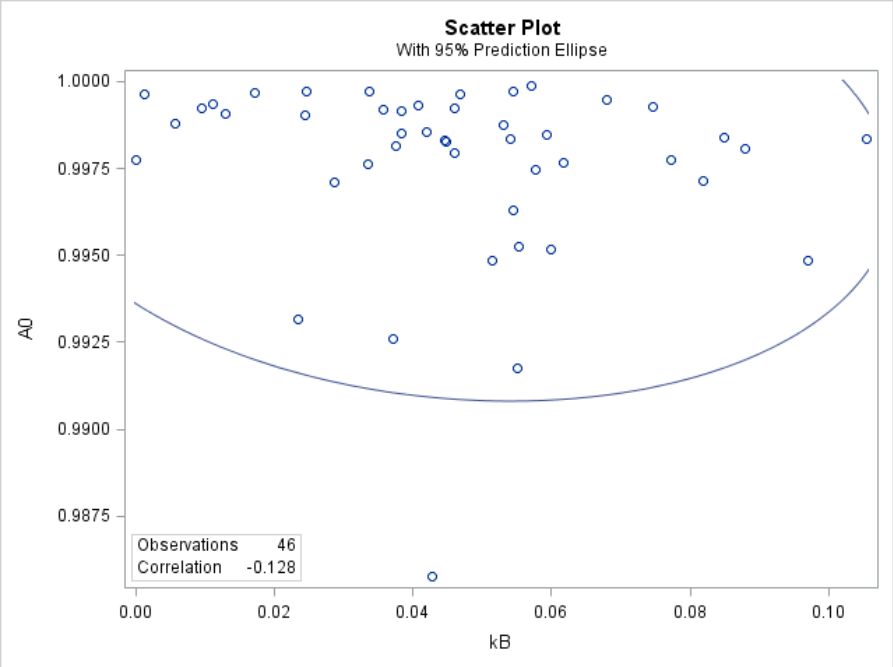

Figure B16. Scatter plot of k_B (cm^2/mJ) vs.A_0 (cfu/100 mL)

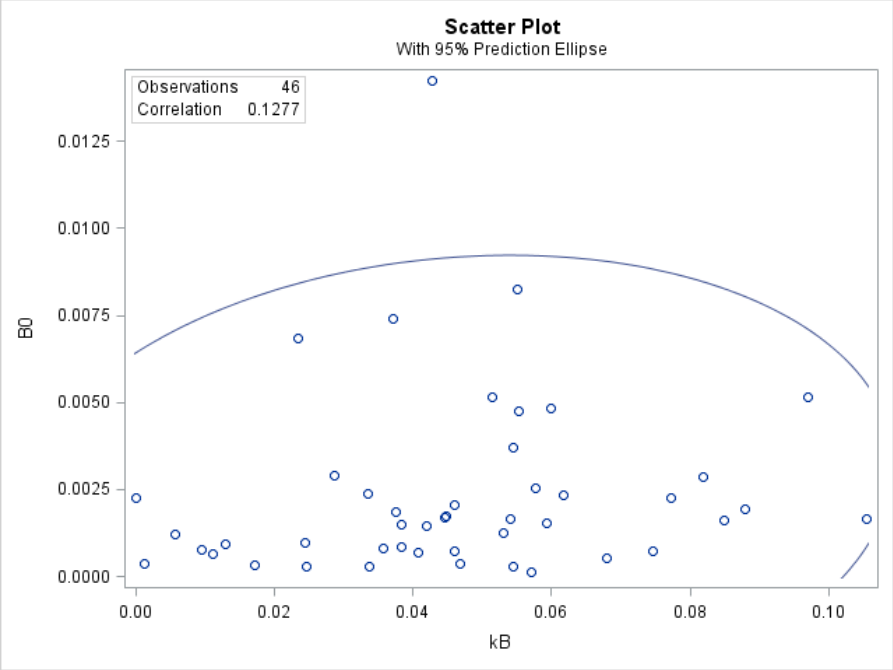

Figure B17. Scatter plot of k_B (cm^2/mJ) vs.B_0 (cfu/100 mL)

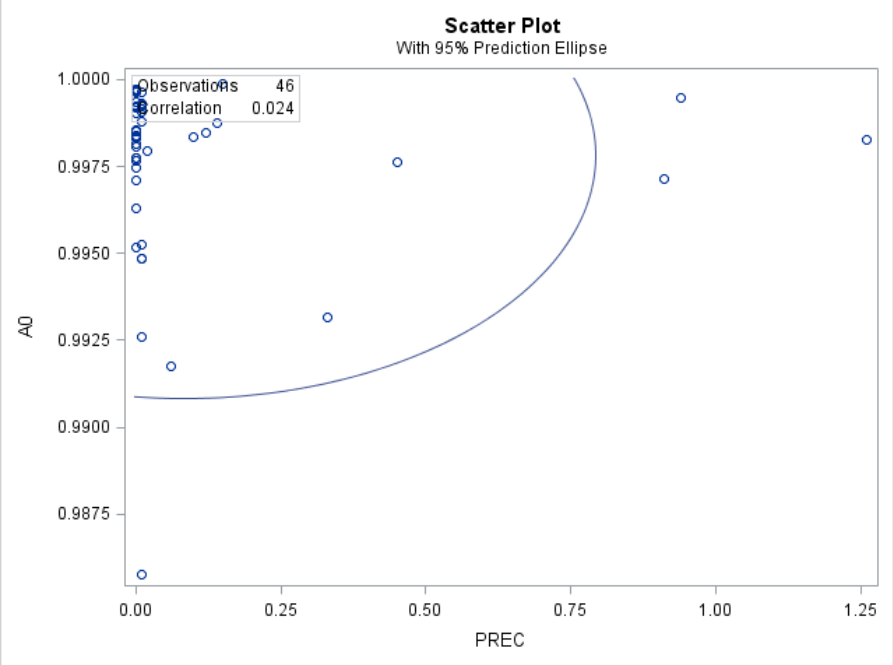

Figure B18. Scatter plot of Precipitation (in) vs.A_0 (cfu/100 mL)

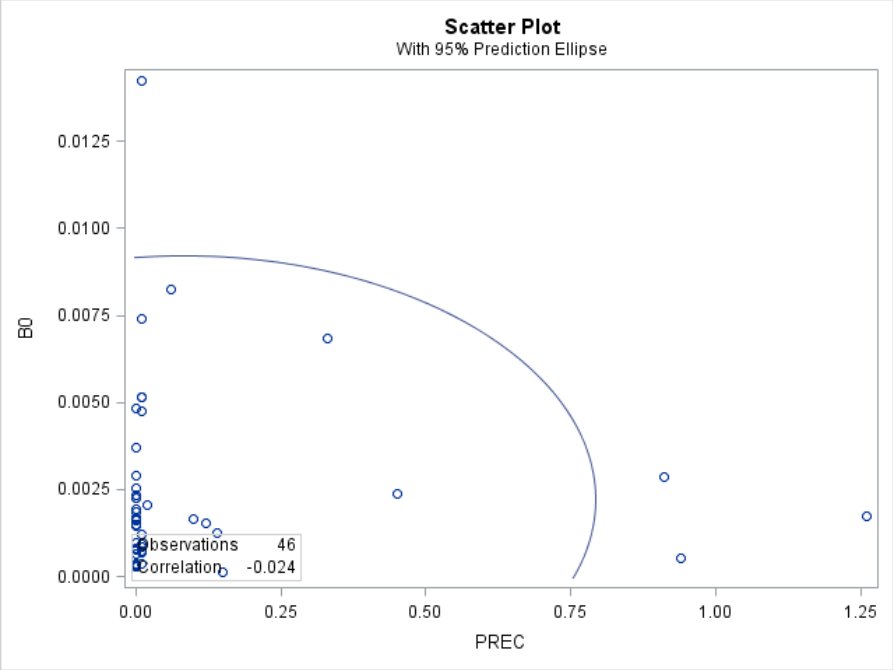

Figure B19. Scatter plot of Precipitation (in) vs.B_0 (cfu/100 mL)

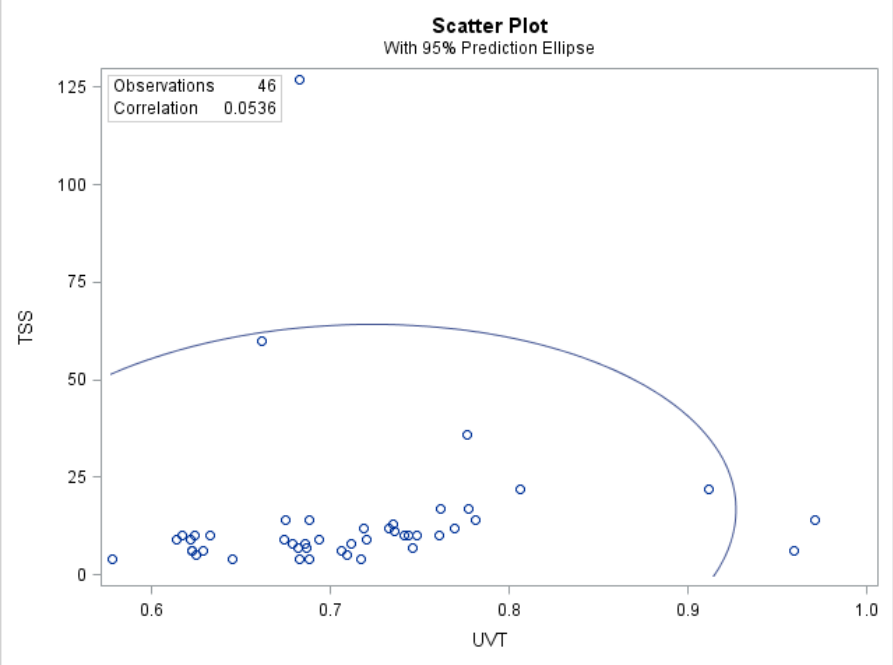

Figure B20. Scatter plot of UVT (fraction) vs. TSS (mg/L)

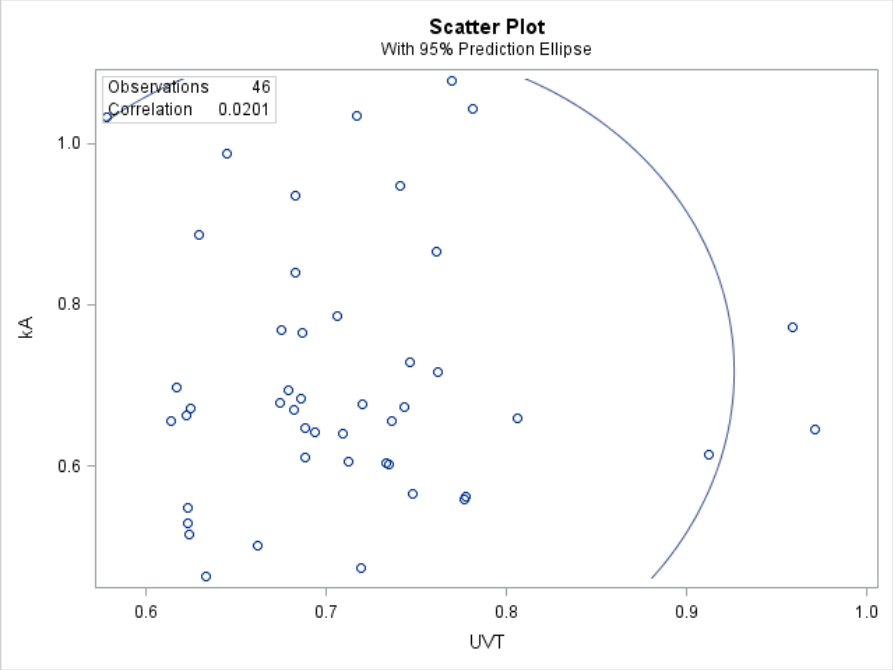

Figure B21. Scatter plot of UVT (fraction) vs. k_A (cm^2/mJ)

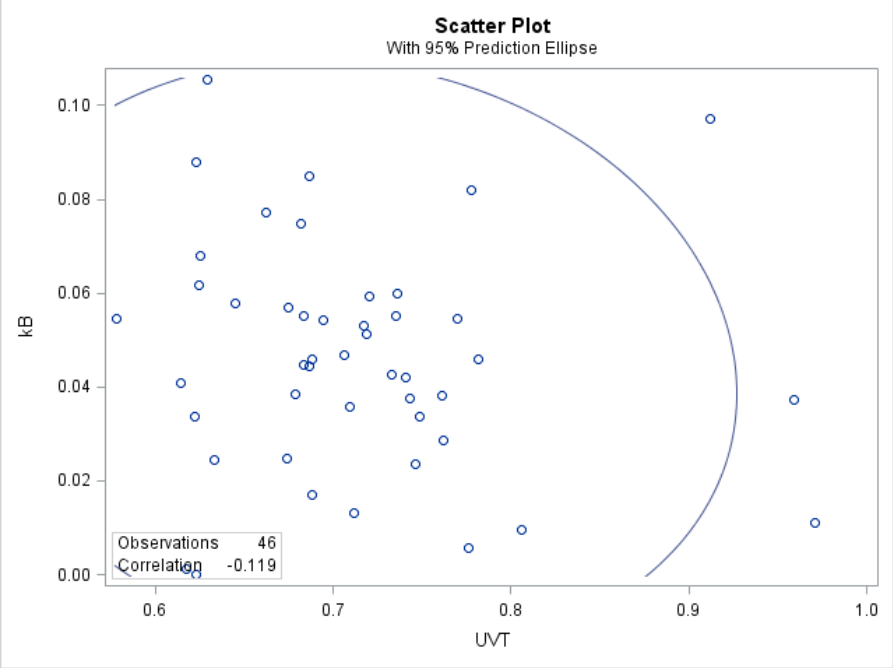

Figure B22. Scatter plot of UVT (fraction) vs. k_B (cm^2/mJ)

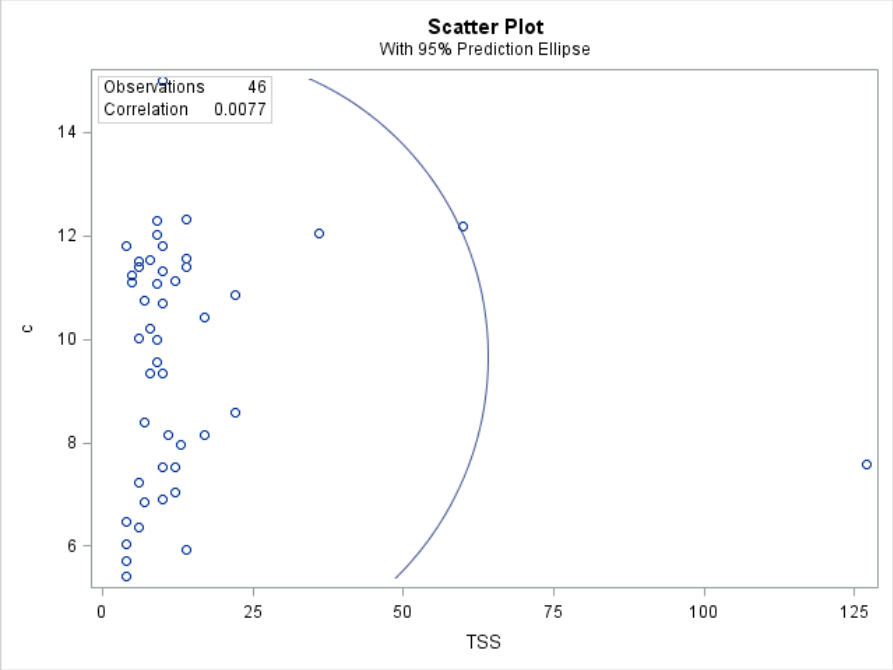

Figure B23. Scatter plot of TSS (mg/L) vs. c (mJ/cm^2)

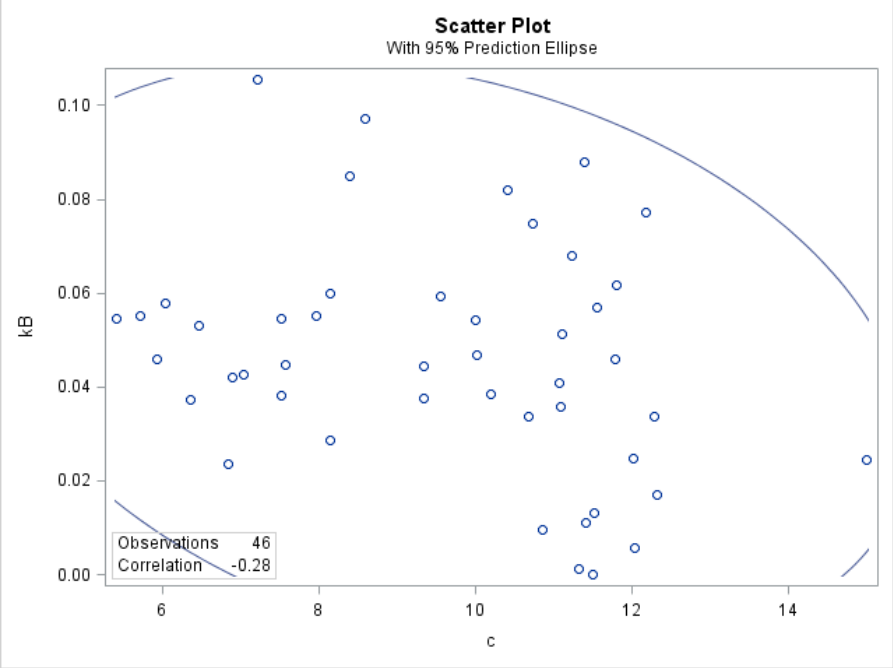

Figure B24. Scatter plot of c (mJ/cm^2) vs. k_B (cm^2/mJ)

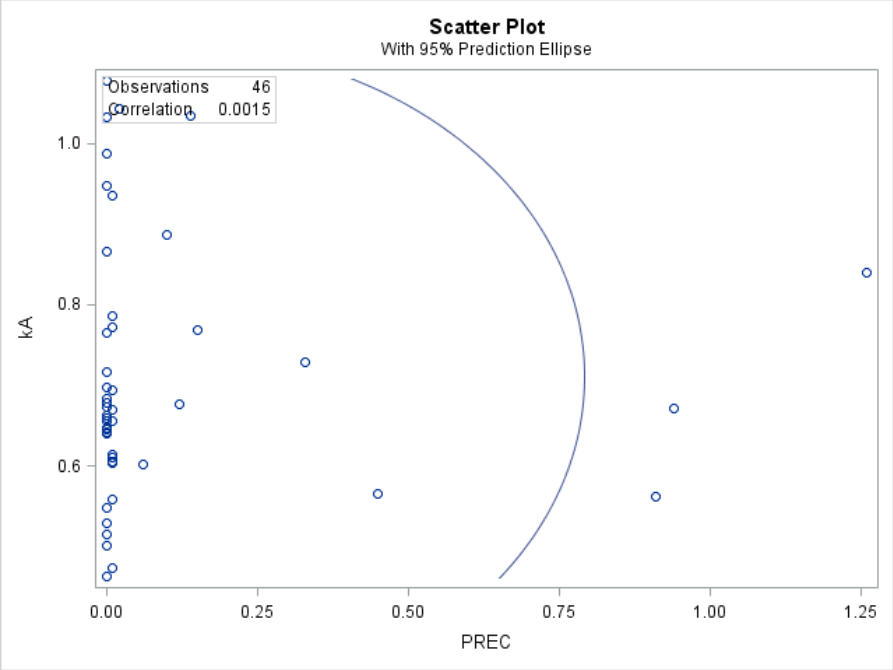

Figure B25. Scatter plot of Precipitation (in) vs. k_A (cm^2/mJ)

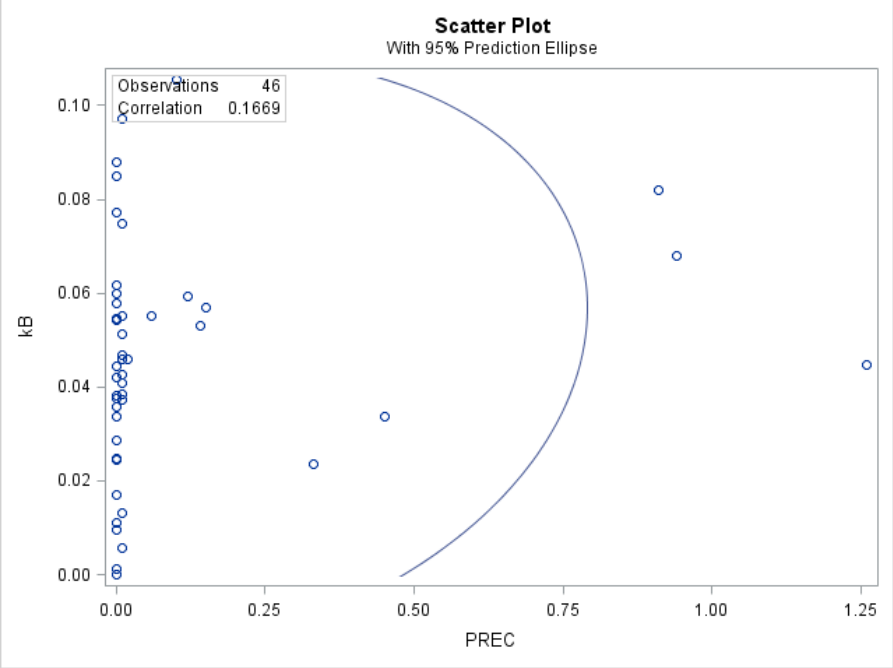

Figure B26. Scatter plot of Precipitation (in) vs. k_B (cm^2/mJ)

Appendix C. AB experiments results

Non-disinfection Season

Table C1. AB flow conditions for experiment executed on 12/13/2012

Flow Condition (Q)	Open Channels	Banks in operation per channel	Sample locations, per operating condition, per channel
1	1,2	A & B	I, II, III
2	1,2,3	A & B	I, II, III
3	1,2,3,4	A & B	I, II, III

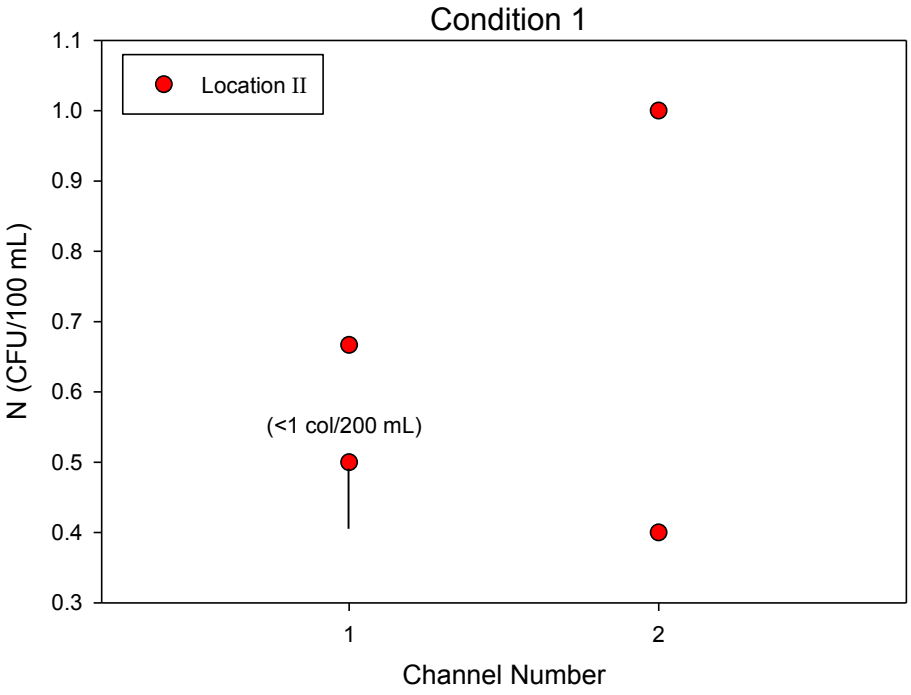

Figure C1. AB Experiment performed on 12/13/12. *E. coli* concentrations per channel. Condition1.

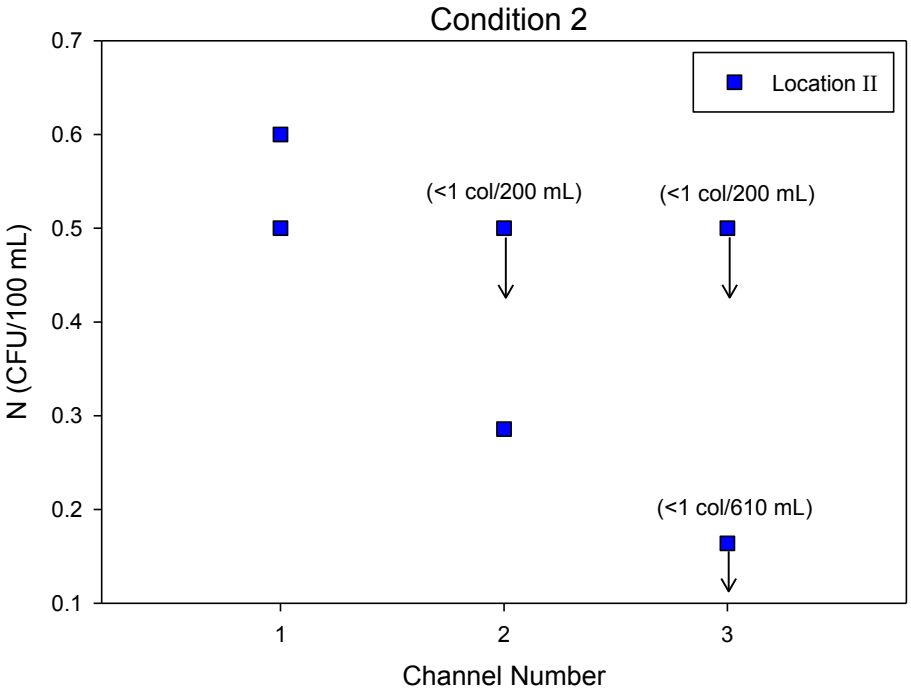

Figure C2. AB Experiment performed on 12/13/12. *E. coli* concentrations per channel. Condition 2.

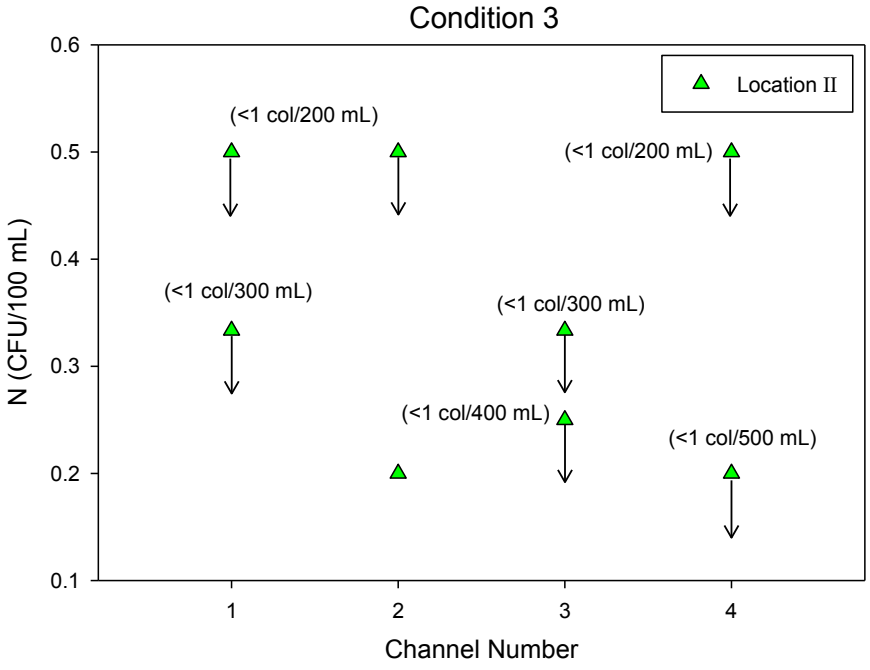

Figure C3. AB Experiment performed on 12/13/12. *E. coli* concentrations per channel Condition 3.

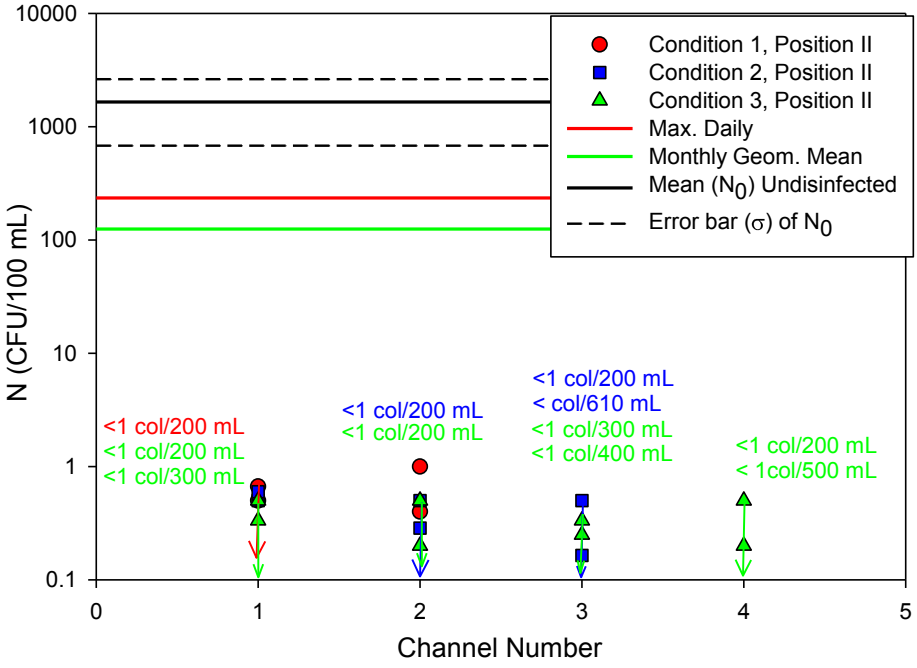

Figure C4. AB Experiment performed on 12/13/12. *E. coli* concentrations per channel, for location II for each of three flow conditions.

Table C2. AB flow conditions for experiment executed on 3/7/2013

Flow Condition (Q)	Open Channels	Banks in operation per channel	Sample locations, per operating condition, per channel
1	1,2,3,4,5,6,7	A & B	I, II, III
2	1,2,3,4	A & B	I, II, III
3	1,2,3	A & B	I, II, III
4	1,2	A & B	I, II, III

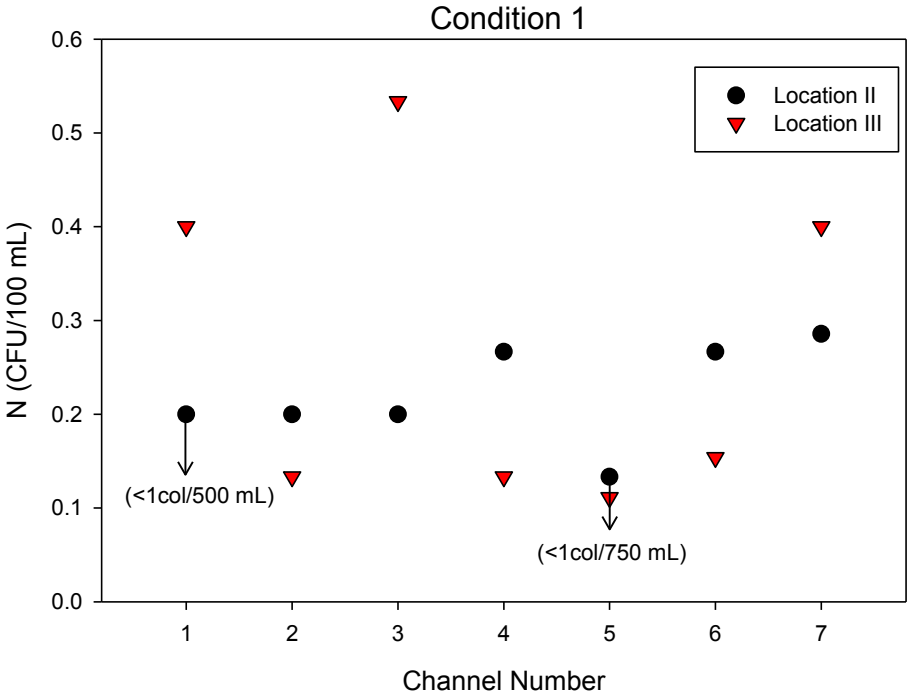

Figure C5. AB Experiment performed on 3/7/13. *E. coli* concentrations per channel Condition 1.

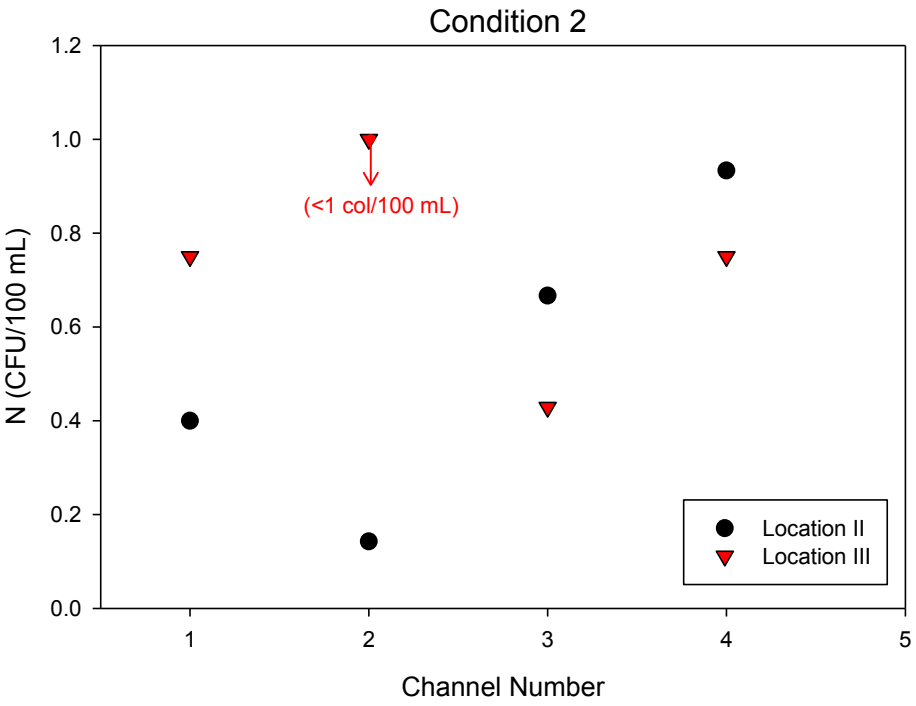

Figure C6. AB experiment performed on 3/7/13. *E. coli* concentrations per channel Condition 2.

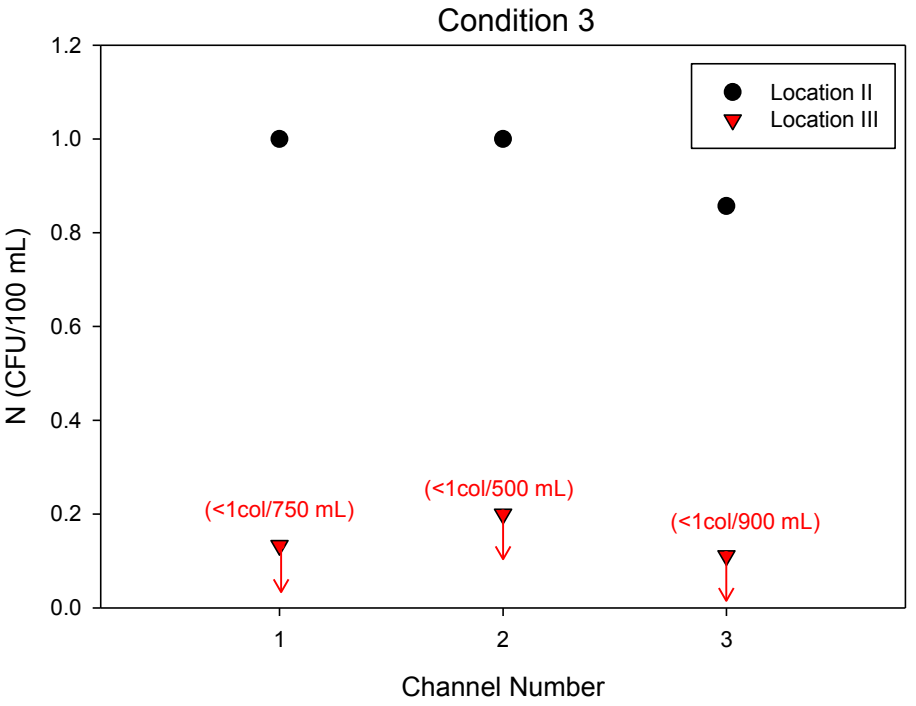

Figure C7. AB experiment performed on 3/7/13. *E. coli* concentrations per channel Condition 3.

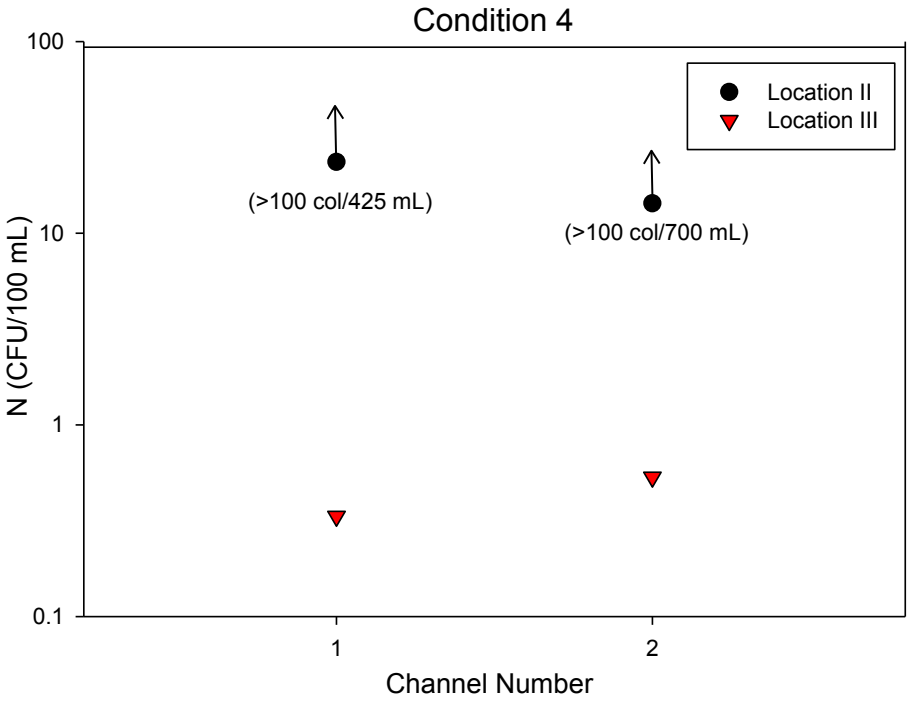

Figure C8. AB experiment performed on 3/7/13. *E. coli* concentrations per channel Condition 4.

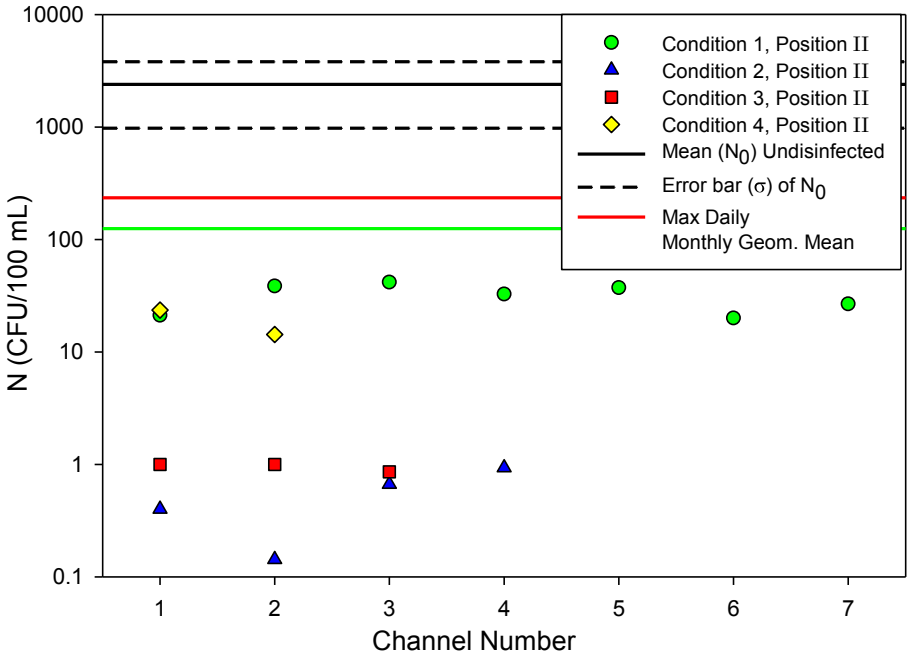

Figure C9. AB Experiment performed on 3/7/13. *E. coli* concentrations per channel, for location II for each of three flow conditions.

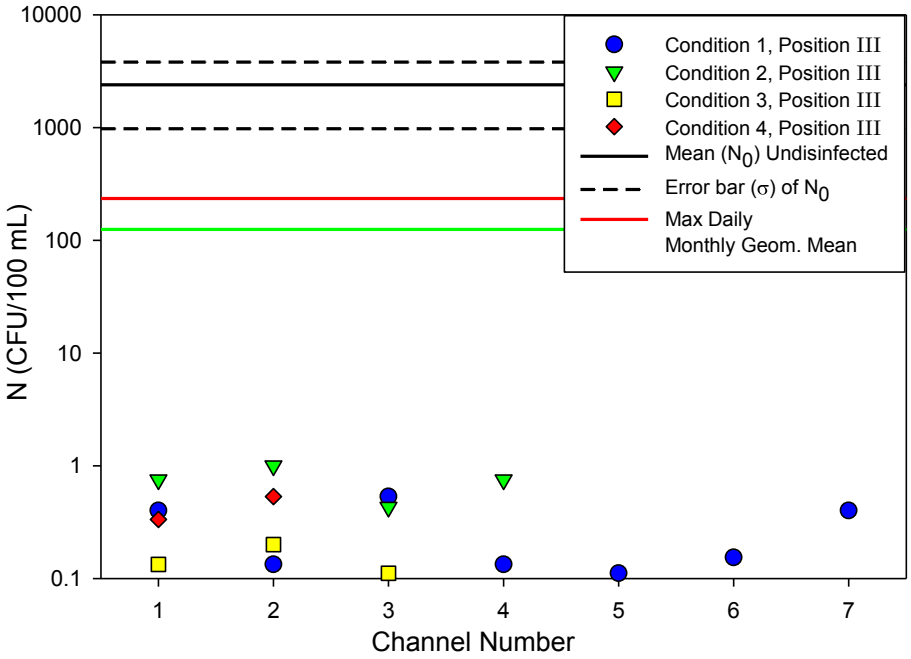

Figure C10. AB Experiment performed on 3/7/13. *E. coli* concentrations per channel, for location III for each of three flow conditions.

Disinfection Season

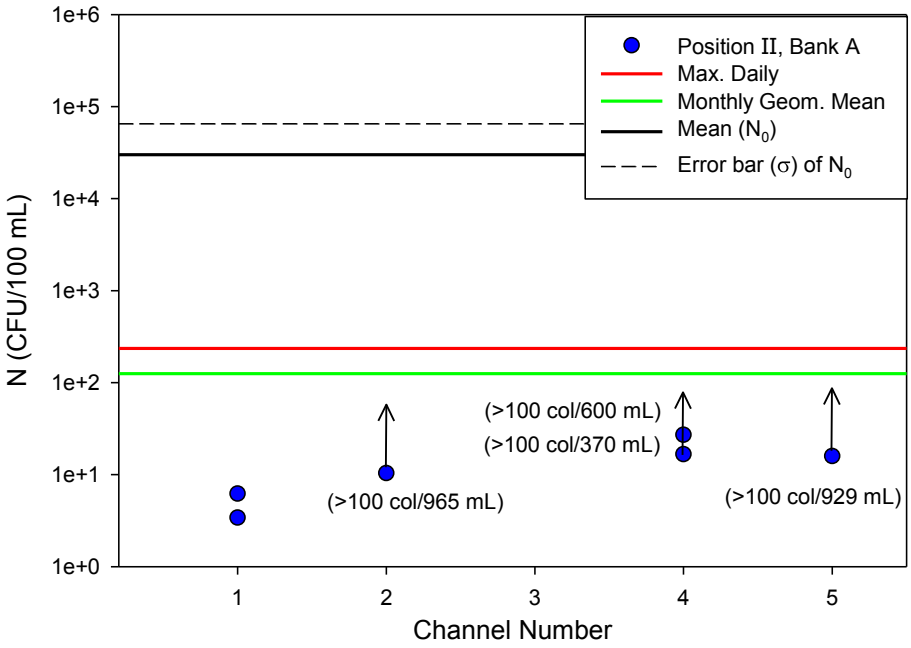

Figure C11. Flow rate at the time of collection of experiments 6/25/13 was Q = 89.7 MGD, UVT = 72.5%, and PLC Dose = 31.2 mJ/cm^2. Channels in operations were 1, 2, 4, and 5. Bank A.

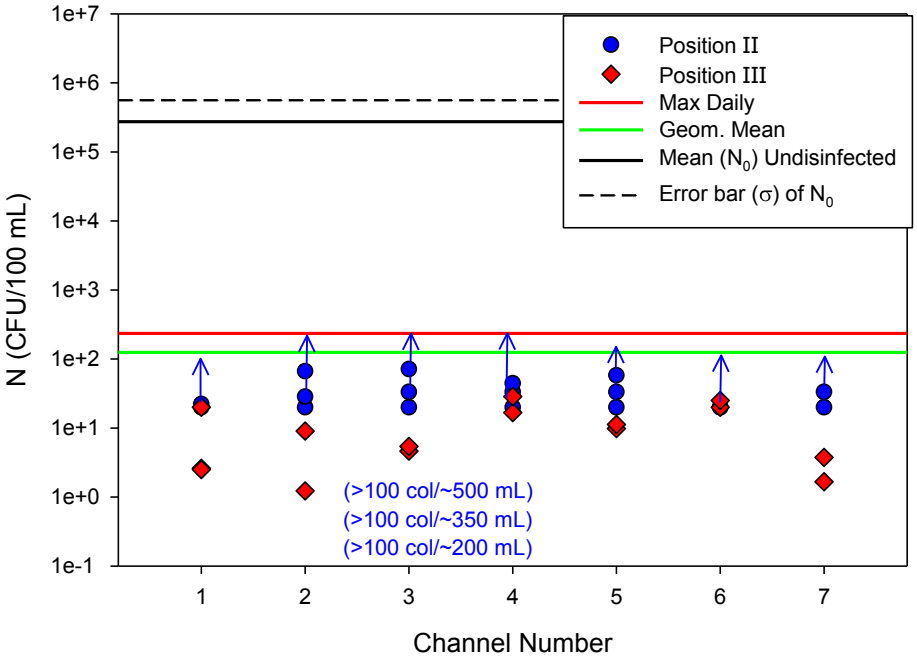

Figure C12. Flow rate at the time of collection of experiments 7/2/13 was Q = 122 MGD, UVT = 68.1%, and PLC Dose = 51.9 mJ/cm^2. All channels in operation. Banks A and B.

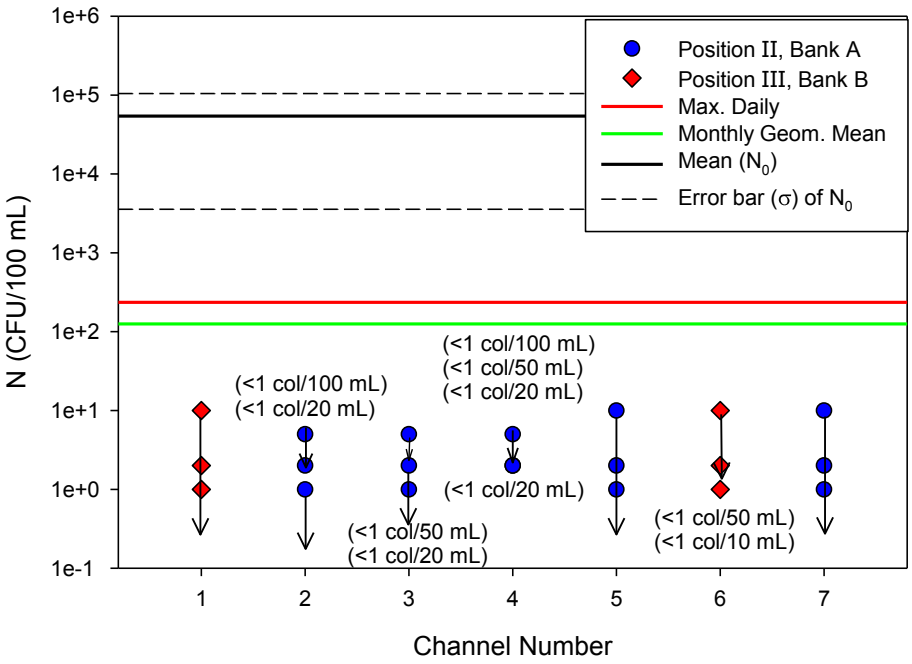

Figure C13. Flow rate at the time of collection of experiments 7/9/13 was Q = 81.8 MGD, UVT = 70.4%, and PLC Dose = 35.5 mJ/cm^2. Operation scheme see Figure 42.

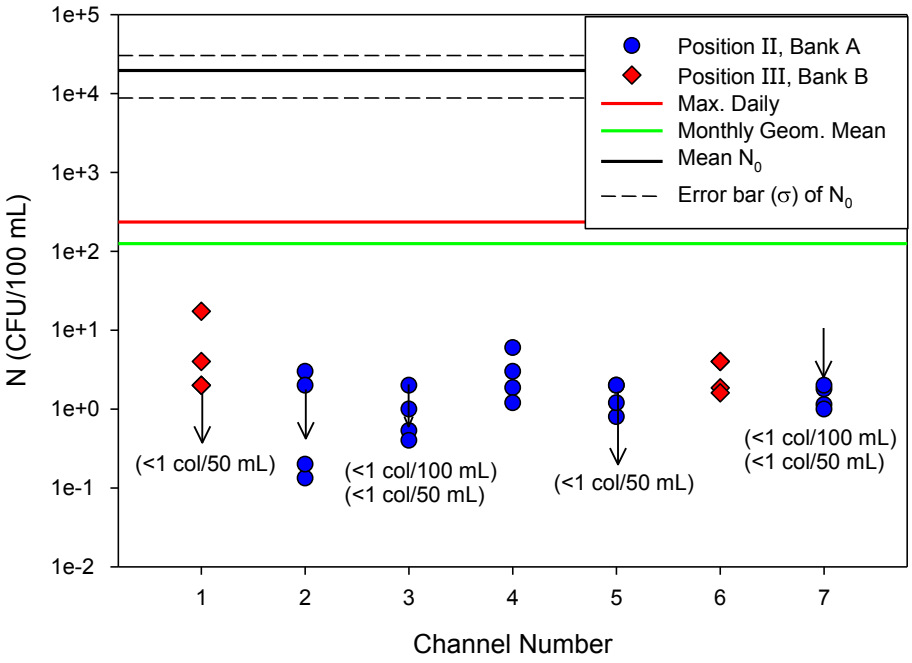

Figure C14. Flow rate at the time of collection of experiments 7/25/13 was Q = 68.4 MGD, UVT = 70.8%, and PLC Dose = 35.1 mJ/cm^2. Operation scheme see Figure 42.

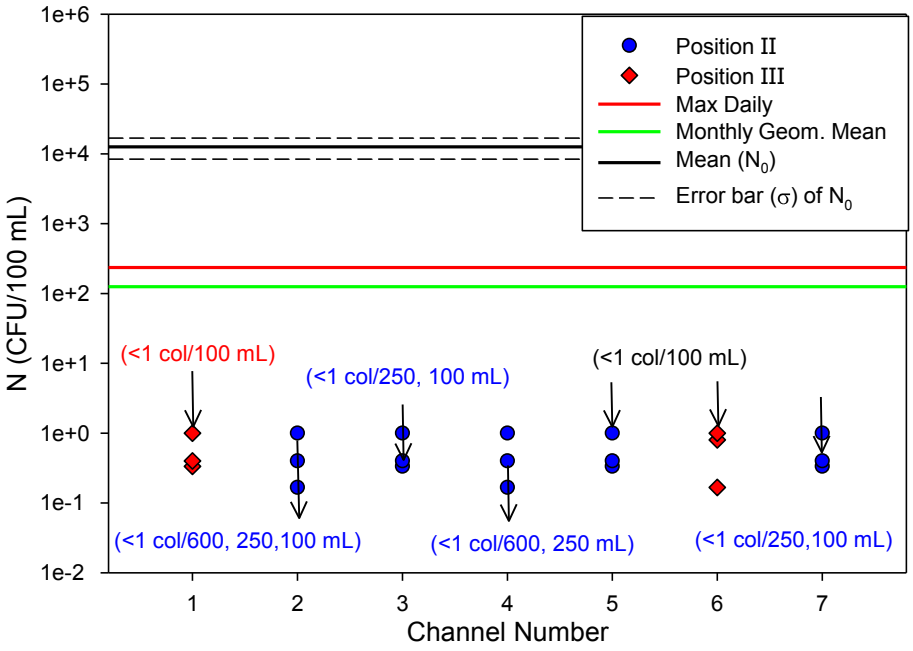

Figure C15. Flow rate at the time of collection of experiments 8/29/13 was Q = 57 MGD, UVT = 72.8%, and PLC Dose = 41.6 mJ/cm^2. Operation scheme see Figure 42.

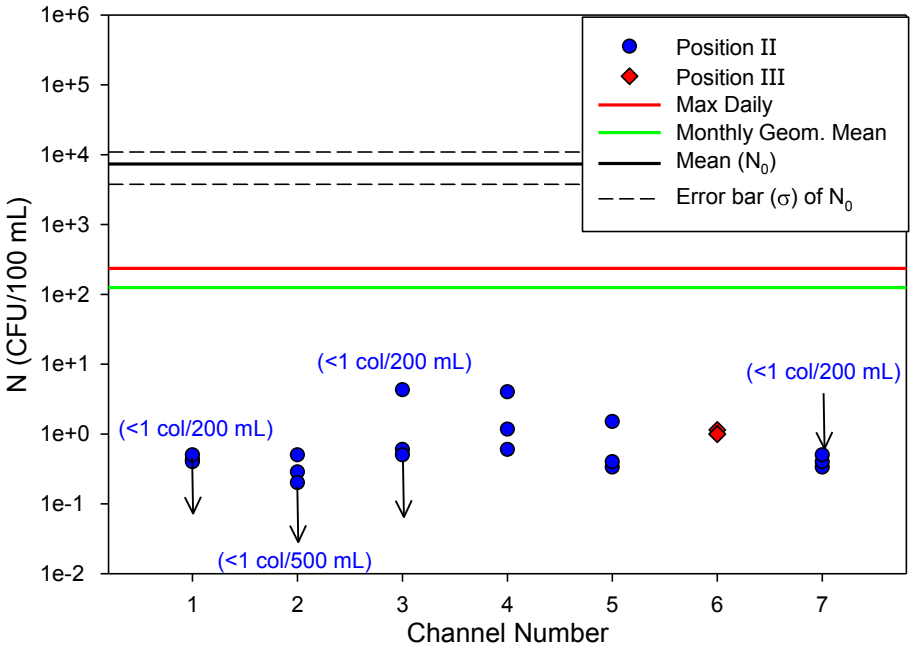

Figure C16. Flow rate at the time of collection of experiments 9/10/13 was Q = 60.2 MGD, UVT = 69.1%, and PLC Dose = 45.15 mJ/cm^2. Bank A operating in channels 1, 2, 3, 4, 5, and 7. Bank B operating in channel 6.

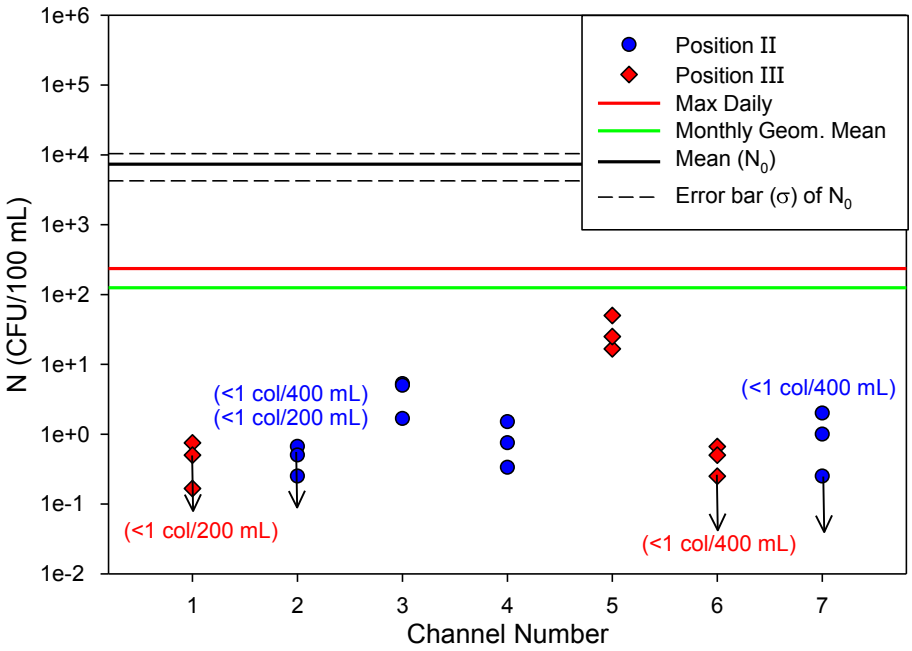

Figure C17. Flow rate at the time of collection of experiments 10/1/13 was Q = 78.4 MGD, UVT = 71.9%, and PLC Dose = 30.8 mJ/cm^2. Bank A operating channels 2, 3, 4, and 7. Bank B operating channels 1, 5, and 6.

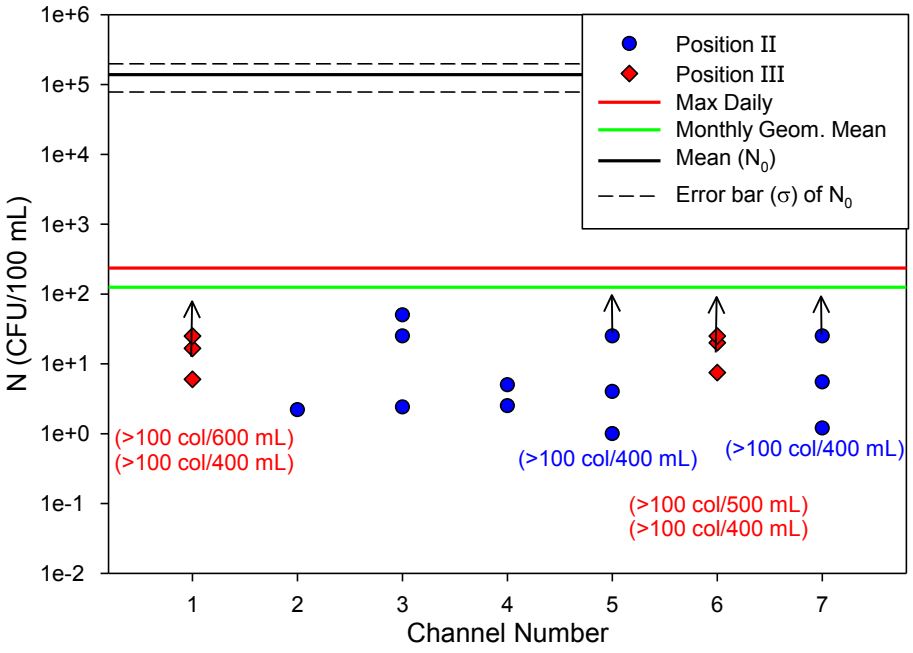

Figure C18. Flow rate at the time of collection of experiments 10/8/13 was Q = 67 MGD, UVT = 70.8%, and PLC Dose = 46.6 mJ/cm^2. Operation scheme see Figure 42.

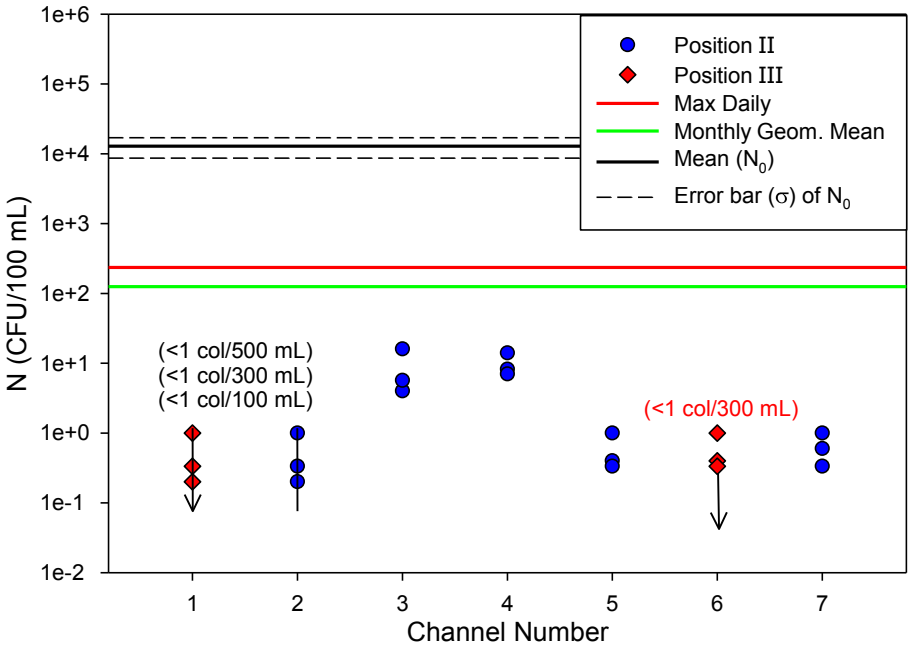

Figure C19. Flow rate at the time of collection of experiments 10/16/13 was Q = 57.5 MGD, UVT = 70.8%, and PLC Dose = 46.3 mJ/cm^2. Operation scheme see Figure 42.